Copy No. **52**

Surface Backscattering
Technical Report under ARL:UT Independent Research and Development Program

Hollis Boehme
Walter M. Amos
Rick S. Bailey

Applied Research Laboratories
The University of Texas at Austin
P. O. Box 8029   Austin, TX 78713-8029

29 August 1995

Technical Report
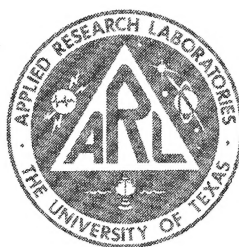
Approved for public release;
distribution is unlimited.

Prepared for:
Applied Research Laboratories
Independent Research and Development Program

19960430 030

DISCLAIMER NOTICE
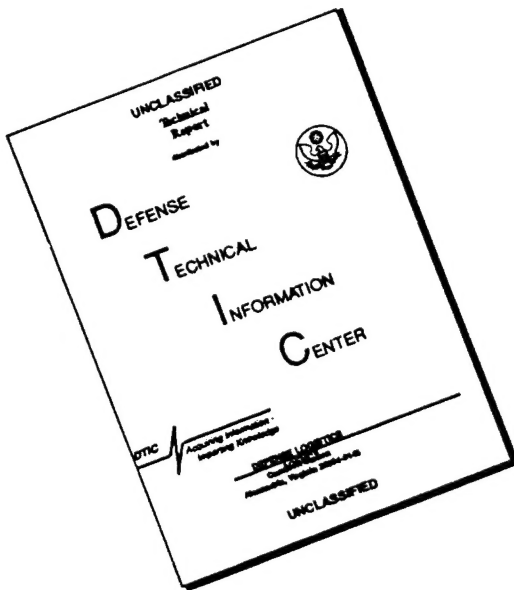
UNCLASSIFIED

REPORT DOCUMENTATION PAGE	Form Approved OMB No. 0704-0188

Public reporting burden for this collection of information is estimated to average 1 hour per response, including the time for reviewing instructions, searching existing data sources, gathering and maintaining the data needed, and completing and reviewing the collection of information. Send comments regarding this burden estimate or any other aspect of this collection of information, including suggestions for reducing this burden, to Washington Headquarters Services, Directorate for Information Operations and Reports, 1215 Jefferson Davis Highway, Suite 1204, Arlington, VA 22202-4302, and to the Office of Management and Budget, Paperwork Reduction Project (0704-0188), Washington, DC 20503.

1. AGENCY USE ONLY (Leave blank)	2. REPORT DATE 29 Aug 95	3. REPORT TYPE AND DATES COVERED technical

4. TITLE AND SUBTITLE	5. FUNDING NUMBERS
Surface Backscattering, Technical Report under the ARL:UT Independent Research and Development Program	ARL:UT Independent Research and Development Program

6. AUTHOR(S)

Boehme, Hollis   Amos, Walter M.   Bailey, Rick S.

7. PERFORMING ORGANIZATION NAMES(S) AND ADDRESS(ES)	8. PERFORMING ORGANIZATION REPORT NUMBER
Applied Research Laboratories The University of Texas at Austin P.O. Box 8029 Austin, Texas 78713-8029	ARL-TR-95-23

9. SPONSORING/MONITORING AGENCY NAME(S) AND ADDRESS(ES)	10. SPONSORING/MONITORING AGENCY REPORT NUMBER
Applied Reseach Laboratories The University of Texas at Austin Austin, Texas 78713-8029	

11. SUPPLEMENTARY NOTES

12a. DISTRIBUTION/AVAILABILITY STATEMENT	12b. DISTRIBUTION CODE
Approved for public release; distribution is unlimited.	

13. ABSTRACT (Maximum 200 words)

Surface and near-surface acoustic backscatter measurements at 108, 72, 36, and 18 kHz made off the coast of Fort Lauderdale, Florida, have been analyzed and the results are presented in this report. The measurements were made with bottom mounted equipment looking upward at the ocean surface; wind speeds encountered varied from about 2.5 to about 16 m/s. Vertical incidence acoustic measurements were used to evaluate near-surface volume backscatter versus depth, which were then used to estimate bubble density versus depth and bubble density versus bubble radius; these results were compared with other reported results. Measured surface backscattering strengths compare well with APL/UW model predictions at high grazing angles; however, measurement results were substantially below MINERAY and somewhat below APL/UW model predictions at intermediate and lower grazing angles when remotely measured wind speeds were used as model inputs.

14. SUBJECT TERMS		15. NUMBER OF PAGES 101
bubble density bubble scattering surface acoustic backscatter	surface bubble loss vertical incidence backscatter volume backscatter	16. PRICE CODE

17. SECURITY CLASSIFICATION OF REPORT	18. SECURITY CLASSIFICATION OF THIS PAGE	19. SECURITY CLASSIFICATION OF ABSTRACT	20. LIMITATION OF ABSTRACT
UNCLASSIFIED	UNCLASSIFIED	UNCLASSIFIED	SAR

NSN 7540-01-280-5500

UNCLASSIFIED

Standard Form 298 (Rev. 2-89)
Prescribed by ANSI Std. 239-18
298-102

This page intentionally left blank.

TABLE OF CONTENTS

This page intentionally left blank.

LIST OF FIGURES

This page intentionally left blank.

LIST OF TABLES

This page intentionally left blank.

EXECUTIVE SUMMARY

High frequency acoustics environmental measurements were made in 1988 off the coast of Fort Lauderdale, Florida, in water depth of about 160 m using a measurement system deployed on the bottom and connected to electronics and power on shore by means of two coaxial cables. This report presents results of acoustic measurements of vertical incidence backscattering from near-surface volume scatterers and of surface backscattering as a function of grazing angle at frequencies of 18, 36, 72, and 108 kHz. The wind speeds encountered were near those adequate for onset of near-surface bubble production at the low end and for onset of near-surface bubble saturation on the high end.

The underwater portion of the acoustic measurement system was located on the bottom about 5.7 km south and 4.9 km east of the harbor entrance to Port Everglades near Fort Lauderdale, Florida. The on-shore portion of the system was located on the south jetty at the Port Everglades harbor entrance. Wind speed and wind direction were measured at the on-shore electronics shelter; sound speed versus depth was measured from a work boat in the vicinity of the in-water equipment.

The acoustic measurement system and deployment conditions provided vertical incidence acoustic backscatter data from scatterers near the sea surface at system frequencies coinciding with resonance frequencies of microbubbles whose density and spatial distribution are of considerable interest. There is general agreement among researchers concerning the gross characteristics of the upper ocean boundary, including bubble generation and spatial density distribution. However, the detailed nature of the near-surface dynamics, including bubble generation and distribution mechanisms, provides incentive for additional research. Near-surface acoustic measurements of volume backscatter and concomitant estimates of bubble density leave little doubt that concentrations of microbubbles are significant constituents of the near-surface scatterer population.

The results obtained from current measurements are generally consistent with a bubble layer model in which the density decays exponentially with depth.

xi

Considerable temporal variation is observed with relatively small, high density cells occasionally moving through the fixed measurement region; however, the mean behavior appears to be relatively constant over periods of several minutes. Bubble density estimates are generally higher within the first few meters of the surface than other reported density estimates, most of which included measurements at deeper depths. The quiescent volume backscatter over the duration of the current measurements also appears to be fairly high but not excessively so for a coastal environment. Bubble density versus bubble radius curves depict an exponential decrease with increasing bubble radius, with little sensitivity to wind speed over the limited range of wind speeds encountered.

The measurements of acoustic backscattering from the sea surface as a function of grazing angle were made by selecting various orientations of the transducer in a vertical plane and echoranging on the sea surface. A mean backscattering strength was determined for each beam in the set of preformed receive beams; a corresponding grazing angle was determined from receive beam vertical angle using raytracing and measured sound speed profile. In most cases overlap of surface regions providing backscatter returns occurred for sequential transducer orientations so that measurements were piecewise continuous in grazing angle. The mean backscattering strength for each receive beam was determined from samples averaged over times equal to transmit pulse lengths, ensemble averaged over valid pings, and corrected by system calibration and estimated propagation losses.

The surface backscattering strength versus grazing angle results were compared with a modified Chapman-Harris submodel used in MINERAY, a sonar performance prediction computer model, and a surface backscattering submodel developed by APL/UW. Both of these submodels have been reduced to dependence upon wind speed only for any selected frequency. Also, the submodel predicted curves are intended for global sonar performance prediction applications. Surface backscattering measurements support a wind speed dependence, and wind speed is relatively easily measured (or at least approximated with some degree of accuracy). Wind measurements were made on shore in the present case at some distance from the deployed equipment.

Surface backscattering measurement results were examined for dependence upon transmitted pulse type; no such dependence was found for the frequencies used and the wind speeds encountered. Only modest wind speed dependence was observed for grazing angles greater than about 60°. However, significant wind speed dependence was observed for all frequencies at intermediate and lower grazing angles. Little if any frequency dependence was seen over the range of wind speeds encountered.

Measured surface backscattering strengths were comparable with APL/UW submodel predictions at high grazing angles. However, measurement results were substantially below MINERAY and APL/UW(89) submodel predictions at intermediate and lower grazing angles. Considerable improvement in wind speed dependence has been made in a revised APL/UW(94) surface acoustic backscatter submodel. Predictions of this revised submodel were in much closer agreement with measurement results at all grazing angles and wind speeds; however, substantial difference in revised submodel predictions and measurements were still noted at intermediate and lower grazing angles for higher wind speeds.

Vertical incidence volume backscatter measurements were used to provide more direct inputs to the bubble component of the APL/UW scattering submodel for prediction of surface backscattering at lower grazing angles. In most cases the model predicted curves, using measured volume backscatter as inputs to the bubble scattering component, match measured surface backscatter strength more closely than comparisons where submodel predictions are based on wind speed as inputs. This is particularly significant with regard to verification of the physical basis of the near-surface bubble layer component of the APL/UW surface backscattering model. The comparisons also serve to illustrate the compatibility of vertical incidence volume backscatter and surface backscatter measurements in the present case. In particular, extremely low surface backscattering strength at low grazing angles is observed to accompany those occasions where no vertical incidence volume backscatter was discernible.

The preferred physical measurement providing model inputs is vertical incidence acoustic backscatter or absorption. When such measurements are impractical, wind speed measurements can provide less direct inputs, but tend to

result in overestimates of surface backscatter at lower grazing angles and higher wind speeds.

1. INTRODUCTION

This report presents results of acoustic measurements of vertical incidence backscattering from near-surface volume scatterers and of surface backscattering as a function of grazing angle. The measurements were made in 1988 off the coast of Fort Lauderdale, Florida, in water depth of about 160 m. The acoustic measurement system included a 2 m high support platform deployed on the bottom which allowed the operator to tilt the soundhead in the vertical plane and rotate the soundhead in the horizontal plane. The underwater equipment was connected to electronics and power on shore by means of two coaxial cables; the test site and equipment will be described in more detail in the next section of this report.

Several characteristics contribute to the uniqueness of the database resulting from the active acoustic measurements and include the following. The frequencies used, 18, 36, 72, and 108 kHz, span almost three octaves, while the beamwidths and pulse types combine to provide good spatial resolution and a variety of insonified surface spot sizes. The wind speeds encountered ranged from about 2.5 to about 16 m/s, which include speeds considered adequate for onset of near-surface bubble production at the low end and for onset of near-surface bubble saturation on the high end. Active acoustic measurements at vertical incidence and at lower grazing angles were interleaved to provide sampling of the same surface environment. Generally good echo-to-noise ratios were achieved over a statistically significant number of pings resulting in valid ensembles from which estimates of mean behavior could be extracted.

Interest in acoustic reverberation from the sea surface developed along with sonar systems, motivated at least in part by desire to circumvent limits imposed on operating systems. Interest has expanded to include acoustic measurements as a means of revealing sea surface dynamics. McDaniel (1993) has recently provided an excellent review of sea surface reverberation including both low frequency and high frequency acoustic characteristics. Earlier acoustic reverberation measurements by Urick and Hoover (1956) and Garrison et al. (1960), as well as more recent measurements by Nützel et al. (1986), McConnell (1988), and Osborn et al. (1992), were discussed in this review.

1

There appears to be a consensus with regard to the significant acoustic role of near-surface gas bubbles as both scatterers and sources of sound [see, for example, Monahan and Lu (1990)]. A near-surface layer of resonant microbubbles can account for observations of initial increase and subsequent quenching of backscattering and ambient noise as wind speeds increase. The contribution of acoustic measurements to knowledge of near-surface bubble density and spatial distribution was included in the review by McDaniel (1993). A comparison with some of the earlier acoustic measurement results will be made in this report. The current acoustic measurement results will also be compared with empirical high frequency backscattering model predictions, specifically, a modified Chapman and Harris model (1962) as currently employed in the sonar performance model MINERAY, and surface backscattering physical models documented by Applied Physics Laboratory, The University of Washington (APL/UW, 1989).

A description of the test site and acoustic measurement equipment will be presented in the following section. Section 3 will include results of vertical incidence backscattering along with estimates of near-surface bubble densities. Surface backscattering versus grazing angle results will be discussed in Section 4; these results will be compared with previously reported measurements and with high frequency backscattering model predictions. Some concluding remarks will be given in Section 5.

2. TEST SITE AND MEASUREMENT EQUIPMENT DESCRIPTION

2.1   TEST SITE

The underwater portion of the acoustic measurement system was located on the bottom in approximately 160 m water depth. The bottom site was about 5.7 km south and 4.9 km east of the harbor entrance to Port Everglades near Fort Lauderdale, Florida. The electronics shelter which housed the on-shore portion of the system was located on the south jetty at the Port Everglades harbor entrance. Wind speed and wind direction were measured at the on-shore electronics shelter. Sound speed versus depth was measured from a work boat in the vicinity of the in-water equipment. The underwater and on-shore equipment were connected by a pair of coaxial cables providing power and command signals from shore to the underwater assembly and providing a signal telemetry link from the underwater assembly to shore. A portion of a navigation chart showing the general test site is shown in Fig. 2.1.

2.2   MEASUREMENT EQUIPMENT

The acoustic measurement equipment was composed of two parts, an underwater assembly and a shore based assembly. The underwater assembly consisted of a support platform which rested on the bottom, an acoustic array, vertical tilt/horizontal scan motor assemblies for positioning the acoustic array, and waterproof canisters to house power and electronic equipment. The support platform was approximately 2 m high and provided a stable base for the acoustic array and electronics canisters. A photograph of the underwater assembly is shown in Fig. 2.2.

The acoustic array was composed of three projector arrays and a receiver array. Separate projector arrays were used for 72 and 108 kHz operating frequencies while a third array was used for both 18 and 36 kHz operating frequencies. The receiver array was composed of 18 horizontal stave pairs arranged to form left and right half arrays; thus, each half array contained 18 half-staves. The combination of left and right half-staves was arranged to approximate a 56 cm diam circular piston. The outputs from each of the 36 half-

3

Figure 2.1
Fort Lauderdale test site.
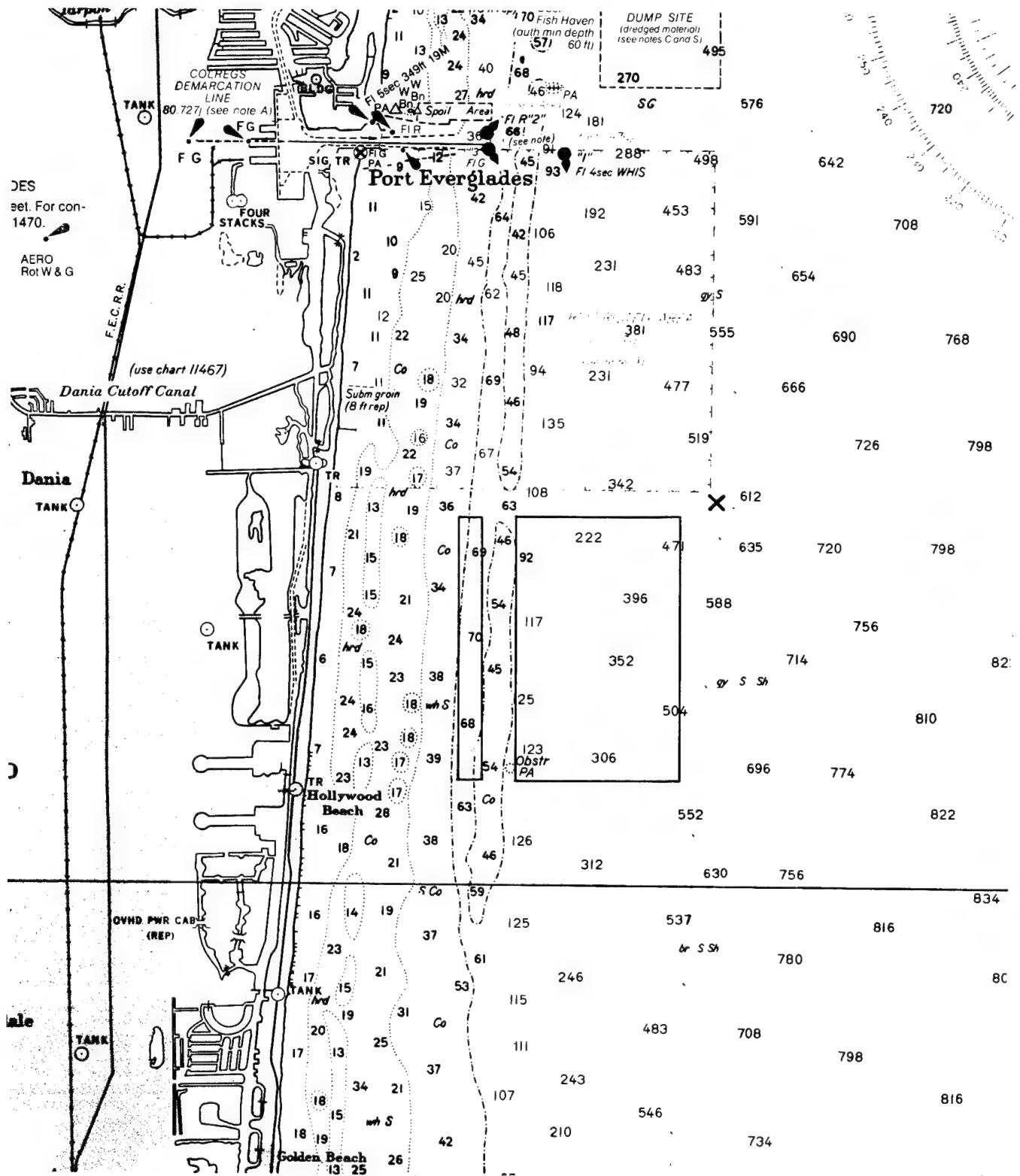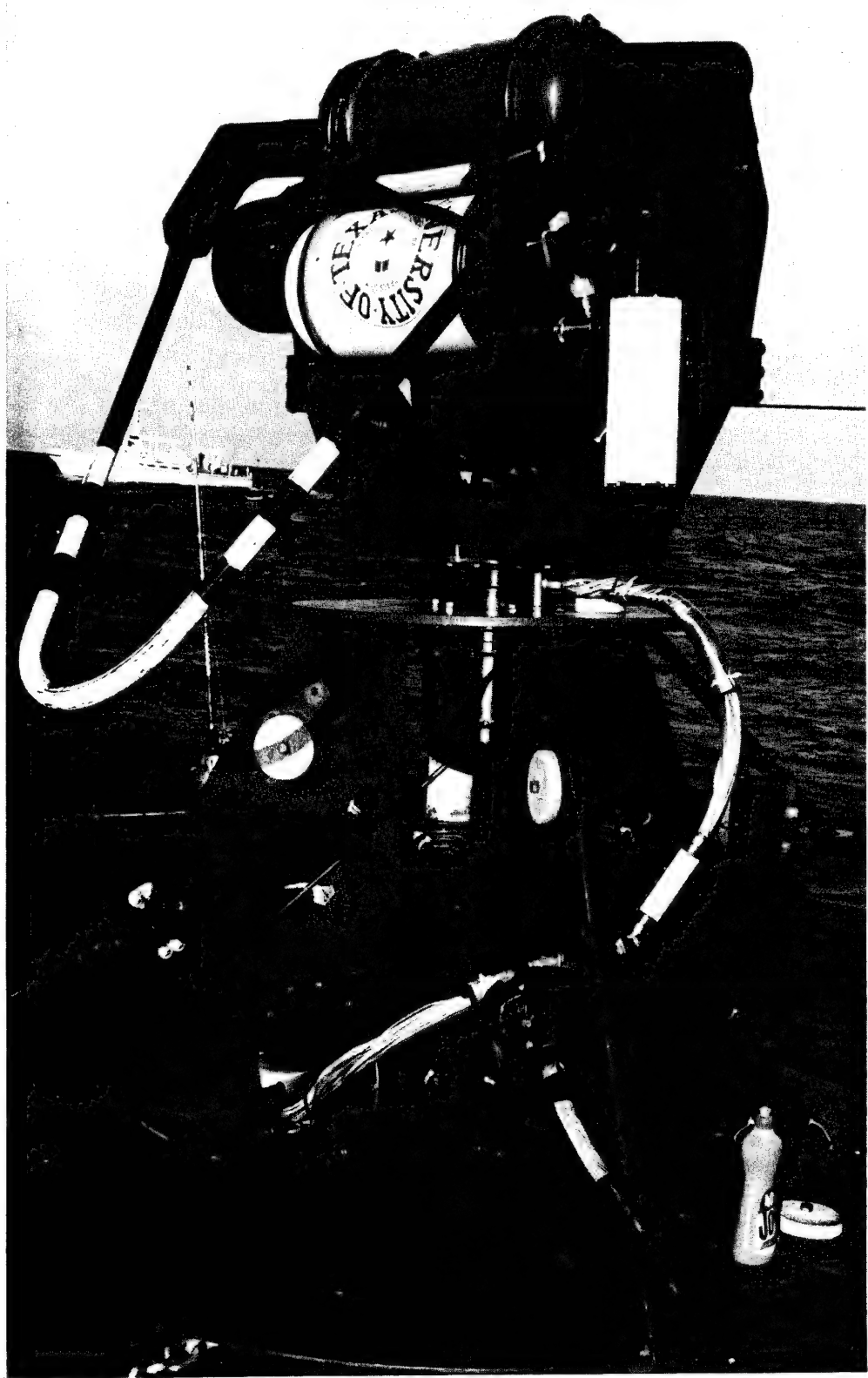
Figure 2.2
Photograph of the underwater assembly
viewed from behind the acoustic array.

staves were quadrature sampled and recorded. A photograph of the acoustic array is shown in Fig. 2.3.

A dc scan motor allowed the operator to tilt the acoustic array in the vertical plane. The depression/elevation (D/E) angle relative to a reference position was sensed and provided as a vertical angle array position to the operator. A second dc scan motor allowed the operator to position the acoustic array vertical plane at any selected azimuthal position. The azimuthal angle relative to a reference position was sensed and provided as an array azimuthal position to the operator. Tilt sensors provided angular readouts to the operator of support platform tilt from vertical caused by bottom slope. All acoustic and auxiliary sensor signals were telemetered to shore via two coaxial cables.

The shore based assembly included a high density digital recorder (HDDR), beamformer, and an operator display and control panel. The HDDR was used to archive all acoustic data, auxiliary sensor data, and time code information. The acoustic data were pre-beamformed sonar signals representing the complex sampled 36 half-stave array outputs. The auxiliary sensor data included system gain settings, array vertical tilt, and horizontal scan positions, as well as additional "housekeeping" information. The time code information provided a realtime clock reference for all recorded data.

The beamformer used for monitoring during data acquisition and for data analysis formed 21 uniformly spaced beams for each of the four operating frequencies. The 21 beams were spaced about half a beamwidth (-3 dB) apart with beam 11 being the center and array boresight beam. Table 2.1 provides the receive beamwidth and sector width for each of the operating frequencies. Vertical incidence backscatter data were taken with beam 11 pointing straight up in most cases; however, on a few occasions, vertical incidence backscatter data were taken with one of the other beams pointing straight up. Surface backscatter versus grazing angle data were taken by stepwise steering in the vertical plane to cause some overlap in sequential sector coverage.
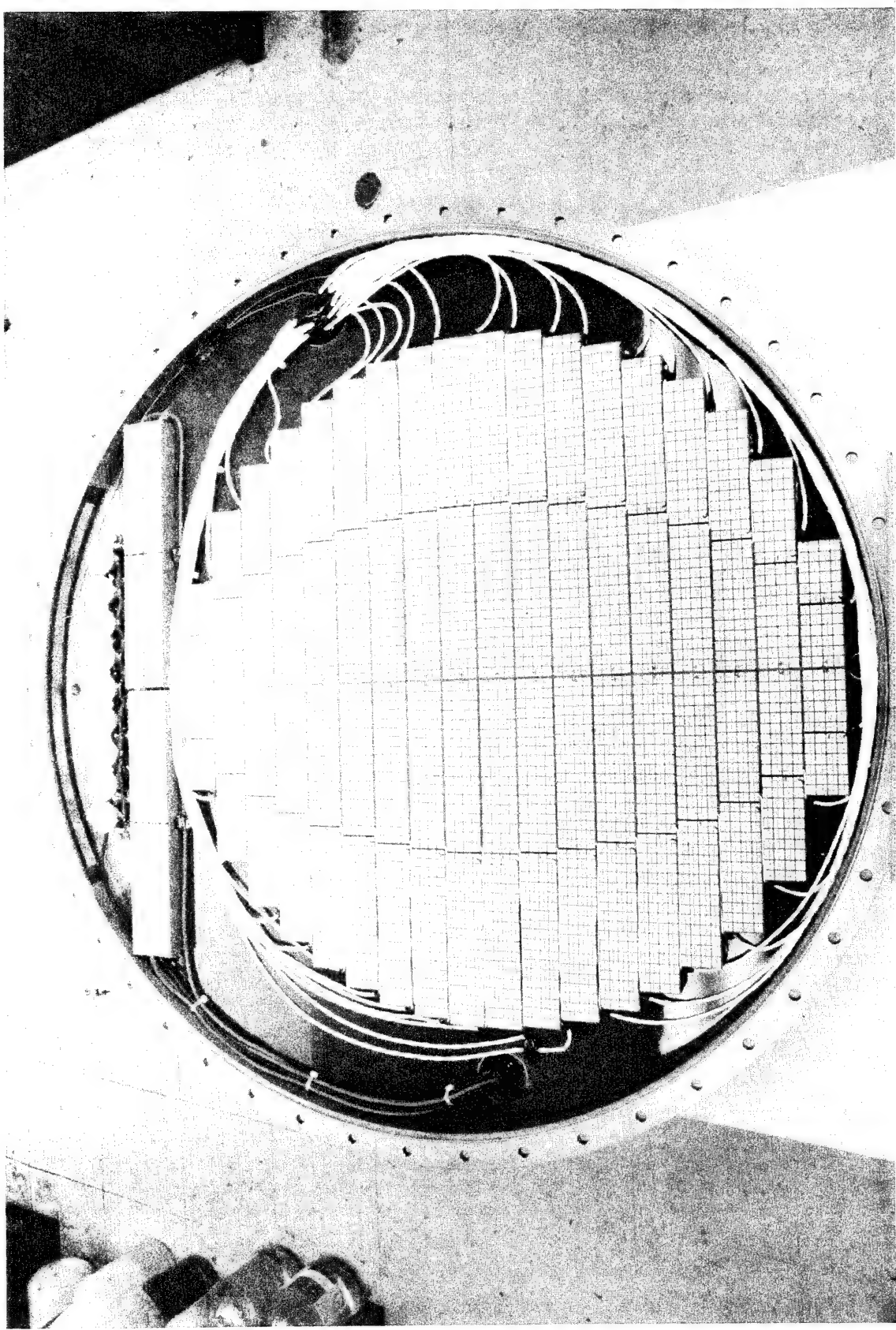
Figure 2.3
Photograph of the transducer array assembly.

Table 2.1
Acoustic measurement system receiver beamwidth
and sector coverage.

Frequency (kHz)	Beamwidth (deg)	Sector Width (deg)
108	1.5	15
72	2.2	22
36	4.4	44
18	8.8	88

The operator control panel provided independent vertical and azimuthal array steering controls and angular readouts. Operating frequency, transmit power, transmit waveform, and receiver gain selection were provided by control switches. Switch positions were sensed and recorded on the HDDR as part of the auxiliary data.

An active display provided the capability of realtime monitoring of data quality during data acquisition. The display format was range (or time) along the vertical axis and beam number along the horizontal axis (i.e., a B-scan format). The operator could elect to display all even numbered (10) beams, all odd numbered (11) beams, or the 11 center beams (beams 6-16). In addition to the multiple beam data, one expanded time display of a single selected beam was provided with operator option of beam number and start range for the expanded time display.

The acoustic subsystems were calibrated at Lake Travis Test Station (LTTS), an acoustic calibration and measurement facility operated by Applied Research Laboratories, The University of Texas at Austin (ARL:UT). System calibration was necessary so that digital signals recorded on archival magnetic tapes could be related to in-water acoustic intensities. Since it was impractical to include the actual telemetry coaxial cables in the system tested at LTTS, provision was made for injecting calibration signals at the receiver preamplifiers. Overall system operation was verified prior to deployment of the underwater equipment.

3. VERTICAL INCIDENCE BACKSCATTER MEASUREMENTS

The acoustic measurement system and deployment conditions provided an opportunity to collect and analyze vertical incidence acoustic backscatter data from scatterers near the sea surface. The system frequencies coincide with resonance frequencies of microbubbles whose density and spatial distribution are of considerable interest. Acoustic measurements of near-surface microbubbles have been reported by several researchers using various techniques to estimate bubble densities; specific references will be cited in the following discussions.

In the present case, a pulse-echo acoustic technique was used wherein relatively narrow beams and short pulses allowed sampling of the near-surface volume. Backscattering from scatterers in volumes ranging from about 350 m^3 for 18 kHz and a 1 ms pulse to about 2.5 m^3 for 108 kHz and a 0.25 ms pulse were used to infer density of scatterers with very good resolution in the vertical dimension. In all cases mean values of volume backscattering were estimated from averages over an ensemble of pings. The start of sampled data in individual pings was not precisely controlled so that alignment in time was necessary in order that selected time windows represent echoes from water volumes at the same depth in each ping of the ensemble. This alignment was accomplished by thresholding on the gradient of the first echo return from the water surface (the first fathometer return) and using this event as a precise time reference.

While the quiescent volume scattering levels were relatively high at all operating frequencies, near-surface volume scatterers, when present, were clearly discernible on the measurement system B-scan display. Figure 3.1 is a print of the B-scan display for one example of vertical incidence backscattering and shows echo returns from two different transmit pulse types. Each set of echo returns represents beams 1-21 from left to right, while time or range increases from bottom to top. The lower part of the dark bands about half way to the top and extending across all beams represents the first returns from the water surface. The dark portions, which are relatively symmetric about the center beam and extending below the first surface return, represent concentrations of near-surface scatterers. Each set of echo returns represents a 'composite ping'
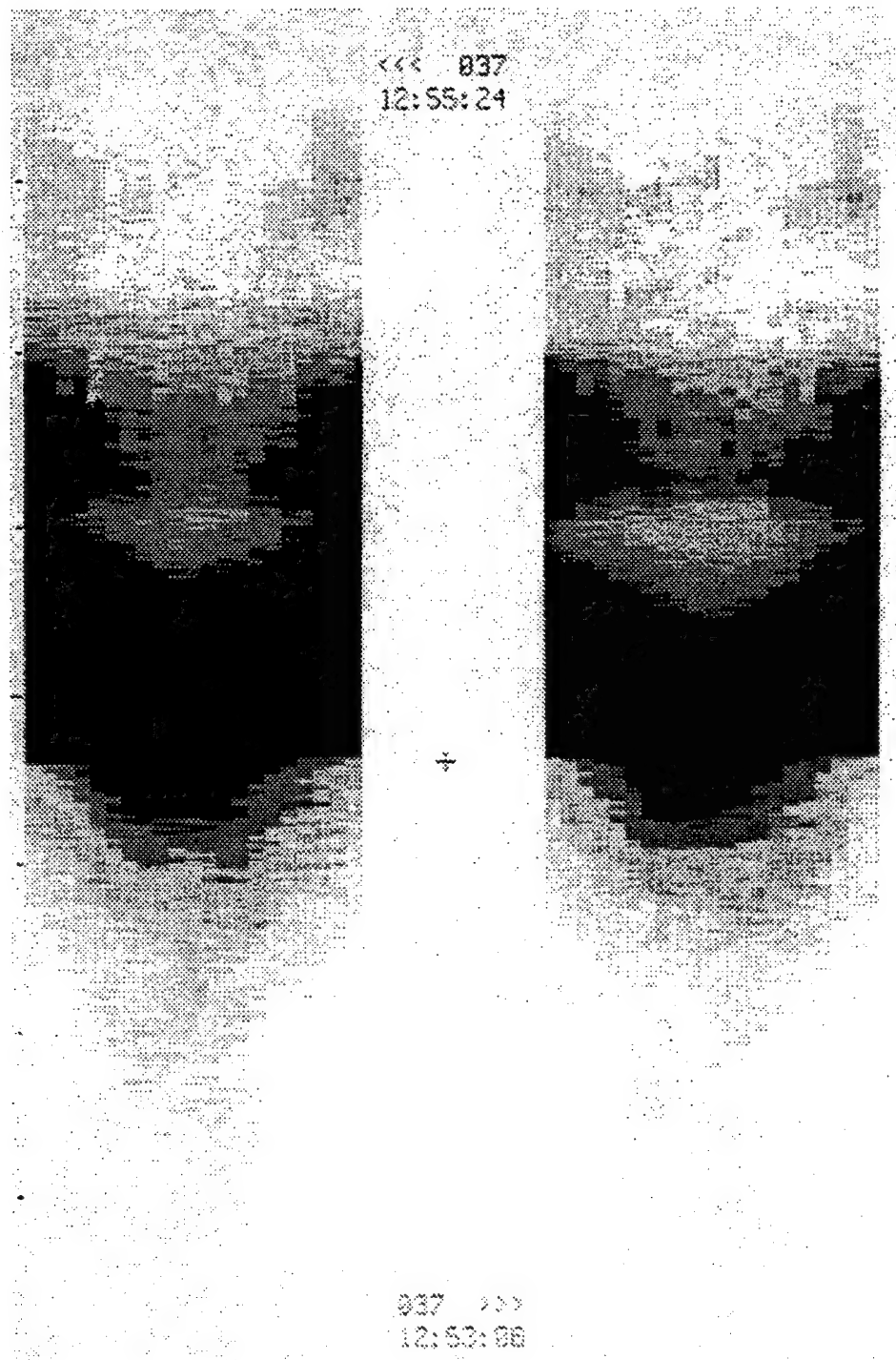
Figure 3.1
Acoustic measurement system example.

consisting of appropriately aligned and ensemble averaged pings of a particular pulse type; the two pulse types were transmitted alternately over a selected interval of time. The numbers at the bottom and top of the display represent the time codes (day:h:min:s) of the start time of the first ping and the last ping, respectively, which form the ping ensembles over the selected time interval.

3.1 VOLUME BACKSCATTER MEASUREMENTS

Within the measurement system analysis software, a target strength TS in dB is computed based upon the received level associated with volume backscatter from a region near the surface at a selected depth z. An analysis window equal to the transmit pulse length is used for all data analyses. The target strength TS and volume backscatter strength V_{bs} are related by

$$10 \log V_{bs} = TS \ (dB) - 10 \log \ (\text{scattering volume}) \ . \tag{3.1}$$

The scattering volume is approximated by a short right circular cylinder (i.e., a pillbox) whose base is determined by receive beamwidth and water depth, and whose height is determined by sound speed and transmit pulse length. Thus,

$$\text{scattering volume} = (\pi b^2)(c\tau/2) \ , \tag{3.2}$$

where $b = s \tan (\theta_r/2)$, s is the distance (in m) to the scattering volume, θ_r is the effective receive beamwidth (in deg), c is the sound speed (in m/s), and τ is the transmit pulse length (in s).

Table 3.1 includes the various data files which were analyzed in order to estimate backscattering strength from near-surface volume elements. The data files in this table are provided in three wind speed categories for each of the four frequencies. The wind speed is in m/s; wind direction is also indicated. The wind measurement system was located on shore and indicated wind speed in knots. Wind speeds were recorded and converted for presentation here by simply dividing wind speed in knots by a factor of 2. The actual conversion is wind speed (m/s) = wind speed (kt) × 0.5144 (Weast, 1979); however, the separation from the underwater equipment and the short term variability in wind speed does

Table 3.1
Vertical incidence backscatter data.

High Wind (> 9 m/s)		Medium Wind (6-9 m/s)		Low Wind (< 6 m/s)	
FILE	WIND (m/s)	FILE	WIND (m/s)	FILE	WIND (m/s)
F1: 108 kHz					
26F1	8-10 NW	17F1	6-8 ESE	42F1	3.5 SE
29F1	8-10 NW	42A1	6-9 SSE	38F1**	3-4.5 SE
10F1	9-10 ENE	14F1	7-9 ESE	18F1	5-6 SE
50F1P7	9-10 ENE				
49F1	9-12 NE				
9F1	11-12 ENE				
F2: 72 kHz					
30F2	8-9 NW	43F2	6-9 SSE	42F2	3.5 SE
27F2	8-10 NW			39F2**	4-4.5 SE
11F2	9-10 ENE			20F2**	5-6 SE
50F2P7	9-11 NE				
22F2W1	9-11 E				
49F2	9-12 NE				
5F2	11-12 ENE				
F3: 36 kHz					
30F3	8-10 NW	43F3	5.5-7.5 SSE	40F3**	2.5-4 SSE
12F3	9-10 ENE	16F3	6-8 ESE	42A3	3.5 SE
28F3	9-10 NW	55F3	7.5-8 SSE	42F3	3.5 SE
22F3W1	9-11 SE			4F3	5 W
50F3P6	9-11 NE			19F3	5-6 SE
50F3P7	9-11 NE				
6F3	11-12 E				
F4: 18 kHz					
31F4	8-10 NW	44F4	5.5-7.5 SSE	40F4**	2.5-4 SE
13F4	9-10 ENE	16F4	6-8 ESE	42F4	3.5 SE
28F4	9-10 NW	55F4	7.5-8 SSE	4F4	5 W
22F4W1	9-11 E	8F4	7.5-9 ENE	19F4**	5-6 SE
50F4P6	9-11 NE				
50F4P7	9-11 NE				
33F4	10-12 E				

** No discernible backscatter

12

not warrant more precise conversion. The measurement height was about 3.5 m and has not been converted to the more customary 10 m height.

Volume backscattering strength versus depth for selected wind regimes is shown in Figs. 3.2 - 3.10; volume backscatter for each frequency is presented when available for each wind speed/wind direction. In each figure the data represent measurements under the same sea state condition, usually within a time interval of several minutes to an hour.

In some cases a sharp decrease in volume backscatter with depth occurred near the surface, followed by a more gradual decrease with depth; comparable behavior was noted by McConnell and Dahl (1991) and is consistent with a two-layer distribution of near-surface scatterers. In Fig. 3.2, representing a low wind speed condition, the volume backscatter is relatively low, consistent with the observation by others that significant near-surface bubble production begins to occur at wind speeds of about 2-3 m/s. In this figure it is also noted that volume backscatter is significantly higher at 72 kHz than at higher or lower frequencies; this trend was fairly consistent at higher wind speeds as well.

The volume backscattering strength represented in Fig. 3.3 for wind speeds of 5-6 m/s is anomalously low at all frequencies. In addition, no volume backscattering above the residual or quiescent level was observable at 72 kHz or 18 kHz at the highest system gain for data files taken during this wind condition. On this occasion the wind speed was diminishing and had been blowing from the east or southeast for more than 24 h. Near-surface volume backscatter from two additional data files at 18 and 36 kHz with wind from the west is also quite low. However, this wind condition persisted for only a few hours and the proximity to land might have partially sheltered the sea surface.

Thorpe (1986) reported acoustic measurements in the form of volume backscattering strength versus depth using an inverted echo sounder operating at 248 kHz. These measurements were made with the transducer pointed upward and suspended at a depth of about 37 m below the sea surface. Two
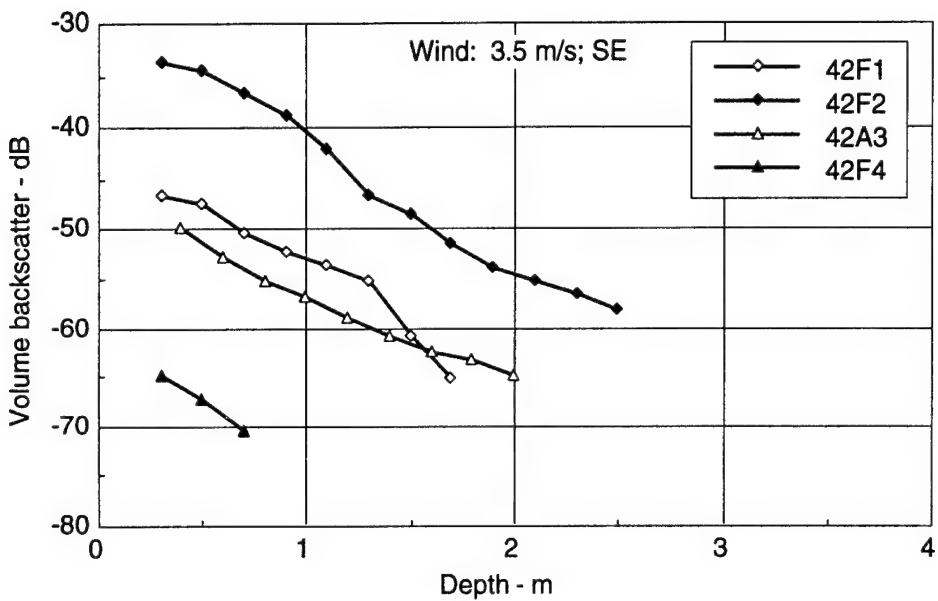
Figure 3.2
Vertical incidence volume backscatter
versus depth (wind speed = 3 .5 m/s).

14
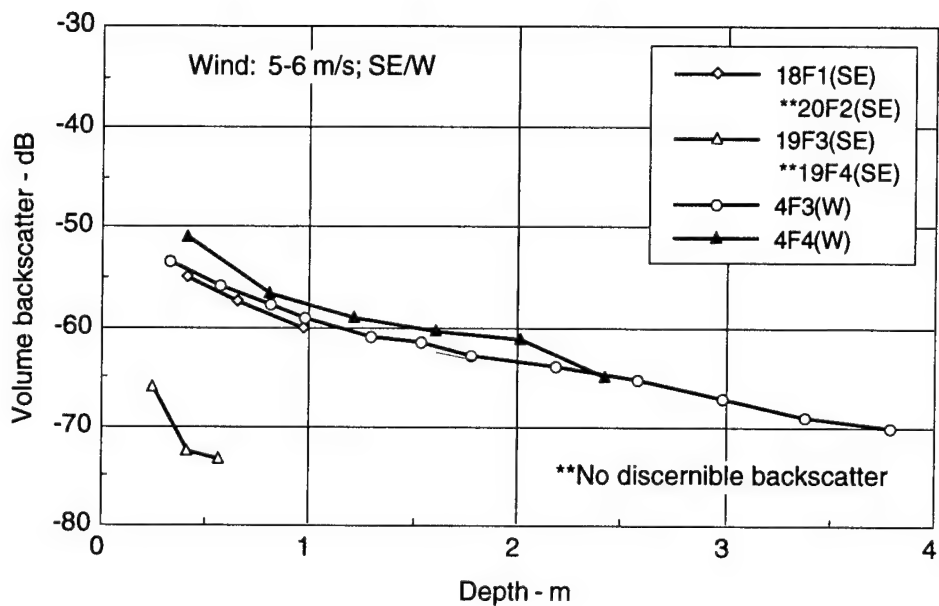
Figure 3.3
Vertical incidence volume backscatter
versus depth (wind speed = 5-6 m/s).

15
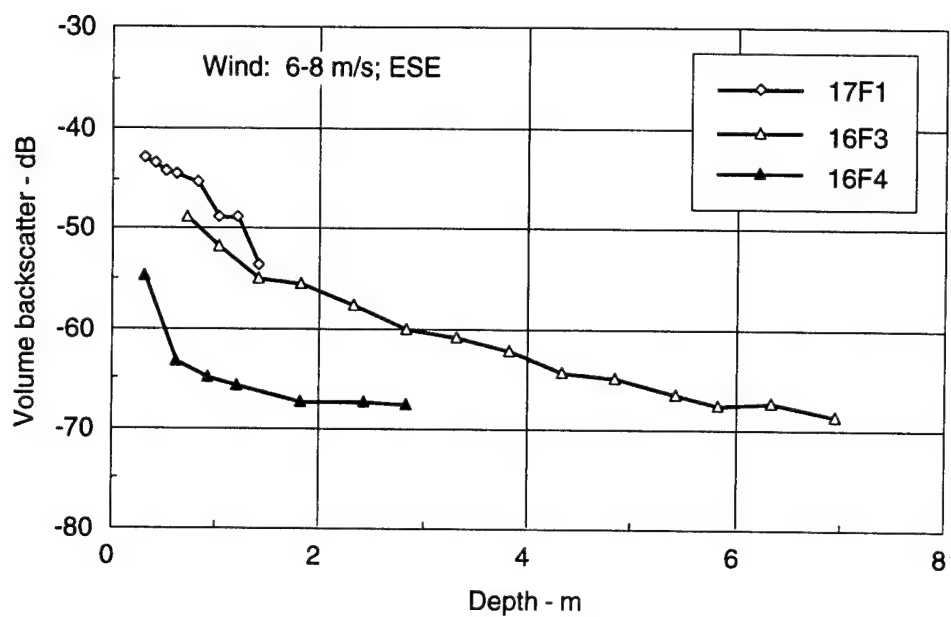
Figure 3.4
Vertical incidence volume backscatter
versus depth (wind speed = 6-8 m/s).

16
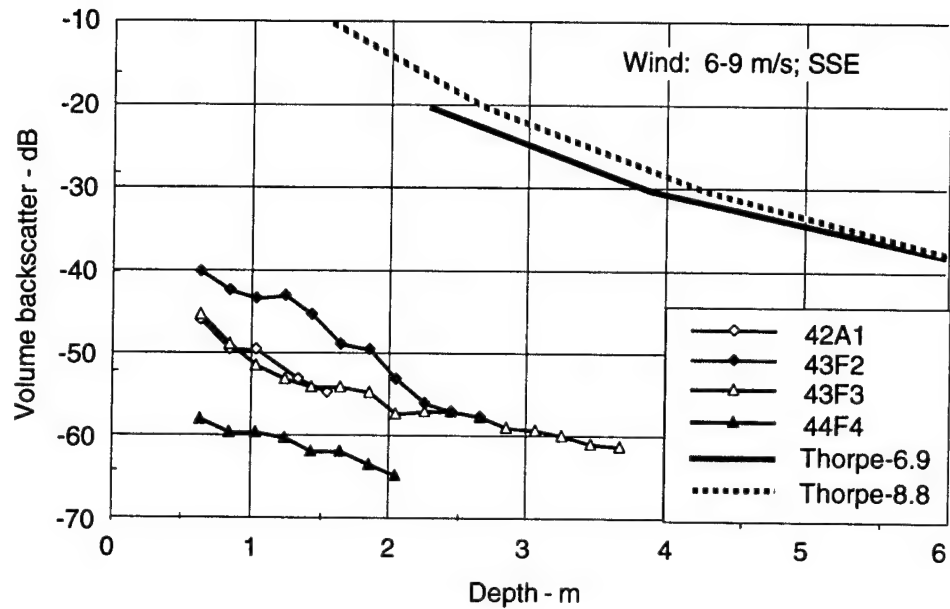
**Figure 3.5
Vertical incidence volume backscatter
versus depth (wind speed = 6-9 m/s).**
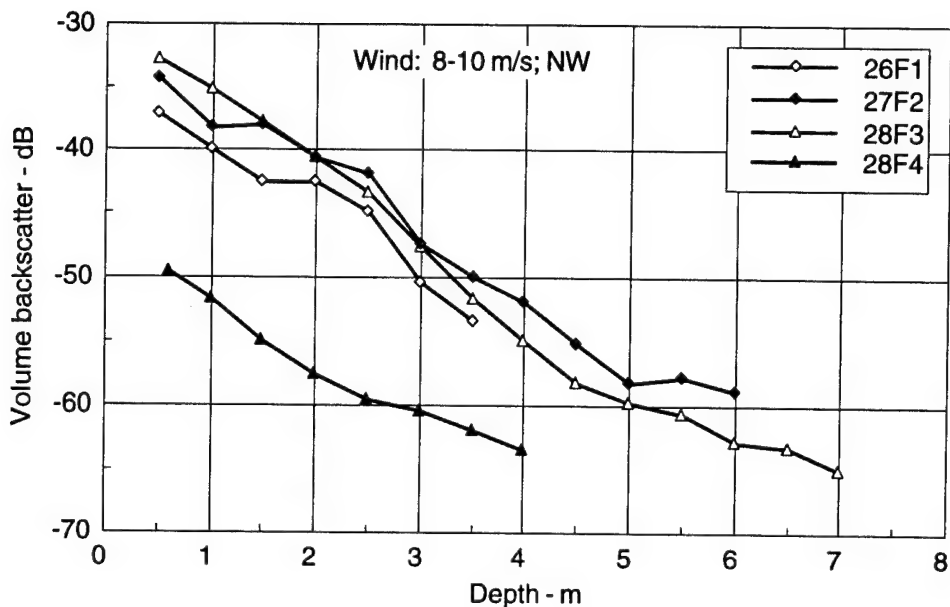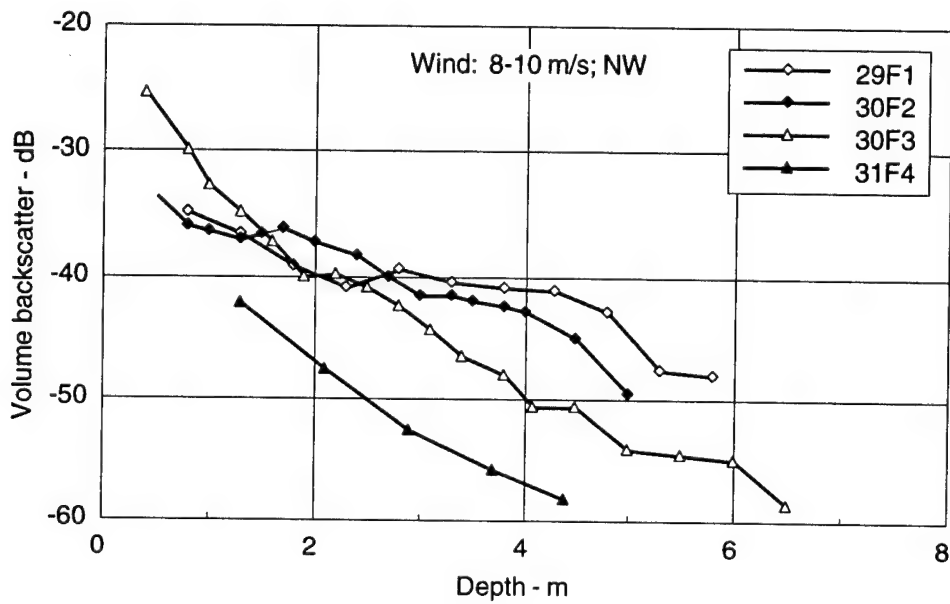
Figure 3.6
Vertical incidence volume backscatter
versus depth (wind speed = 8-10 m/s).

18
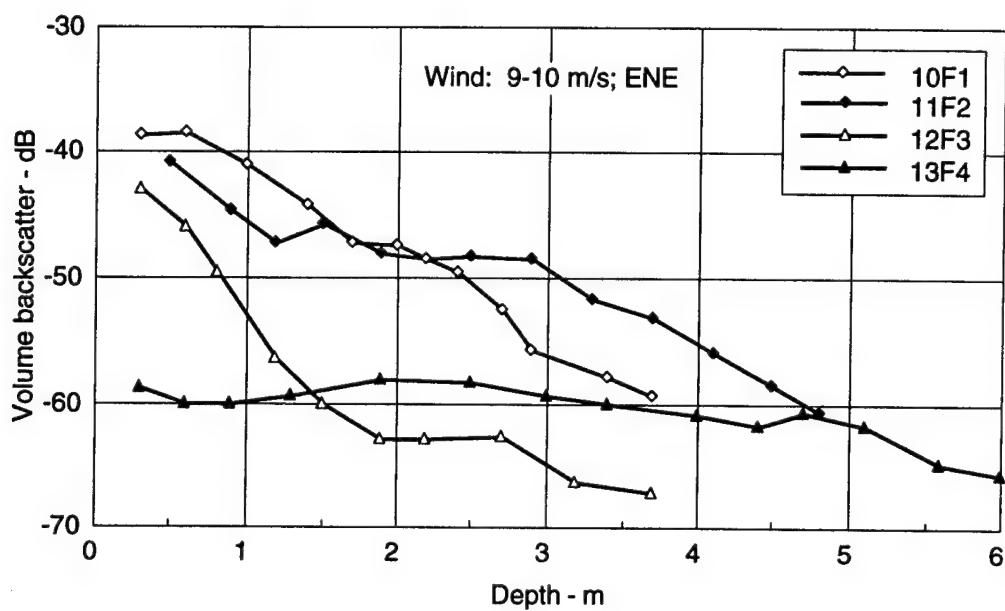
Figure 3.7
Vertical incidence volume backscatter
versus depth (wind speed = 9-10 m/s).
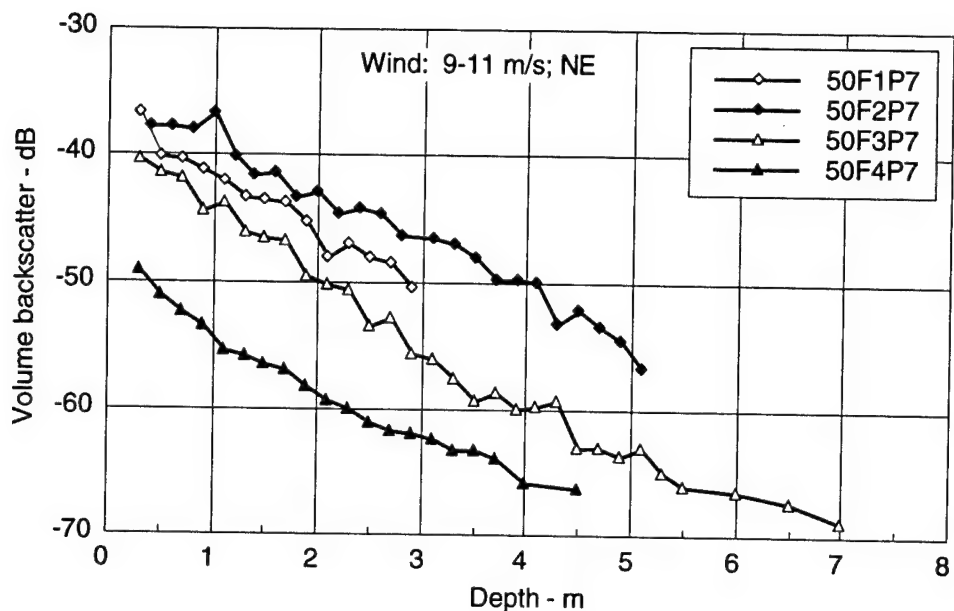
(a)
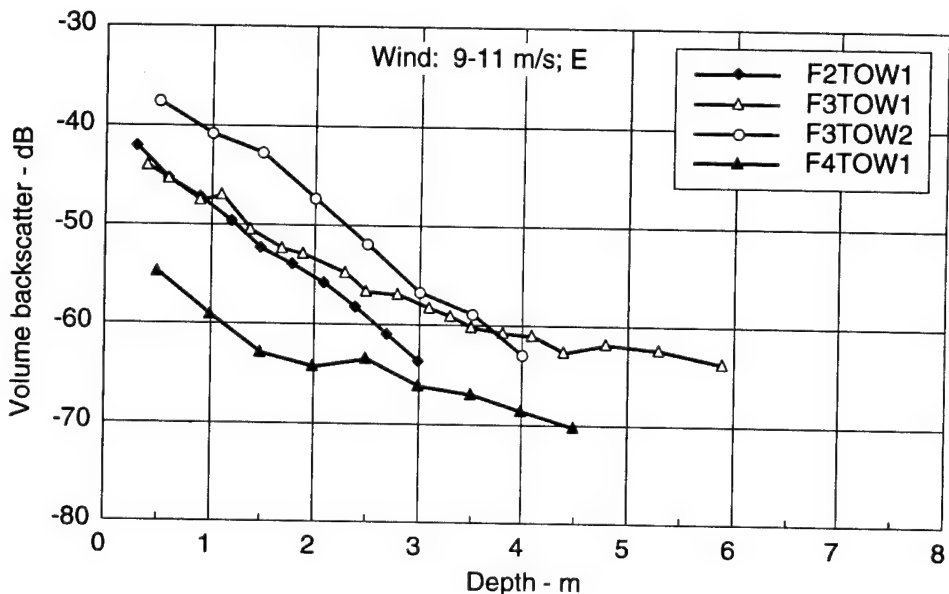
(b)

Figure 3.8
Vertical incidence volume backscatter
versus depth (wind speed = 9-11 m/s).
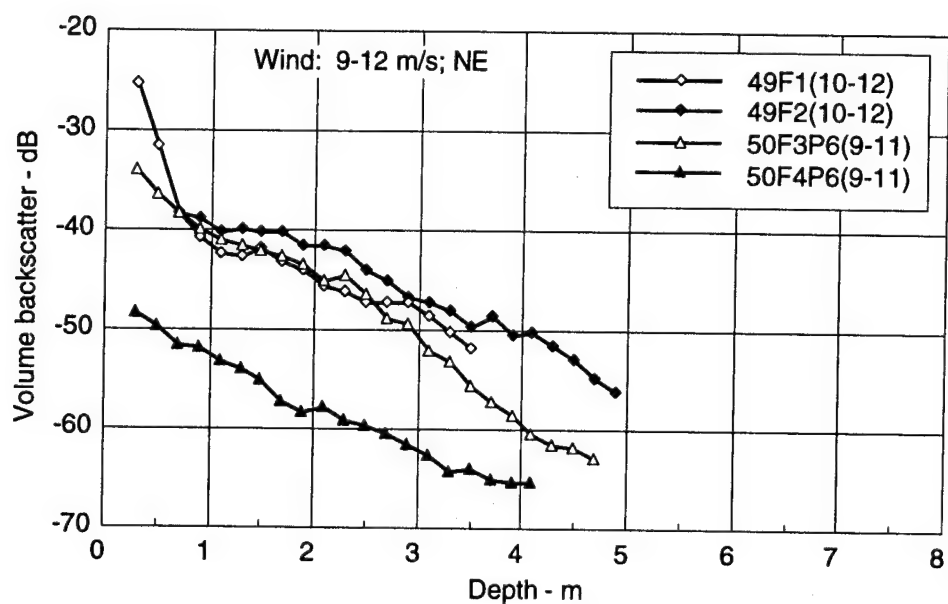
Figure 3.9
Vertical incidence volume backscatter
**versus depth (wind speed = 9-12 m/s).**

21
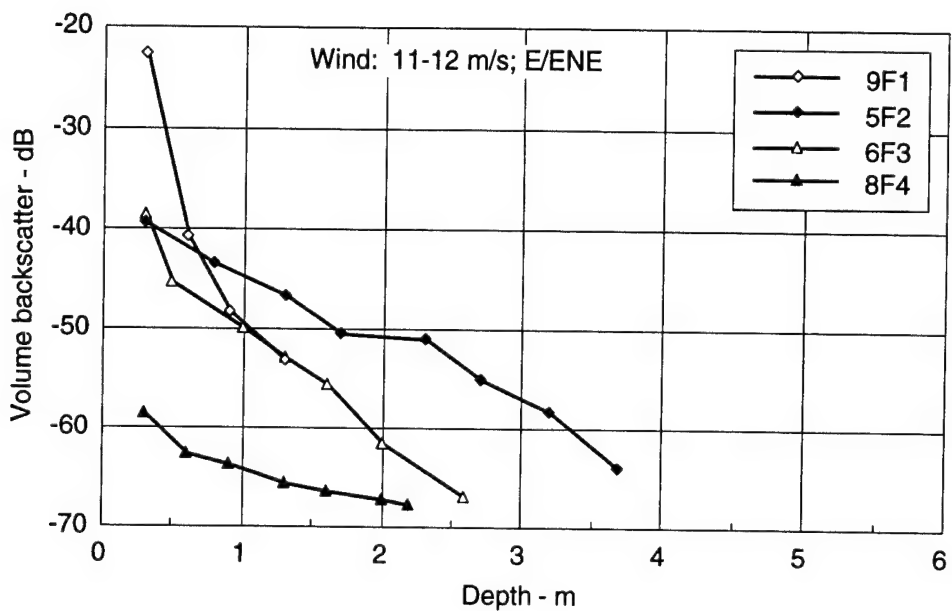
**Figure 3.10
Vertical incidence volume backscatter
versus depth (wind speed = 11-12 m/s).**

22

sets of measurements are compared with current measurement results in Fig. 3.5. The current measurements are significantly lower for all frequencies than those reported by Thorpe. Other comparisons can be made by estimating the integrated volume scattering strength (McConnell and Dahl, 1991), bubble density versus depth (Medwin, 1970; Løvik, 1980; Schippers, 1980; Dalen and Løvik, 1981; Crawford and Farmer, 1987), and bubble density versus bubble radius (Medwin, 1977a; Medwin and Breitz, 1989; Farmer and Vagel, 1989). Such comparisons will be made in subsequent sections.

3.2 INTEGRATED VOLUME SCATTERING

The integrated volume backscattering strength is a simplified comparative parameter in that a single number is used to represent near-surface backscattering for each measurement trial. The simplification derives from the scatterer distribution being modeled as a near-surface layer whose density decreases exponentially with depth. When the volume backscatter versus depth behavior follows a single exponential, the integrated volume backscattering strength can be written as

$$(V_{bs})_I = (V_{bs})_o \int \exp(-z/z_o) \, dz \quad , \tag{3.3}$$

where $(V_{bs})_o$ is the volume backscattering strength extrapolated to the surface and z_o is an e-folding depth characterizing the exponential depth dependence of scatterer density. The integral is evaluated from zero to infinity with the result that $(V_{bs})_I = (V_{bs})_o \, z_o$. Both $(V_{bs})_o$ and z_o can be determined from fitting an exponential curve to measured volume backscattering versus depth plots.

A correction for attenuation by the bubble distribution may be necessary and can be written as (Medwin, 1977b; McConnell and Dahl, 1991)

$$SBL(dB) = 8026 \, \delta \, (V_{bs})_o \, z_o \quad , \tag{3.4}$$

where δ is the total bubble damping coefficient given by

$$\delta = 2.55 \times 10^{-3} \, f^{1/3} \quad , \tag{3.5}$$

where f is in Hz, as a fit by McConnell and Dahl to data reported by Devin (1959). Table 3.2 shows the estimated values of $(V_{bs})_I$ in dB and SBL(dB) for the vertical incidence backscatter measurements reported here. The estimated surface bubble loss does not appear to be a significant factor in these vertical incidence measurements, nor is it expected to be.

The integrated volume scattering strength versus frequency is presented in Fig. 3.11(a) for low to medium wind speeds and in Fig. 3.11(b) for higher wind speeds. The paucity of data at the lower wind speeds and the anomalous behavior of the measurements at 5-6 m/s wind speeds, as mentioned earlier, fail to provide a reliable trend. The integrated volume scattering strength of the higher wind speed data increases with increasing frequency, at least over a portion of the frequency range, but exhibits considerable variability. Measurements reported by McConnell and Dahl (1991) under similar wind speed conditions have been included for comparison. The two data sets are generally comparable in level and trend but less supportive than might be desired, with significant variability evident in both sets of measurements. A comparison of the same data sets representing integrated volume backscattering strength versus wind speed with frequency as a parameter is shown in Fig. 3.12(a) and (b). In this figure both data sets indicate increased backscattering for increasing wind speed.

3.3 BUBBLE DENSITY versus DEPTH

The inversion of volume backscattering measurements follows that of Medwin (1977a) wherein scattering from a near-surface bubble layer is described by the expression

$$V_{ex} = \int (\sigma_a + \sigma_s)\, n(a)\, da \quad , \tag{3.6}$$

where V_{ex} is the volume extinction resulting from bubbles with absorption and scattering cross-sections σ_a and σ_s, respectively, and $n(a)da$ is the bubble density in an increment of bubble radius da. With several simplifying assumptions, the above expression can be written as

$$V_{ex} = 2\pi^2 (a_R{}^3/\delta_R)\, N(a_R) \quad , \tag{3.7}$$

24

Table 3.2
Integrated volume backscatter and
surface bubble loss.

High Wind (> 9 m/s)			Medium Wind (6-9 m/s)			Low Wind (< 6 m/s)		
FILE	$(V_{bs})_I$ (dB)	SBL (dB)	FILE	$(V_{bs})_I$ (dB)	SBL (dB)	FILE	$(V_{bs})_I$ (dB)	SBL (dB)
F1: 108 kHz								
26F1	-34.8	0.3	17F1	-42.7	0.05	42F1	-46.1	0.02
29F1	-30.9	0.8	42A1	-46.1	0.02	38F1**	xxx	xxx
10F1	-36.8	0.2	14F1	-39.5	0.1	18F1	-53.8	0.0
50F1P7	-37.1	0.2						
49F1	-33.3	0.5						
9F1	-26.8	2.0						
F2: 72 kHz								
30F2	-30.6	0.7	43F2	-38.9	0.1	42F2	-33.7	0.4
27F2	-32.4	0.5				39F2**	xxx	xxx
11F2	-39.5	0.1				20F2**	xxx	xxx
50F2P7	-34.7	0.3						
22F2W1	-42.9	0.04						
49F2	-34.0	0.3						
5F2	-39.7	0.09						
F3: 36 kHz								
30F3	-28.7	0.9	43F3	-47.4	0.01	40F3**	xxx	xxx
12F3	-47.2	0.01	16F3	-48.5	0.0	42A3	-50.6	0.0
28F3	-32.0	0.4	55F3	-44.2	0.03	4F3	-53.3	0.0
22F3W1	-44.5	0.02				19F3	-67.9	0.0
50F3P6	-34.2	0.3						
50F3P7	-40.7	0.05						
6F3	-41.9	0.04						
F4: 18 kHz								
31F4	-37.1	0.1	44F4	-56.4	0.0	40F4**	xxx	xxx
13F4	-51.1	0.0	16F4	-58.7	0.0	42F4	-65.7	0.0
28F4	-48.0	0.0	55F4	-54.7	0.0	4F4	-51.0	0.0
22F4W1	-54.6	0.0	8F4	-59.1	0.0	19F4**	xxx	xxx
50F4P6	-48.4	0.0						
50F4P7	-49.8	0.0						
33F4	-43.7	0.02						

** No discernible backscatter
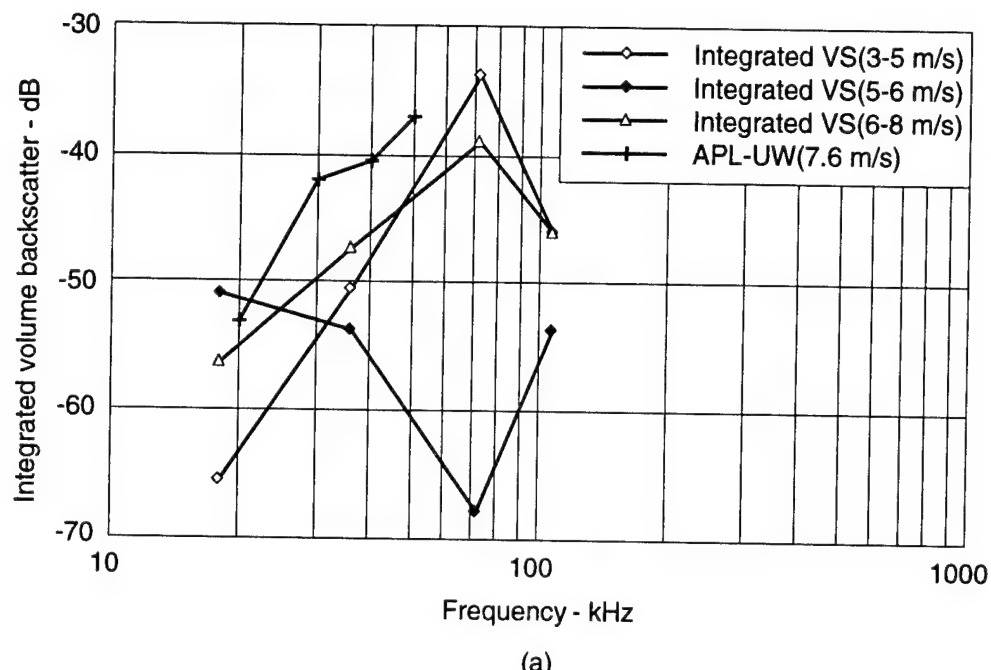
(a)
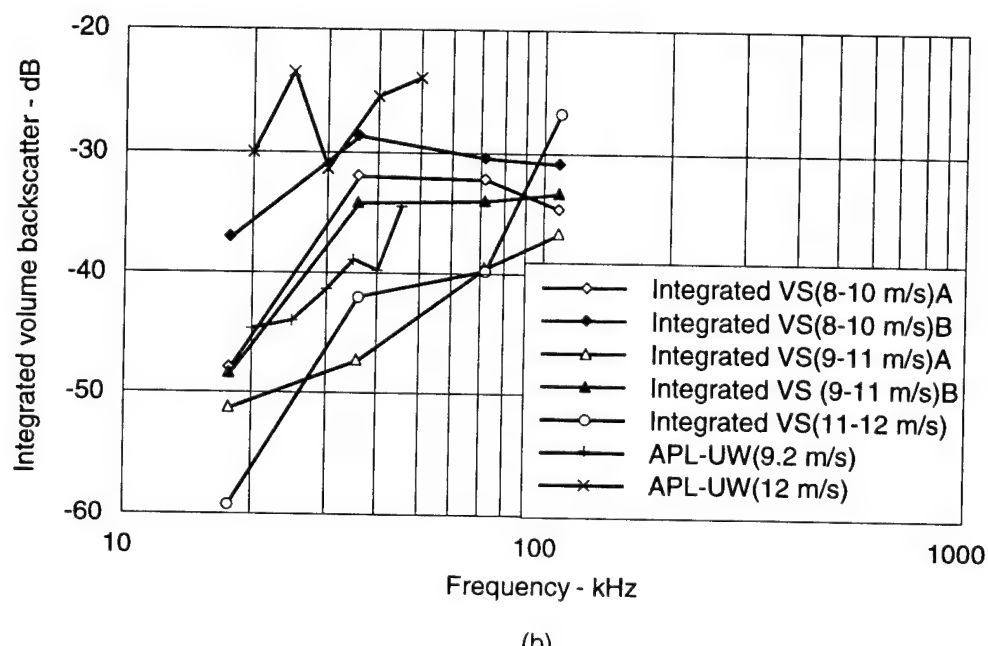
(b)

Figure 3.11
Integrated volume backscatter
versus frequency for various wind speeds.

26
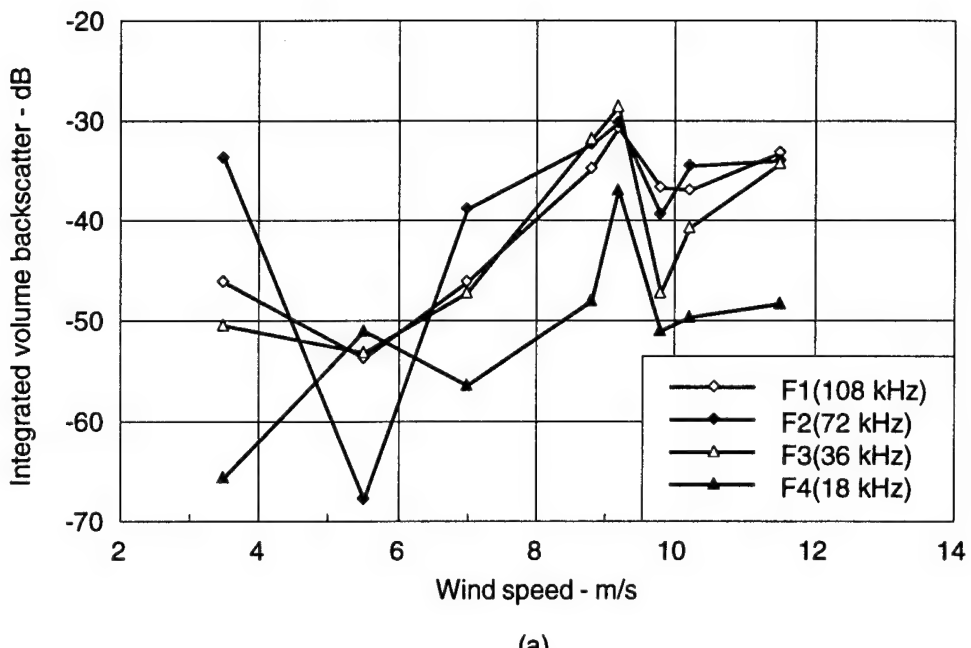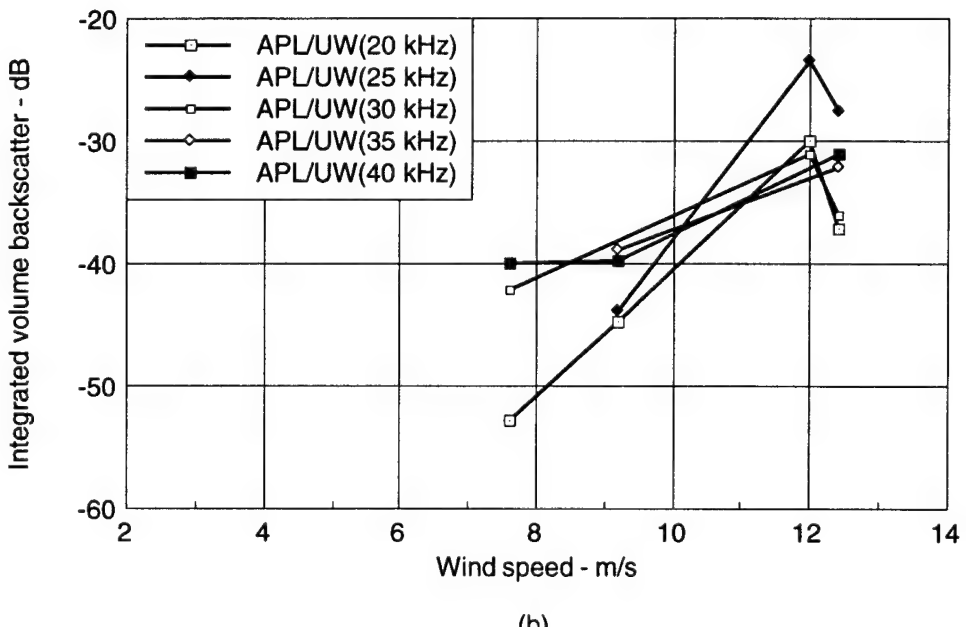
Figure 3.12
Integrated volume backscatter versus wind speed
for each of the measurement frequencies.

27

where a_R is the resonant bubble radius (in m) related to frequency f (in kHz) and depth z (in m) by

$$a_R = [3.25 \times 10^{-3}/f][1 + 0.1z]^{1/2} \text{ (m)} \quad . \tag{3.8}$$

The bubble radiation damping coefficient $\delta_R = 0.0136$, and $N(a_R)$ is the near-resonant bubble density contributing to volume extinction. Since backscatter is the measured quantity in the pulse-echo technique, we substitute $V_{bs}=(V_{ex}/4\pi)(\delta_r/\delta)$, so that

$$V_{bs} = (\pi/2)\,(a_R^3/\delta)\,N(a_R) \quad . \tag{3.9}$$

This simplified expression will be used to relate measured volume backscattering strength to estimates of bubble densities.

The quantity most often represented in the literature is resonant bubble density in a 1 μm range of bubble radius and not $N(a_R)$ directly (e.g., Medwin, 1977c; Løvik, 1980; Schippers, 1980). For a constant frequency, we will assume that near-resonant bubbles in a frequency band determined by δ (i.e., $\delta=\Delta f/f_R$) will contribute to backscattering. Additionally, near-resonant bubbles in a frequency band determined by the transmit pulse spectrum (i.e., $b=\Delta f/f_c$) will contribute to backscattering. Thus, the resonant bubble density in a 1 μm range of bubble radius, $n(a_R)da_R$, will be represented in the following discussions as

$$n(a_R)da_R = N(a_R)[(\delta+b)a_R]^{-1} \quad , \tag{3.10}$$

where a_R in the denominator of the right side is in μm.

Bubble density versus depth estimated from near-surface volume backscatter measurements are shown in Figs. 3.13 - 3.17 for various wind conditions. In Fig. 3.13(a) bubble densities for a low wind speed condition are shown along with the bubble density equivalent of measured receiver noise level for each of the four frequencies. The bubble density estimates shown in Fig. 3.13(a) are comfortably above the equivalent noise floors at all frequencies. The noise levels for this data set correspond to measurements made following a retrieval, repair, and redeployment of the in-water acoustic measurement

28
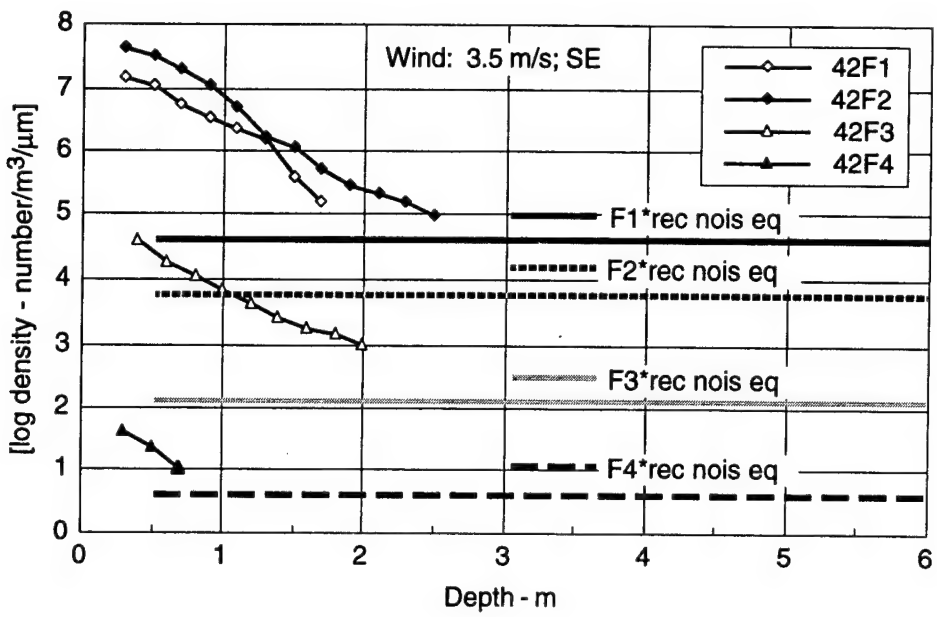
(a)
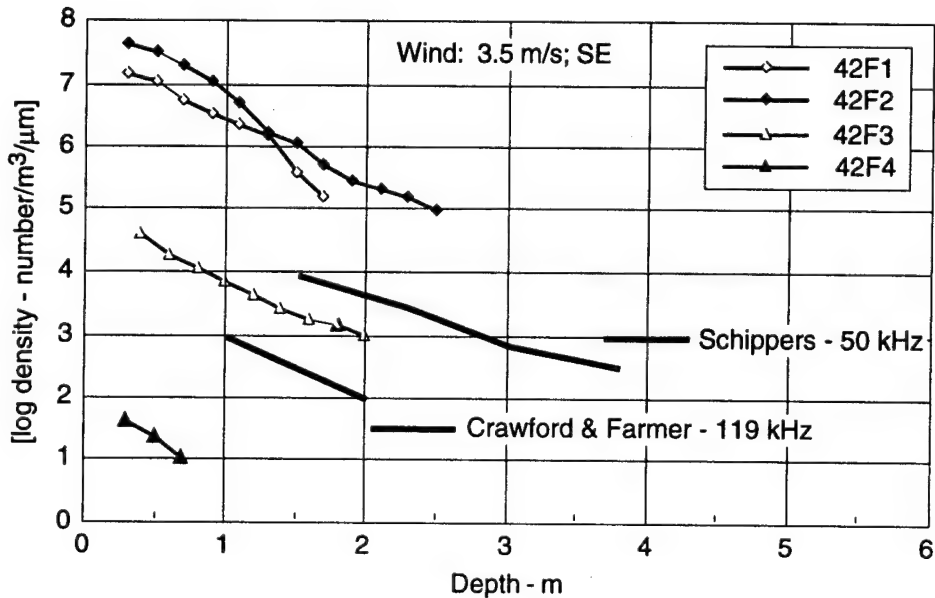
(b)

Figure 3.13
Bubble density versus depth estimated from
near-surface volume backscatter (wind speed = 3.5 m/s).
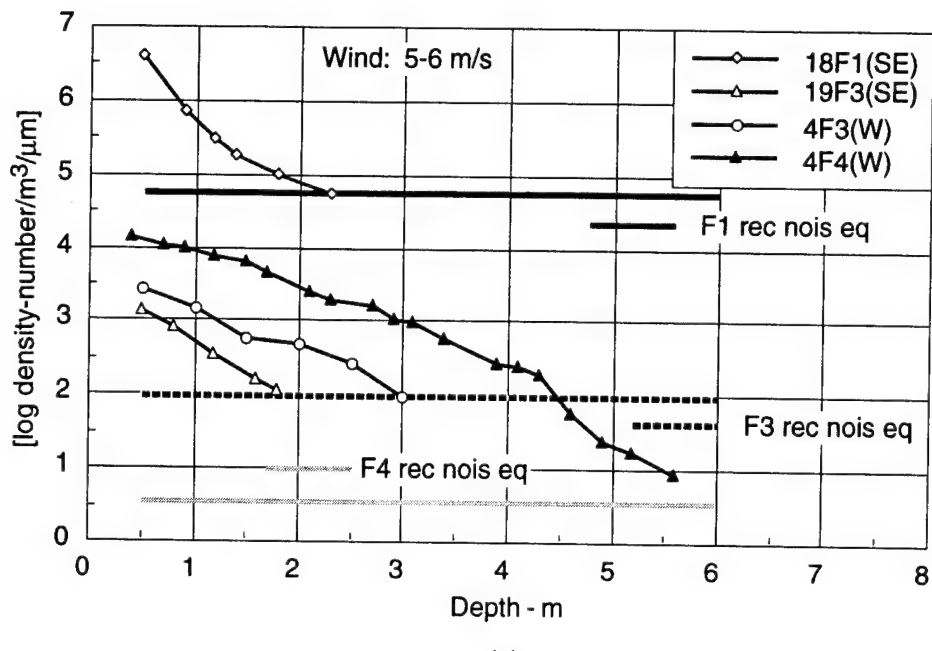
(a)
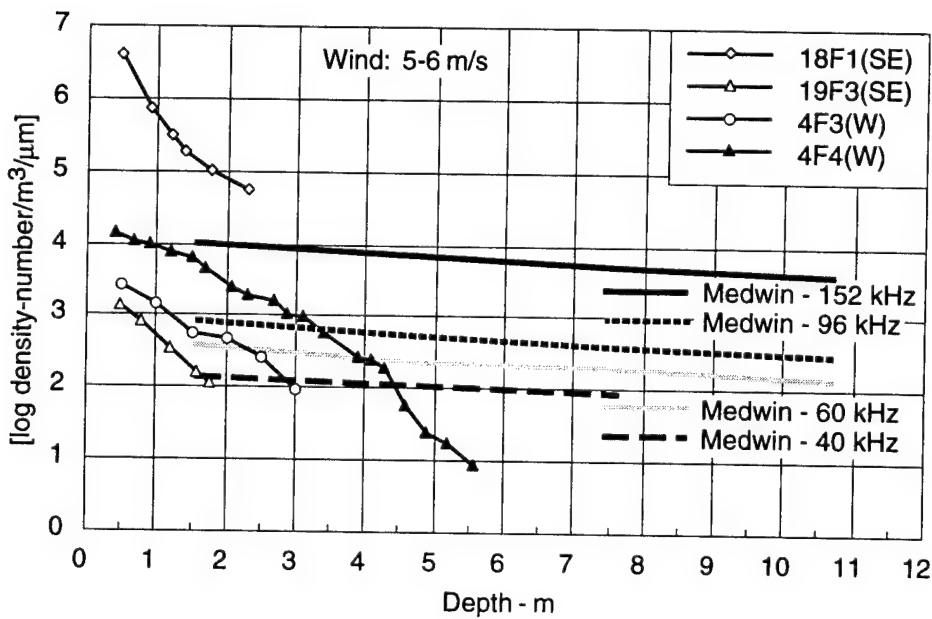
(b)

Figure 3.14
Bubble density versus depth estimated from
near-surface volume backscatter (wind speed = 5-6 m/s).

30
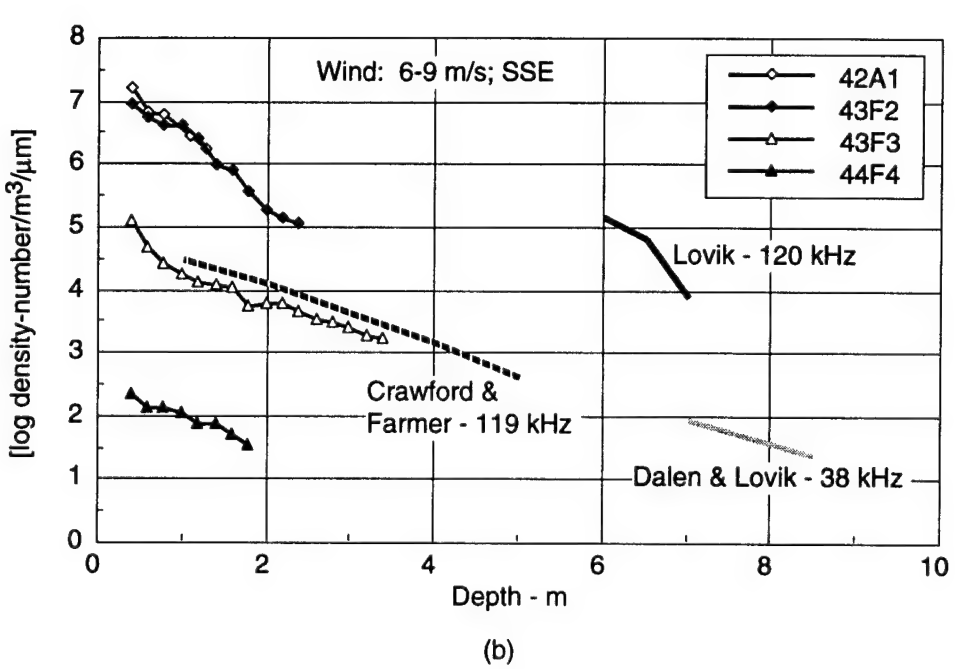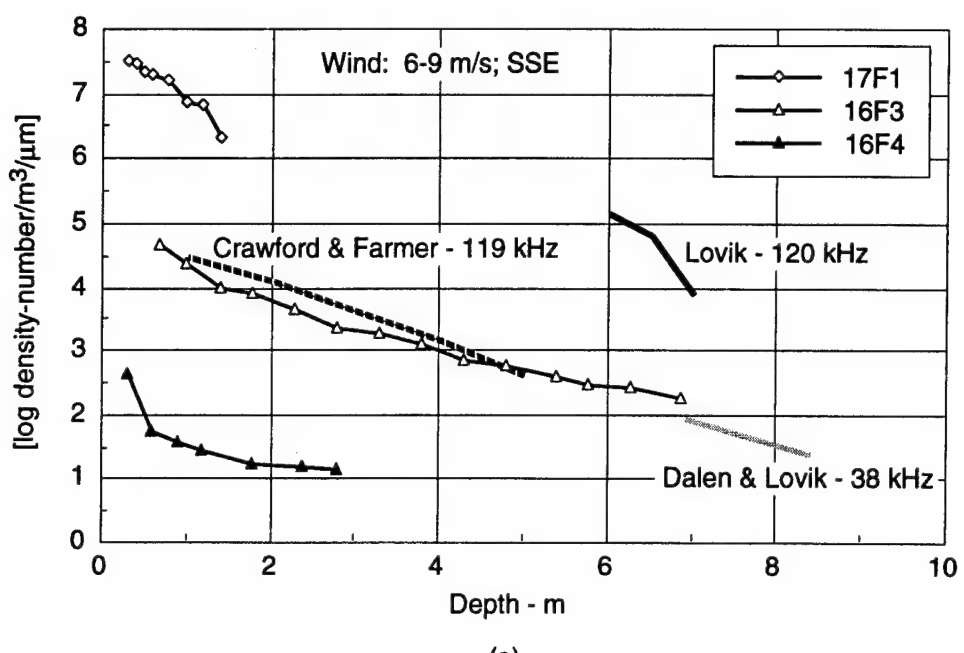
Figure 3.15
Bubble density versus depth estimated from
near-surface volume backscatter (wind speed = 6-9 m/s).
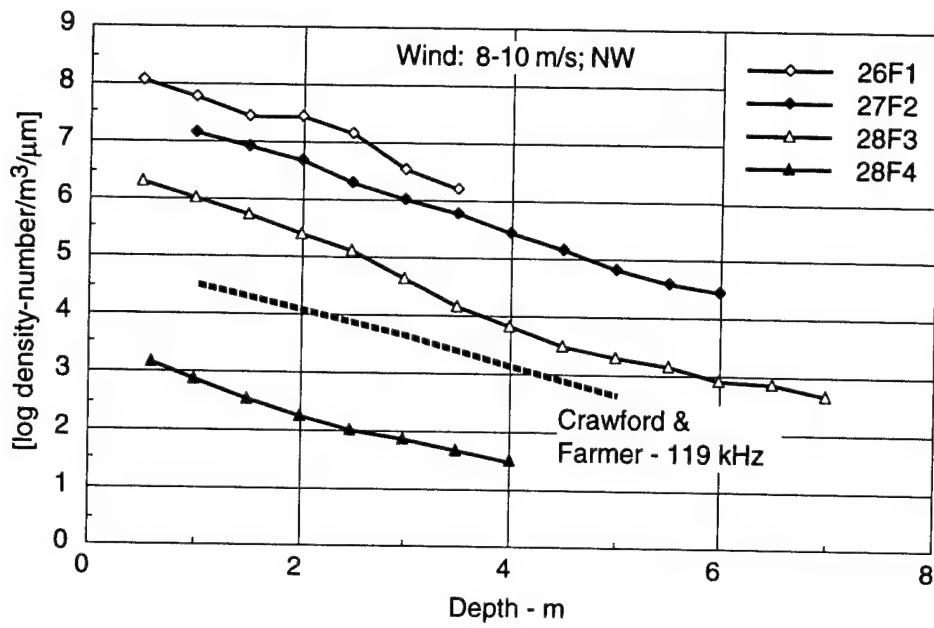
(a)
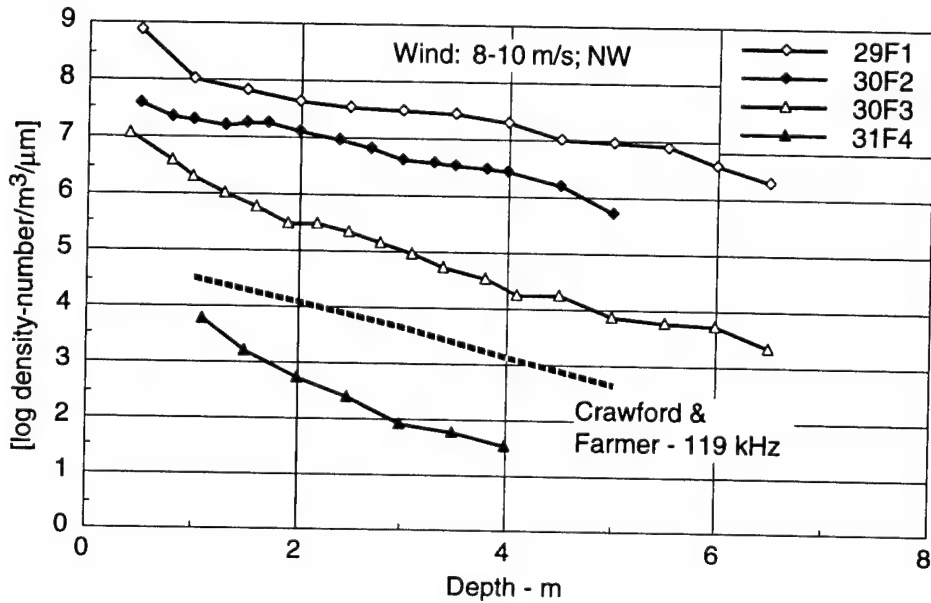
(b)

Figure 3.16
Bubble density versus depth estimated from
near-surface volume backscatter (wind speed = 8-10 m/s).

32
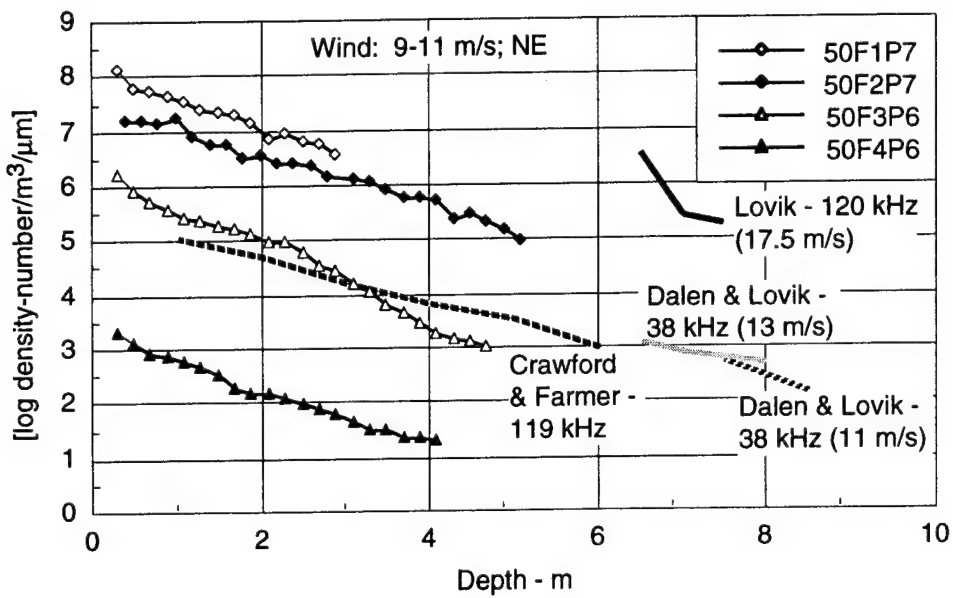
Figure 3.17
Bubble density versus depth estimated from
near surface volume backscatter (wind speed = 9-12 m/s).

equipment; the system electronic noise levels were significantly improved during the repair process.* Receiver noise levels as measured here are determined by a relatively constant (with depth) quiescent volume backscatter (as well as possibly ambient and system noise contributions). The receiver noise levels determine a lower limit of near-surface volume backscatter measurements and are appropriate for data comparisons.

An additional data set at low wind speed for all four frequencies was analyzed in an attempt to augment bubble density estimates. This additional data set is shown in Table 3.2 as data files 38F1, 39F2, 40F3, and 40F4 at wind speeds of 2.5-4 m/s; however, no near-surface backscattering was discernible. Only upper limits for bubble densities corresponding to the quiescent volume backscatter equivalent (i.e., measured receiver noise) associated with each frequency can be determined for this data set.

In Fig. 3.13(b) the bubble density estimates shown in Fig. 3.13(a) are compared with those reported by Schippers (1980) and by Crawford and Farmer (1987). Schipper's measurements were made in the North Sea at 50 kHz under sea state 1 conditions, and used a bottom mounted, pulse-echo transducer pointed upward in 18 m water depth. Crawford and Farmer used an upward looking acoustic transducer mounted on the upper deck of the submarine USS DOLPHIN (AGSS 555) operating near Monterey, California. Bubble density versus depth estimates were reported for 119 kHz and wind speeds of 3, 7, and 11 m/s. The bubble density estimates from current measurements at 36 kHz are comparable with the results of Schippers and Crawford and Farmer, but are significantly greater at the higher frequencies. [Note: Even the highest bubble density estimate shown here, at 72 kHz, corresponds to a near-surface bubble volume fraction of less than 0.04%.]

In Fig. 3.14 bubble estimates are shown at 36 and 108 kHz for wind speeds of 5-6 m/s from the southeast and at 18 and 36 kHz for a wind speed of 5 m/s from the west. Since near-surface volume backscatter appears to be anomalous for these wind conditions, the receiver noise floor was determined for

---

* Data files beginning with No. 37 and higher correspond to this redeployment.

34

each frequency and converted to an equivalent bubble density estimate.[*] A comparison of estimated bubble density with receiver noise equivalent density is shown for each frequency in Fig. 3.14(a). The measured receiver noise for these data files is essentially the same as that shown in Fig. 3.13(a), and is consistent with domination by volume backscatter of -70 to -75 dB/m^3 in both instances. In those cases for which near-surface scatterers were clearly discernible (on the measurement system display), the estimated densities near the surface were substantially above the equivalent receiver noise densities. For those cases in which no near-surface scatterers were discernible, bubble densities can only be estimated as being lower than the equivalent noise density values.

Observed bubble densities are compared with density estimates reported by Medwin (1970) in Fig. 3.14(b). Medwin's acoustic measurements were made in 60 ft water depth near Mission Bay (San Diego), California, at several frequencies and under sea state 1 surface conditions. The measurements reported here for the southeast wind condition resulted in backscattering above the system noise limits only from scatterers very near the surface and only at the two frequencies shown. The bubble density estimates at both frequencies show a strong decrease with increasing depth. The density estimates for 36 kHz data for both wind directions, and for 18 kHz data for the westerly wind condition, are comparable with values reported by Medwin; however, the decrease with depth is much greater in the present data. The bubble density estimates shown here for 108 kHz data are considerably higher than estimates reported by Medwin. Again, there appears to be a sharper decrease with depth in the current data.

Bubble densities at intermediate wind speeds are shown in Figs. 3.15 - 3.17 and compared with estimates reported by Løvik (1980), Dalen and Løvik (1981), and Crawford and Farmer (1987). The measurements reported by Løvik and by Dalen and Løvik used depth sounders at three different frequencies operated from a surface research vessel. The mean depth and receiver electronic recovery time following a transmission for the depth sounders prevented measurements being made at very shallow depths. The measurements reported by Crawford and Farmer used the equipment described earlier.

---

[*] All the subject data files were acquired prior to the improvements made in system electronic noise floor mentioned above.

The current measurements at 72 and 108 kHz do not reveal significant depth dependent scatterers extending to depths reported by Løvik for 120 kHz; however, the current measurements at 36 kHz are comparable with densities at 38 kHz reported by Dalen and Løvik and at 119 kHz reported by Crawford and Farmer, as shown in Fig. 3.15. The current estimated densities at 72 and 108 kHz are significantly higher than those reported by Crawford and Farmer at 119 kHz. The density estimates at 18 kHz are considerably lower than the reported values shown in Fig. 3.15. This trend extends over the range of wind speeds encountered, as shown in Figs. 3.15 - 3.17.

3.4 BUBBLE DENSITY versus BUBBLE RADIUS

The estimated bubble densities versus bubble radius from current measurements are shown in Fig. 3.18 for a sample depth of 1 m and various wind speeds. There is no distinct trend with wind speed indicated by these measurement results. Estimates from three of the higher wind speed data files are compared with results reported by Medwin and Breitz (1994) in Fig. 3.18(b). The measurements made by Medwin and Breitz employed a floating acoustic resonator with a sample depth of 25 cm. The densities estimated from current measurements are considerably higher than those determined by Medwin and Breitz; the rate of decrease in density with increasing bubble radius is much higher also. If one considers that $n(a_R)=n_o a_R^{-m}$, the current data provide a value of m=5.8 with a standard deviation of 0.8 from averaging the slopes over all wind speeds. This compares with about m=2.7 for the Medwin and Breitz data.

The estimated bubble density versus bubble radius from current measurements at 4 m depth are compared with results reported by Medwin (1977b) and by Farmer and Vagle (1989) in Fig. 3.19. The results by Medwin in Fig. 3.19(a) are also at 4 m depth while those by Farmer and Vagle in Fig. 3.19(b) are at 3 m depth. The current results are somewhat higher than Medwin's, but were also obtained at somewhat higher wind speeds. The mean slope at this sample depth was m=6.9 with a standard deviation of 1.1. This is higher than that of the overall slope of Medwin's curves (about 3.5), but less so and more comparable with the slope for the smaller bubble radii.
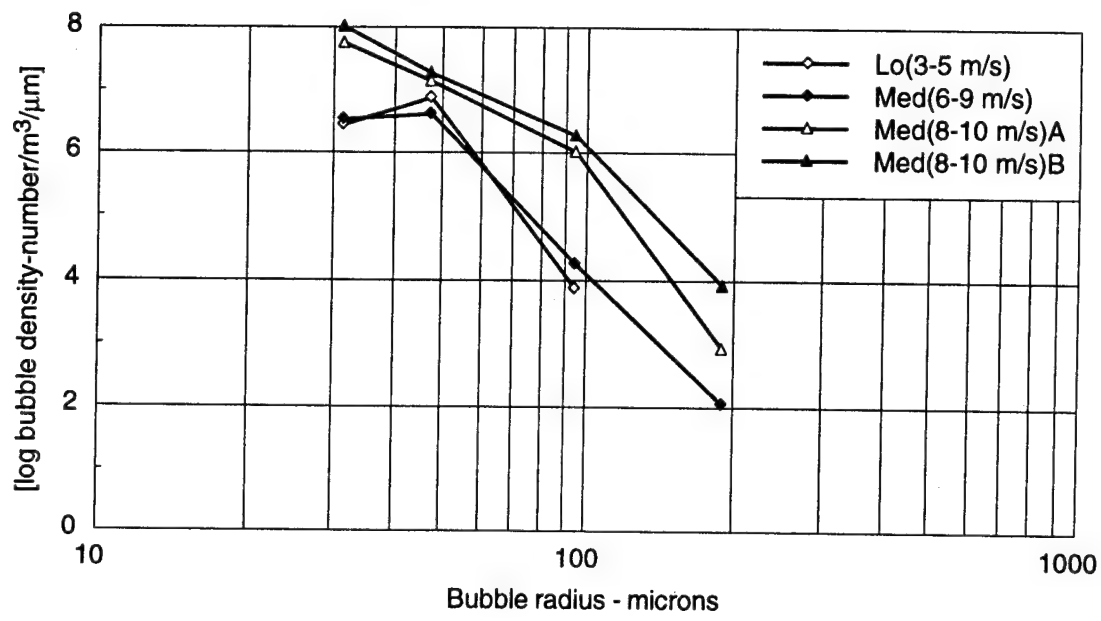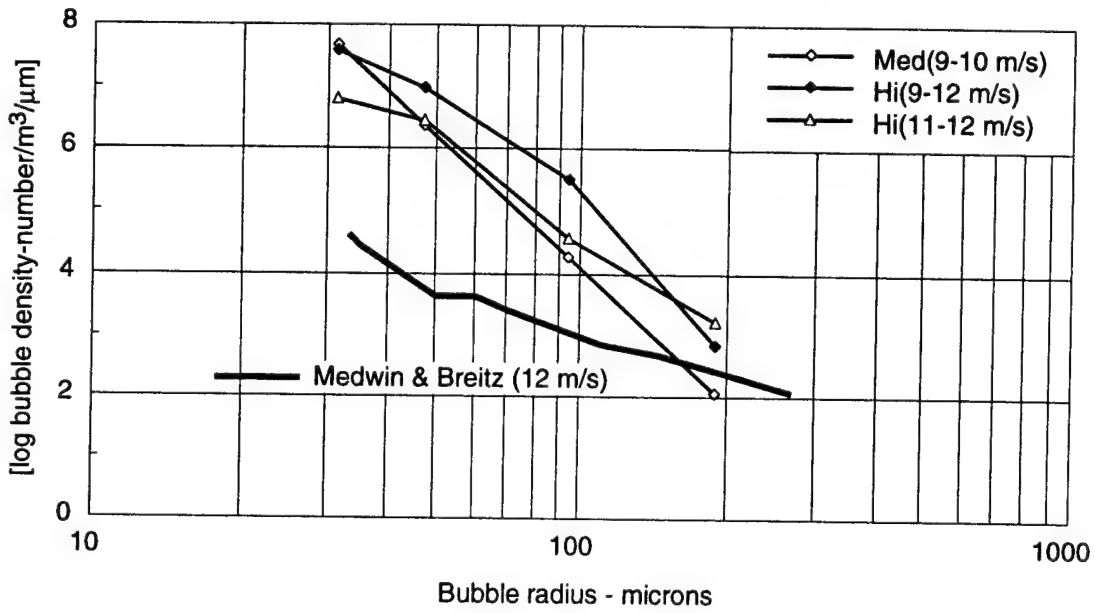
Figure 3.18
Bubble density versus bubble radius
for various wind speeds (depth = 1 m).

37
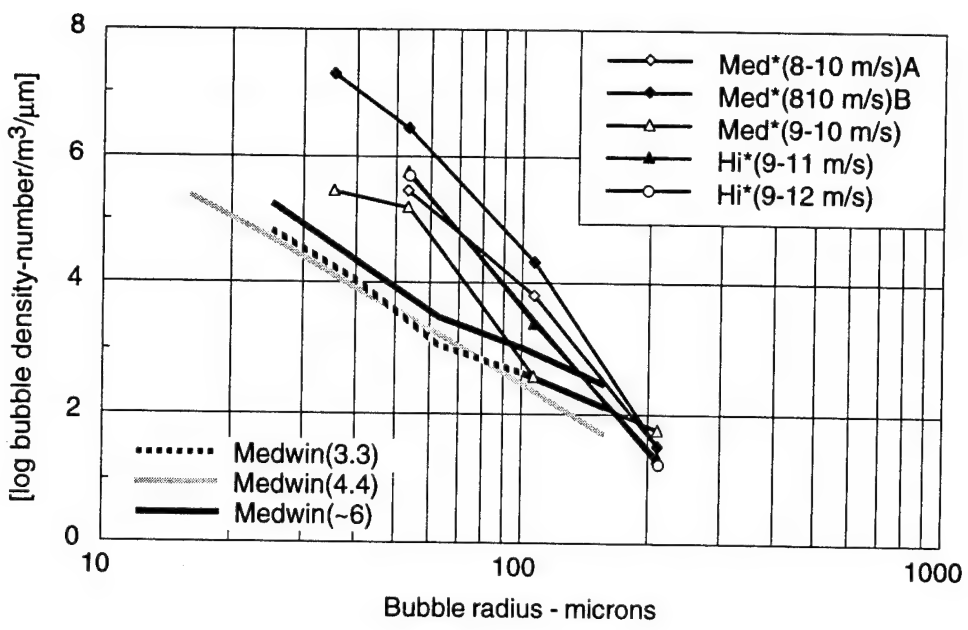
(a)
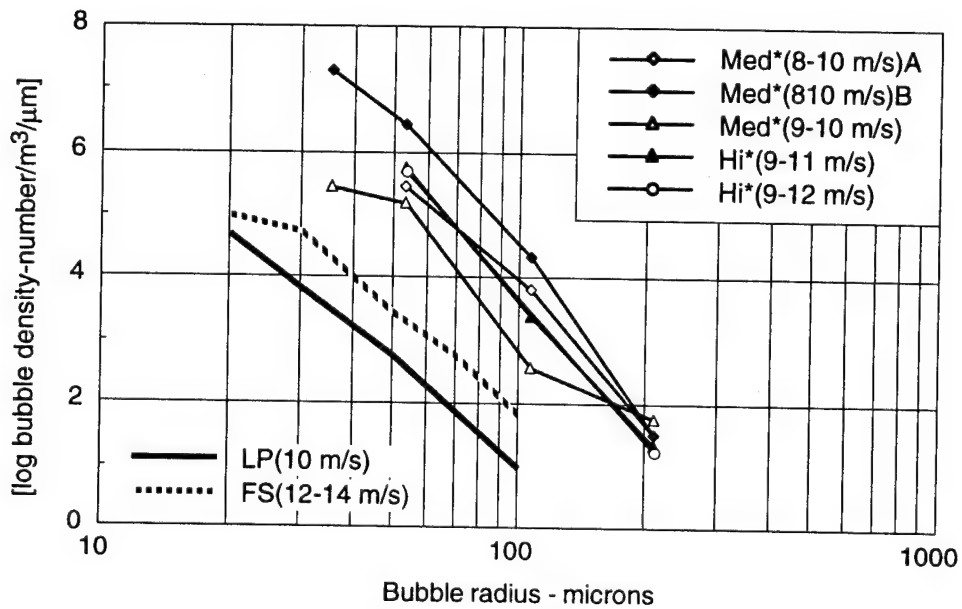
(b)

**Figure 3.19
Bubble density versus bubble radius
for various wind speeds (depth = 4 m).**

The bubble density estimates in Fig. 3.19(b) are significantly higher than those reported by Vagle and Farmer (1992) for comparable wind speeds at a sample depth of 3 m. In Fig. 3.19(b), the curve identified as LP corresponds to their LA PEROUSE data while the curve identified as FS corresponds to their FASINEX data. The average slope for their data is about 5.

3.5   VARIABILITY IN VERTICAL INCIDENCE BACKSCATTER

The degree of variability from ping to ping is perhaps the most noticeable characteristic of the vertical incidence backscatter data as one observes the measurement system B-scan display over a sequence of pings. An attempt was made to quantify the variability and proceeded in the following manner. The sequence of N pings of a selected pulse type comprising a specific data file was first "stacked" by aligning all pings to a common time reference associated with the first fathometer return as described earlier. Quadrature sampled values were then averaged over the ensemble of pings to create a representative "composite" ping over an epoch of interest, based upon shortest and longest ranges of interest. Such composite pings were particularly useful for qualitative diagnostics when presented on the B-scan display.

If we define $z_{ik}=x_{ik}+jy_{ik}$, where x and y are quadrature samples, the index i identifies the sample position in time, and the index k identifies the ping number $(1 \leq k \leq N)$, a composite ping can be represented as

$$<z_i> = N^{-1} \sum_{k=1}^{N} z_{ik} \quad . \tag{3.11}$$

Physical quantities of interest can be extracted from the composite ping over the full epoch or over any desired sub-epoch, such as a pulse length. Generally, an average power over a time interval equal to the transmit pulse was related to the quantity of interest. This can be expressed as

$$<u> = [(n-m+1)]^{-1} \sum_{i=m}^{n} u_i \quad , \tag{3.12}$$

where

39

$$u_i = (2N)^{-1} \sum_{k=1}^{N} (z_{ik} \cdot z_{ik}{}^*) \quad , \tag{3.13}$$

where * refers to complex conjugate, the factor 2 arises due to complex samples, and (n-m+1) constitutes the number of samples in a time interval equal to the transmit pulse length.

When a composite ping is not required for qualitative diagnostics, a computationally simpler approach may be used whereby the position of an interval in time (or the equivalent interval in range) is first selected and appropriate (complex) samples are averaged within each ping. An average over the ensemble of pings is then performed; this procedure can be expressed as follows.

$$<u> = N^{-1} \sum_{k=1}^{N} u_k \quad , \tag{3.13}$$

where

$$u_k = [2(n-m+1)]^{-1} \sum_{i=m}^{n} (z_{ik} \cdot z_{ik}{}^*) \quad . \tag{3.14}$$

Using this procedure a measure of variability can be expressed as

$$\sigma_u{}^2 = N^{-1} \sum_{k=1}^{N} [u_k - <u>]^2 \quad . \tag{3.15}$$

The procedure described above is straightforward and commonly used; however, its utility is diminished in the present application. Consider a physical quantity of interest (such as sound pressure level, SPL) which is estimated by appropriate scaling (using system gain and receiver sensitivity) of sample derived elements. Then

$$\text{SPL (in dB)} = 10 \log <u> + B \quad , \tag{3.16}$$

40

where $B = 10 \log b$ encompasses the system calibration parameters (in dB). If v represents the physical quantity of interest, $<v> = b<u>$ and $v_k = bv_k$, so that $\sigma_v^2 = b^2 \sigma_u^2$, which depends upon the scaling.

Of course, this situation can be avoided in a number of ways; one of the more common methods involves normalization with respect to the mean value [coefficient of variation (COV)]. The method we choose here simply uses the dB values directly, which is also a relatively common practice in spite of producing less physically intuitive results. Thus, we make use of the following relations,

$$v_k = 10 \log u_k + B; \quad <v> = 10 \log <u> + B \quad , \tag{3.17}$$

and use a measure of variation of the dB quantities expressed as

$$\sigma_v^2 = N^{-1} \sum_{k=1}^{N} [v_k - <v>]^2 \quad . \tag{3.18}$$

An example of the above variability measure is shown in Fig. 3.20 for volume backscatter versus depth under moderately windy conditions (8-10 m/s). The relatively high variability, particularly at deeper depths, is quite apparent in this figure and is likely due to patches of bubbles migrating through the fixed acoustic beams.

3.6 COMMENTS ON VERTICAL INCIDENCE BACKSCATTER

The acoustic echoes from vertical incidence transmissions clearly reveal the presence of near-surface scatterers (e.g., Urick and Hoover, 1956; McConnell, 1988; Nützel et al., 1994). Near-surface acoustic measurements of volume backscatter, attenuation, and sound speed, combined with ambient noise and bubble density measurements, leave little doubt that concentrations of microbubbles are significant constituents of the near-surface scatterer population. There is general agreement among researchers concerning the gross characteristics of the upper ocean boundary, including bubble generation and spatial density distribution (Thorpe, 1985; Monahan and Lu, 1990; Thorpe, 1992; McDaniel, 1993). The detailed nature of the near-surface dynamics, including
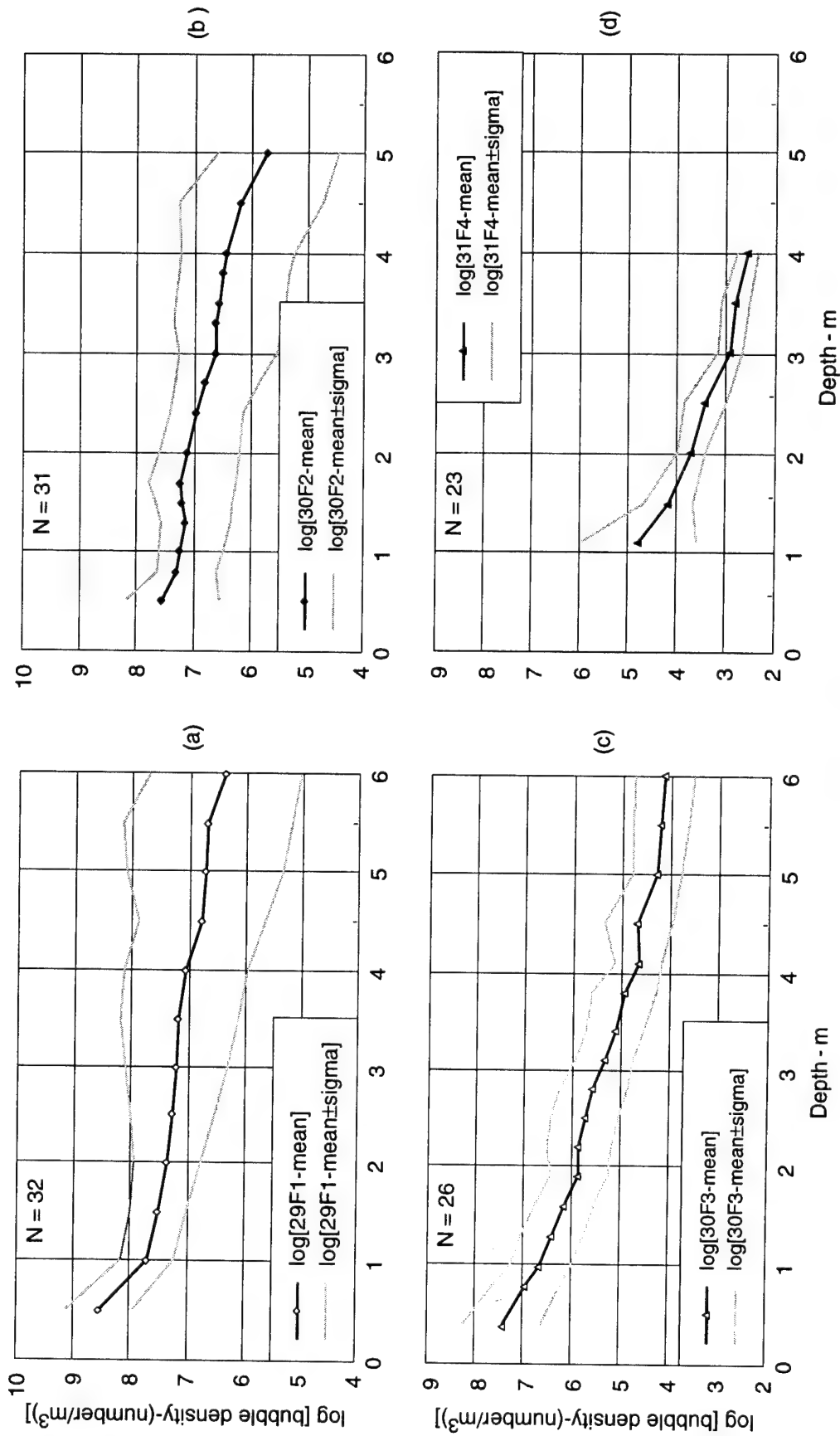
Figure 3.20

An example of near-surface volume backscatter variability for a moderately windy condition (wind speed = 8-10 m/s).

42

bubble generation and distribution mechanisms, provides incentive for additional research.

The results presented here are generally consistent with a bubble layer model in which the density decays exponentially with depth. Considerable temporal variation is observed with relatively small, high density cells occasionally moving through the fixed measurement region; however, the mean behavior appears to be relatively constant over time periods of several minutes. Figure 3.21 shows three successive measurements at 108 kHz of near-surface volume backscatter versus depth taken over a time period of 18 min. The vertical tilt was changed between data sets so that different preformed beams were used to extract vertical incidence data. The three curves are quite similar in magnitude and slope.

Bubble density estimates based on volume backscatter data are generally higher within the first few meters of the surface than other reported density estimates, most of which included measurements at deeper depths. The quiescent volume backscatter over the duration of the current measurements also appears to be fairly high but not excessively so, particularly when considering the likelihood of contributions from marine organisms in the coastal environment.

The bubble density versus bubble radius curves depict an exponential decrease with increasing bubble radius; the curves show little sensitivity to wind speed over the limited range of wind speeds encountered.
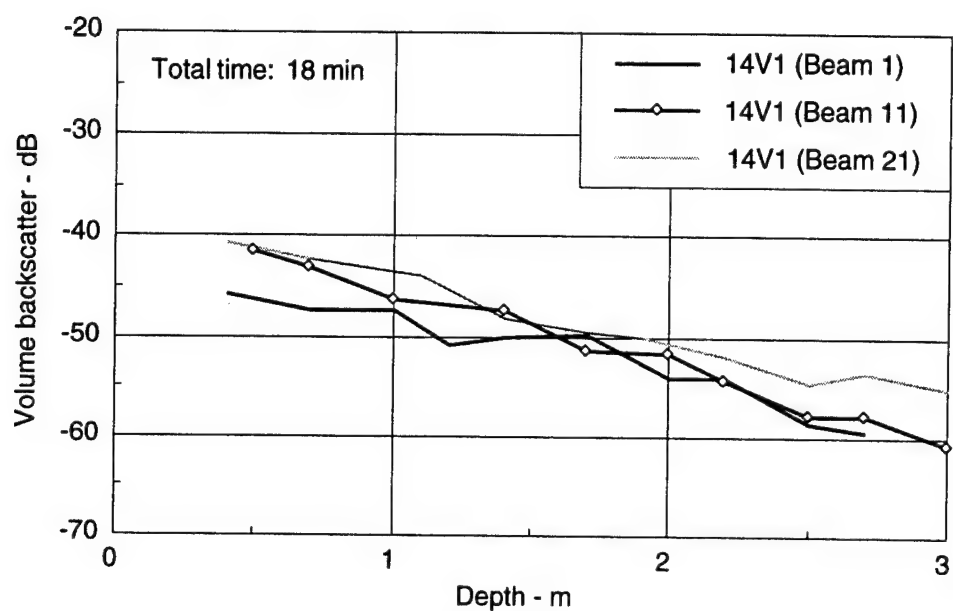
Figure 3.21
An example of near-surface volume backscatter
temporal stability for 108 kHz data.

44

4. SURFACE ACOUSTIC BACKSCATTER MEASUREMENTS

Acoustic backscatter from scatterers distributed below the sea surface as determined by vertical incidence measurements was discussed in the preceding section.   The measurement results discussed in this section concern backscattering from the sea surface and, particularly, backscatter as a function of grazing angle. The measurements were made by selecting various orientations of the transducer in a vertical plane and echoranging on the sea surface. A mean backscattering strength was determined for each beam in the set of preformed receive beams; a corresponding grazing angle was determined from receive beam vertical angle using raytracing and measured sound speed profile. Figure 4.1 provides an example of the system B-scan display presentation for a particular transducer orientation during surface backscattering measurements. The surface backscatter forms a parabolic trace for each of two different pulse types in this display presentation.

In most cases overlap of surface regions providing backscatter returns occurred for sequential transducer orientations so that measurements were piecewise continuous in grazing angle. When time permitted, measurements were made in the vertical plane containing the wind velocity (with/against wind) and in a perpendicular plane (cross wind).

The mean backscattering strength for each receive beam was determined from samples averaged over times equal to transmit pulse lengths, ensemble-averaged over valid pings, and corrected by system calibration and estimated propagation losses as described earlier in Section 3. Generally, two different pulse types were selected for transmission on alternate pings; the time between pings was always 2 s. The influence of pulse type on mean backscattering strength and variability results will be addressed first in the following topical discussions.

The mean backscattering strength measurement results will be compared with predicted results using two different surface acoustic backscattering

45
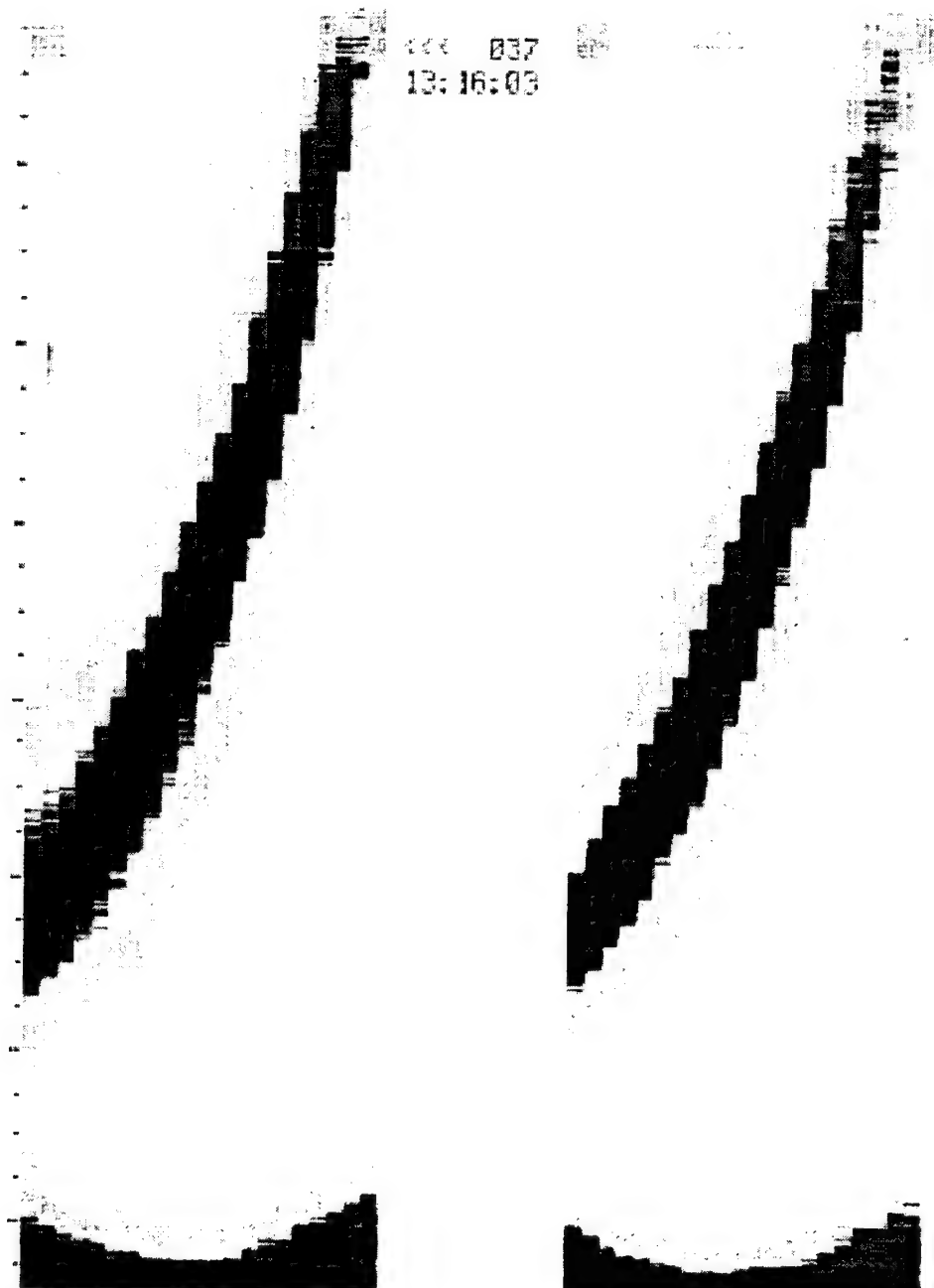
Figure 4.1
An example of the measurement system B-scan display
for surface backscattering strength analyses.

submodels.* One of these submodels is used in a minehunting sonar performance prediction model, MINERAY (Jaster and Boehme, 1984) and the other submodel is developed within APL/UW's high frequency environmental acoustics models (APL/UW, 1989). These high frequency sonar performance prediction models have historical significance, as well as current applications, in Navy mine countermeasures and weapon systems programs. The MINERAY and APL/UW surface backscattering strength submodels are described in the appendix.

The remainder of this section will be devoted to the presentation, comparison, and discussion of surface backscattering strength data analysis results.

4.1   PULSE TYPE DEPENDENCE

A brief opportunity was afforded during acoustic measurements when wind speeds were the highest experienced (14-16 m/s); advantage was taken during this period to record data using various pulse types for each of the four frequencies. Surface backscattering strength measurements were made with the transducer (boresight axis) tilted about 45° with respect to the vertical. Measurements were made pointing into the wind and cross wind at 108 kHz, and pointing into the wind only at 72 and 36 kHz under maximum wind speed conditions. Cross wind measurements were subsequently made at 72, 36, and 18 kHz after the wind had diminished somewhat (to about 10-13 m/s).

The mean surface backscattering strength versus grazing angle determined from the above measurements at each of the four frequencies is shown in Fig. 4.2. Figure 4.2(a)-(c) includes several pulse types as well as both up wind and cross wind conditions; two pulse types and measurement under cross wind conditions are shown in Fig. 4.2(d). These data analysis results

---

* While this report was undergoing internal ARL:UT review, a revised APL/UW surface acoustic backscattering submodel was received (APL/UW, 1994). APL/UW graciously provided the computer code which allowed some comparative analyses with this latest submodel. These results are presented later in Figs. 4.19 - 4.22. Comparisons of measurement results with the earlier submodel are identified as APL89, while comparisons with the revised submodel are identified as APL94.
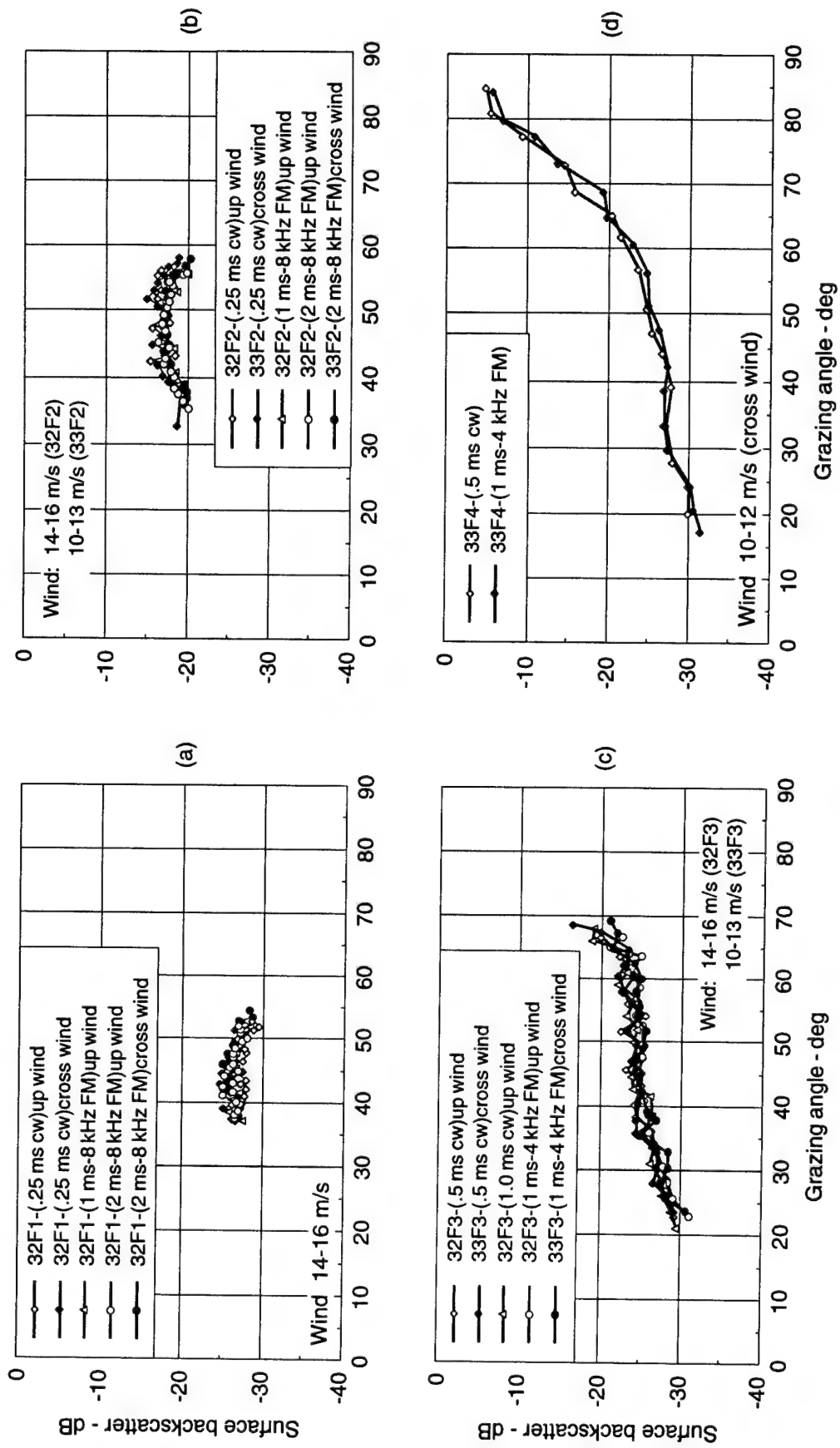
Figure 4.2

Surface backscattering strength versus grazing angle for various pulse types under high wind speed conditions.

indicate no significant dependence of mean backscattering strength on pulse type or orientation with respect to the wind direction.

The mean surface backscattering strength versus grazing angle resulting from data at a lower wind speed and a cross wind orientation is shown in Fig. 4.3. In this figure the same two pulse types are indicated for all four frequencies; again, no significant dependence on pulse type is indicated.

The behavior of the data points at high grazing angles, in Figs. 4.3(a) and 4.3(c), and at low grazing angles in Fig. 4.3(a), require some comment. The observed 'saturation' effect at high grazing angles is a result of exceeding the measurement system dynamic range. This effect occurred during acoustic measurements when the operator selected a receiver gain which was too high for the echo levels being received on near vertically oriented beams. While the system was designed to provide the operator an indication of this condition during data acquisition, receiver gain selection was required before data acquisition commenced and was not changed once a ping sequence had begun.

The behavior of the data points at low grazing angle in Fig. 4.3(a) (and possibly in Fig. 4.3(b), to a lesser extent) is due to the influence of system noise. The receiver noise was measured for several data files and will be shown as equivalent backscattering strength in figures later in the discussion.

In order to provide a quantitative measure of significant variation, a standard deviation was calculated for each of the pulse types in each of the data files shown in Fig. 4.3 according to the method described in some detail earlier in Section 3. The mean backscattering strength versus grazing angle results shown in Fig. 4.3 are again presented in Fig. 4.4. In addition, curves representing mean ±1 standard deviation computed for each pulse type are shown for each data file. The light/(dark) dashed curves apply to the short/(long) pulse data. As stated, the mean backscattering strength is not significantly dependent upon pulse type according to the error criterion displayed in Fig. 4.4. A reduction in standard deviation of the longer pulse relative to that of the shorter pulse is noted and attributed to the difference in time-bandwidth product of the two pulse types.

49
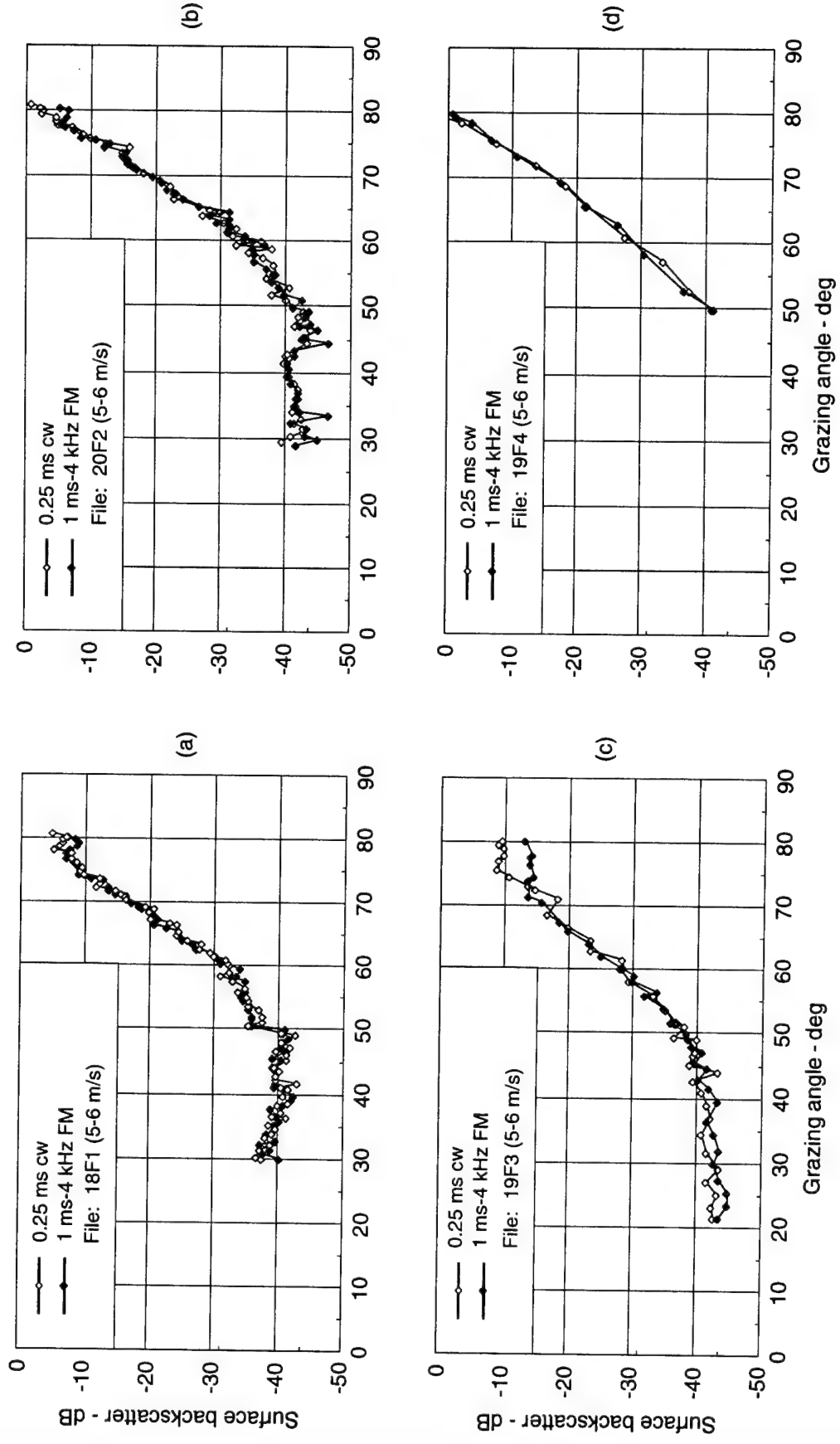
Figure 4.3
Surface backscattering strength versus grazing angle
for two pulse types under lower wind speed conditions.

50
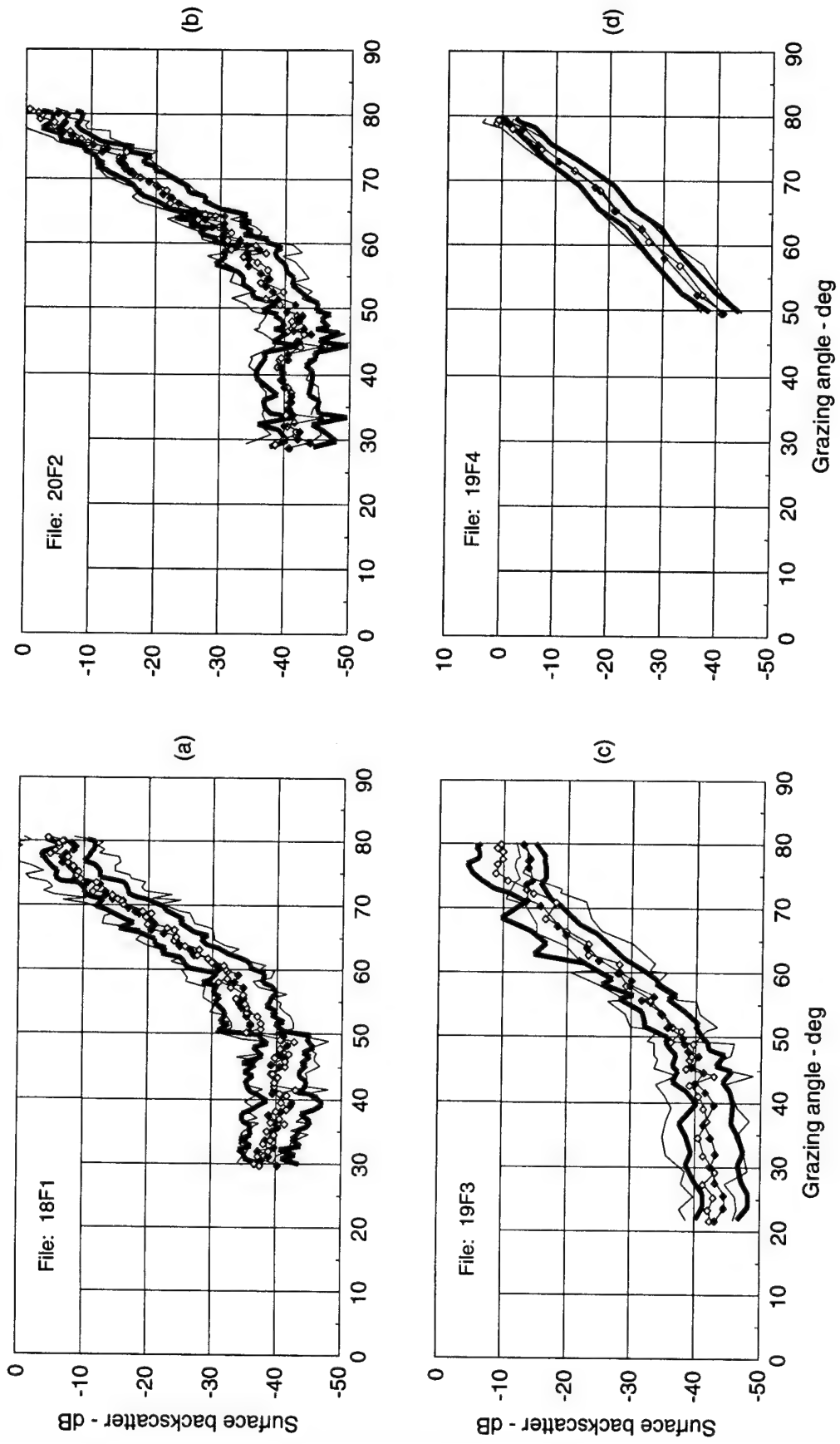
Figure 4.4

An example of mean surface backscattering strength variability.

4.2 SURFACE BUBBLE LOSS

In using received echo levels at a bottom mounted measurement system to infer surface backscattering strength, the path loss to and from the surface must be estimated. The data analysis software includes ray path calculations based upon sound speed versus depth derived from temperature versus depth measurements. Spreading and absorption loss along the two-way paths are accounted for; absorption loss is based upon the Francois and Garrison (1982) equation.

When a concentration of near-surface bubbles exists, an added loss is encountered in transit to and from the sea surface; this added loss has been termed SBL (dB) and for vertical incidence is represented in Eq. (3.4). When the two-way path is that of an acoustic ray encountering the surface at a grazing angle, Eq. (3.4) can be modified as follows (see McConnell and Dahl, 1991).

$$SBL \text{ (dB)} = [8026 \, \delta(V_{bs})_I]/\sin \theta \quad , \tag{4.1}$$

where $(V_{bs})_I$ is the volume integrated bubble scattering. The values of $(V_{bs})_I$ estimated in Section 3 (provided in Table 3.2, in dB) from vertical incidence backscattering measurements can be used to estimate the additional propagation loss within a near-surface bubble distribution for any grazing angle.

Even for the relatively high bubble densities estimated for vertical incidence backscatter measurements, the limited depth extent of significant bubble concentrations in the current experiment results in propagation loss corrections that are trivial in most cases. However, when this is not the case, surface bubble loss corrections have been made to subsequent surface backscattering strength versus grazing angle data.

4.3 FREQUENCY DEPENDENCE AND MODEL COMPARISONS

Surface backscattering strength versus grazing angle measurements were made over a limited range of wind speed conditions for all four system frequencies. In most cases measurements were made in the vertical planes parallel and perpendicular to the wind direction. The measurement results for all

frequencies under similar wind conditions are shown in Figs. 4.5 - 4.8; MINERAY and APL/UW (1989) model predictions for representative frequencies at either 5 m/s or 10 m/s wind speed are also shown for comparison.

Measurement results for relatively low wind speeds and a cross wind orientation are shown in Fig. 4.5. The results for a 5-6 m/s wind speed condition which resulted in anomalously low volume backscatter discussed in Section 3 are also shown in Fig. 4.5(b). No consistent frequency dependence is apparent in either of Fig. 4.5(a) or (b). For grazing angles below about 60°, the measured backscatter is substantially below that predicted by either of the surface backscatter models.

The system noise at frequencies of 108 and 72 kHz (F1 and F2) influences the measurements at these frequencies at the lower grazing angles; the equivalent backscatter strength of the measured system noise levels at 72 kHz, for the measurement conditions of Fig. 4.5(a) and (b), are also shown for comparison. In Fig. 4.5(b), the equivalent system noise includes the higher receiver electronic noise experienced during the initial deployment period and the influence on low grazing angle measurements is more dramatic. While only the 72 kHz equivalent system noise is shown in Fig. 4.5, the measured system noise at 108 kHz resulted in similar low grazing angle limitations.

Surface backscattering strength versus grazing angle for somewhat higher wind speeds and down wind, up wind, and cross wind conditions is shown in Fig. 4.6. The measured data for the up and down wind conditions appear to follow the APL/UW model predictions quite well at the higher grazing angles and the MINERAY model predictions moderately well at intermediate grazing angles. The measured data at intermediate grazing angles appear to be anomalously low for all frequencies, except 108 kHz for the cross wind condition. Again, no consistent trend with frequency is apparent in the measured results.

In Fig. 4.7 measurement results for even higher wind speed conditions are presented. The up and down wind orientations provide essentially identical results that are slightly below both model predicted curves at intermediate to
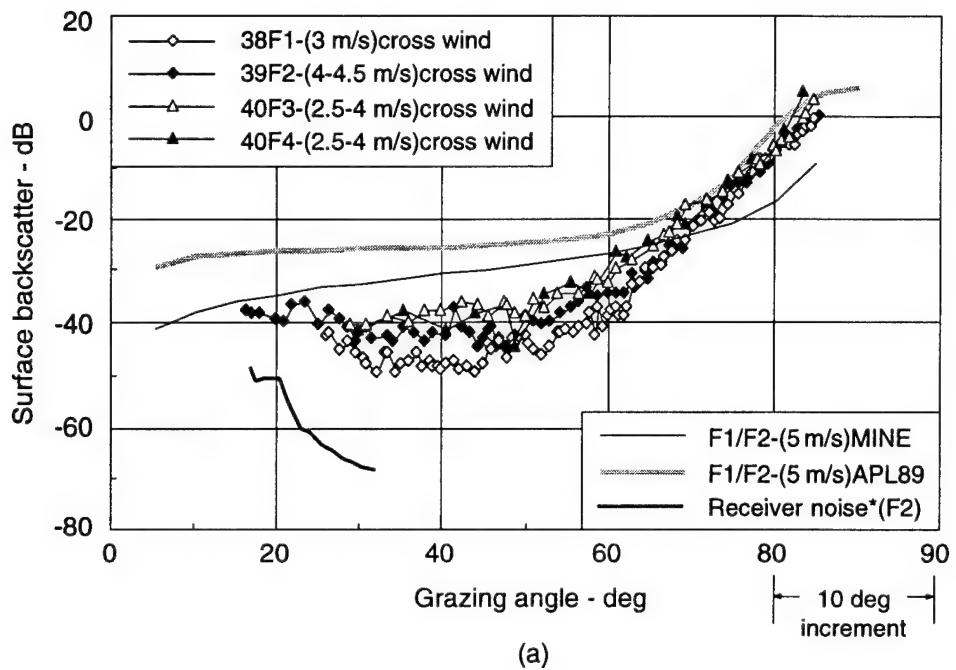
(a)
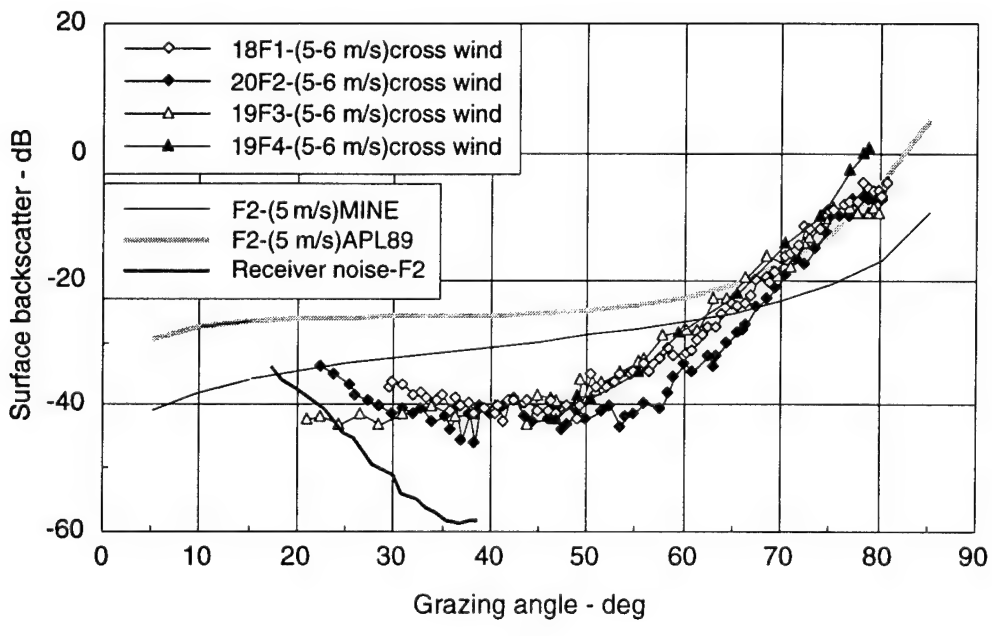
(b)

**Figure 4.5
Frequency dependence/model comparisons of surface
backscattering strength versus grazing angle (wind ≤ 6 m/s).**

54
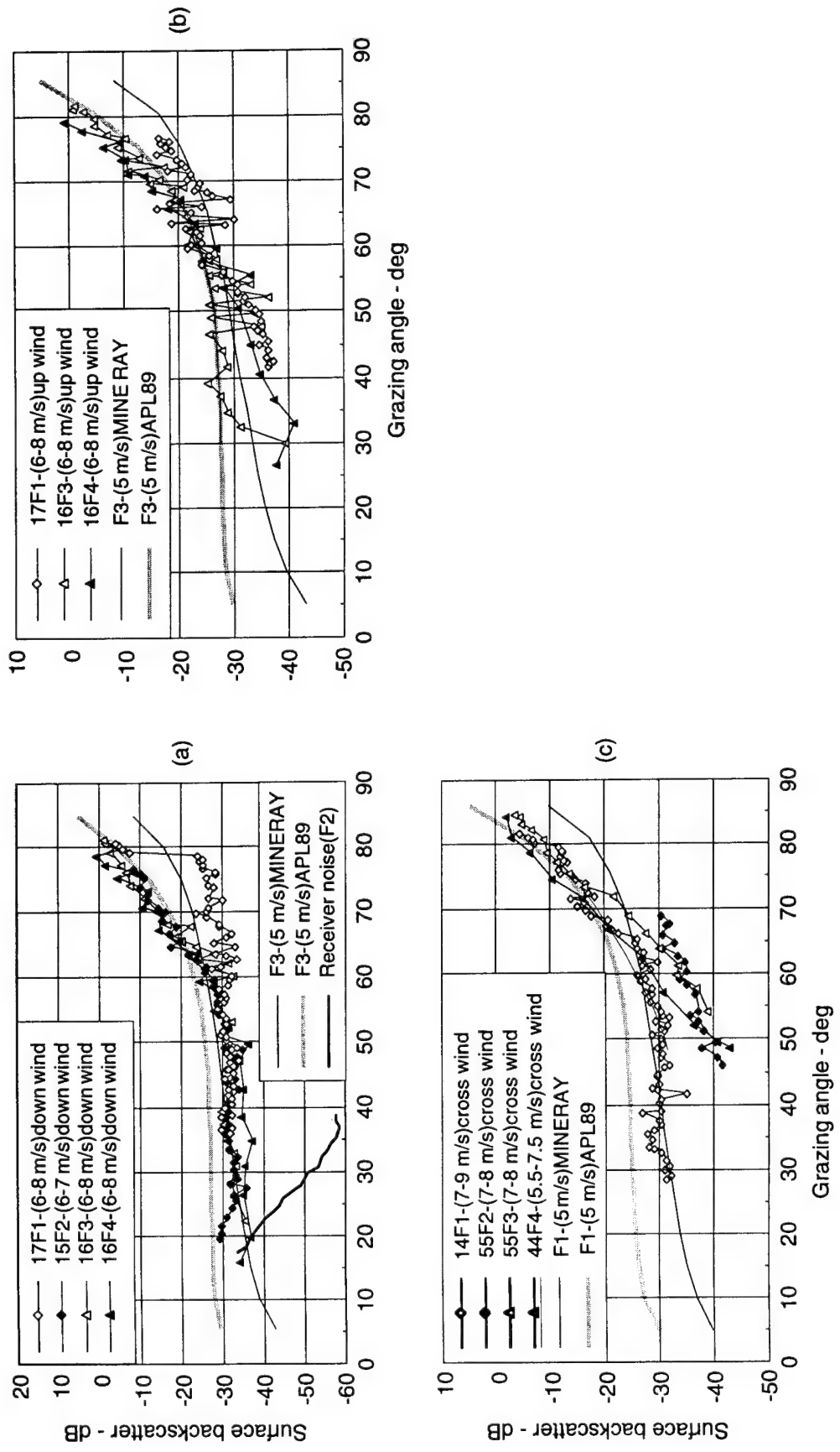
Figure 4.6

**Frequency dependence/model comparisons of surface backscattering strength versus grazing angle (wind = 6-8 m/s).**
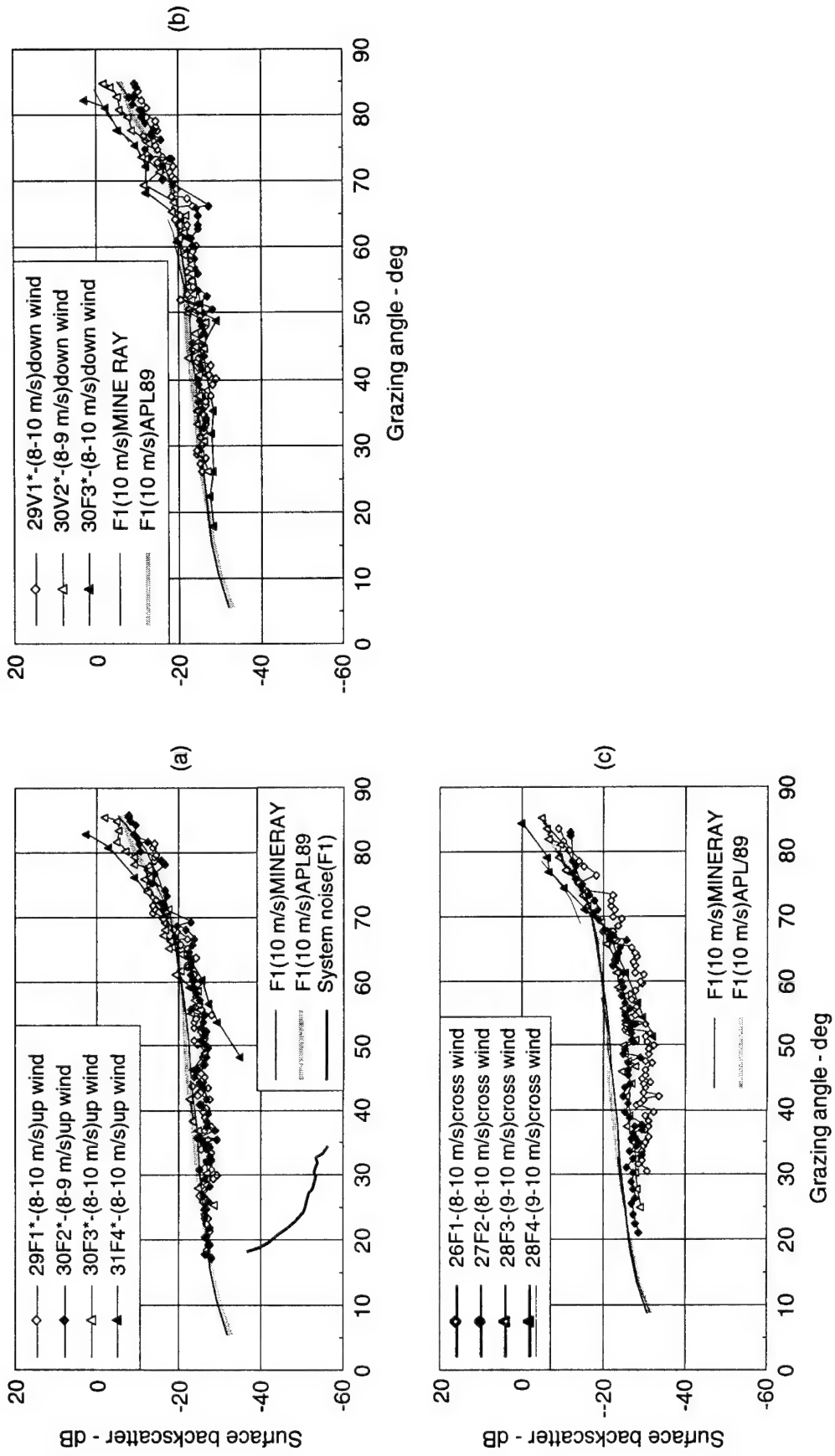
Figure 4.7

Frequency dependence/model comparisons of surface backscattering strength versus grazing angle (wind = 8-10 m/s).
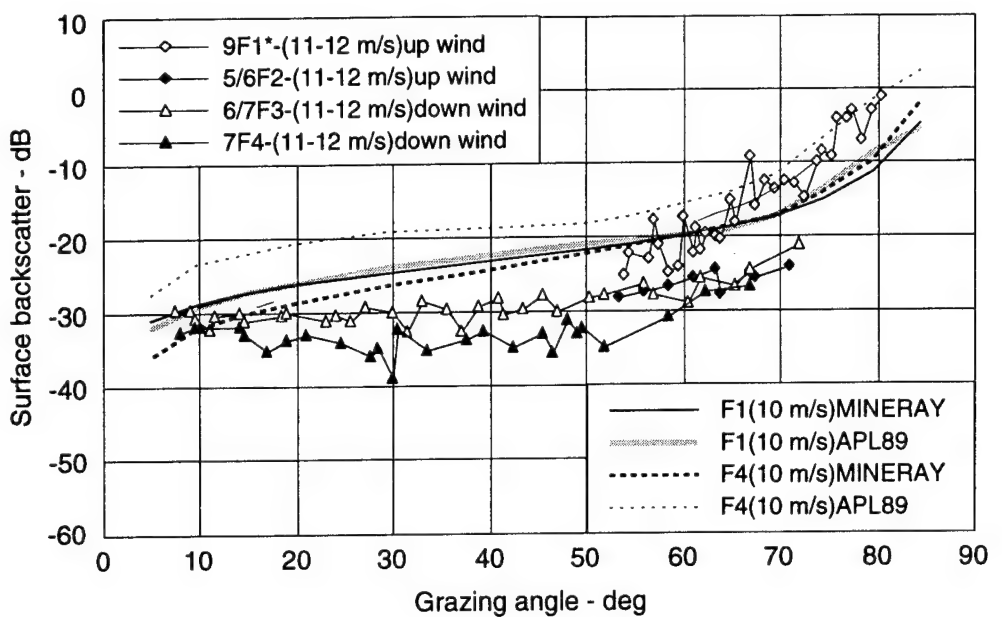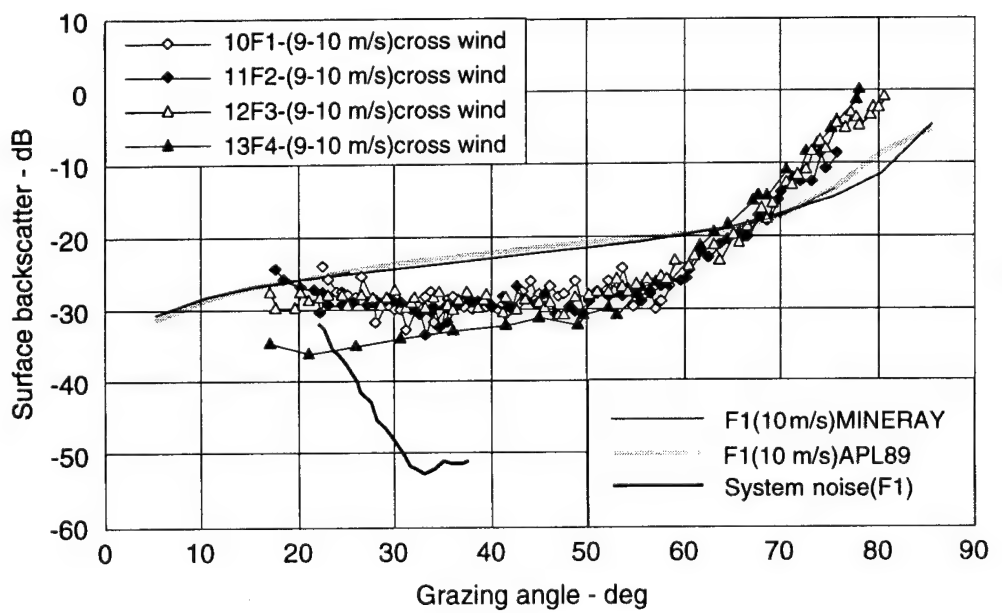
Figure 4.8
Frequency dependence/model comparisons of surface
backscattering strength versus grazing angle (wind = 9-12 m/s).

lower grazing angles. For the cross wind measurements shown in Fig. 4.7(c), the surface backscattering strength is substantially lower than model predictions at all but the highest grazing angles. No significant frequency dependence is predicted at these wind speeds and none is observed.

Measurement results under the highest wind speed conditions for which an appreciable range of grazing angles were included are shown in Fig. 4.8. Figure 4.8(a) includes only down wind conditions at 18 and 36 kHz and up wind conditions at 72 and 108 kHz. The 72 and 108 kHz data extend only over a limited range of higher grazing angles, but appear to correspond with the MINERAY model predictions moderately well. The 18 and 36 kHz data are substantially below the model predicted curves throughout the intermediate and most of the lower grazing angle ranges. The variability of the data in Fig. 4.8(a) (and the limited grazing angle coverage) precludes definitive frequency comparisons. However, it is worth noting that at these wind speeds MINERAY predicts a decrease in surface backscatter with decreasing frequency over intermediate and lower grazing angles, while the APL/UW model predicts an increase in surface backscatter with decreasing frequency over the entire range of grazing angles.

In Fig. 4.8(b) cross wind measurements at slightly lower wind speeds are shown for all four frequencies. No dependence on frequency is apparent and the APL/UW model prediction compares reasonably well with measurement results at higher grazing angles. However, the measurements are substantially below predictions of either model at intermediate to low grazing angles. The equivalent measured system noise at 108 kHz is presented to reveal the influence on backscatter measurements at low grazing angles, particularly at 72 and 108 kHz.

The data set obtained over a limited range of grazing angles under the highest wind speed condition experienced, shown earlier in Fig. 4.2, is presented again in Fig. 4.9 along with MINERAY model predicted curves for 10 m/s wind speeds. Even at wind speeds 50% higher than modeled wind speed, the measured backscattering strength values fall substantially below model predictions for both MINERAY and APL/UW models in the intermediate to lower grazing angle ranges. The cumulative data results imply a frequency
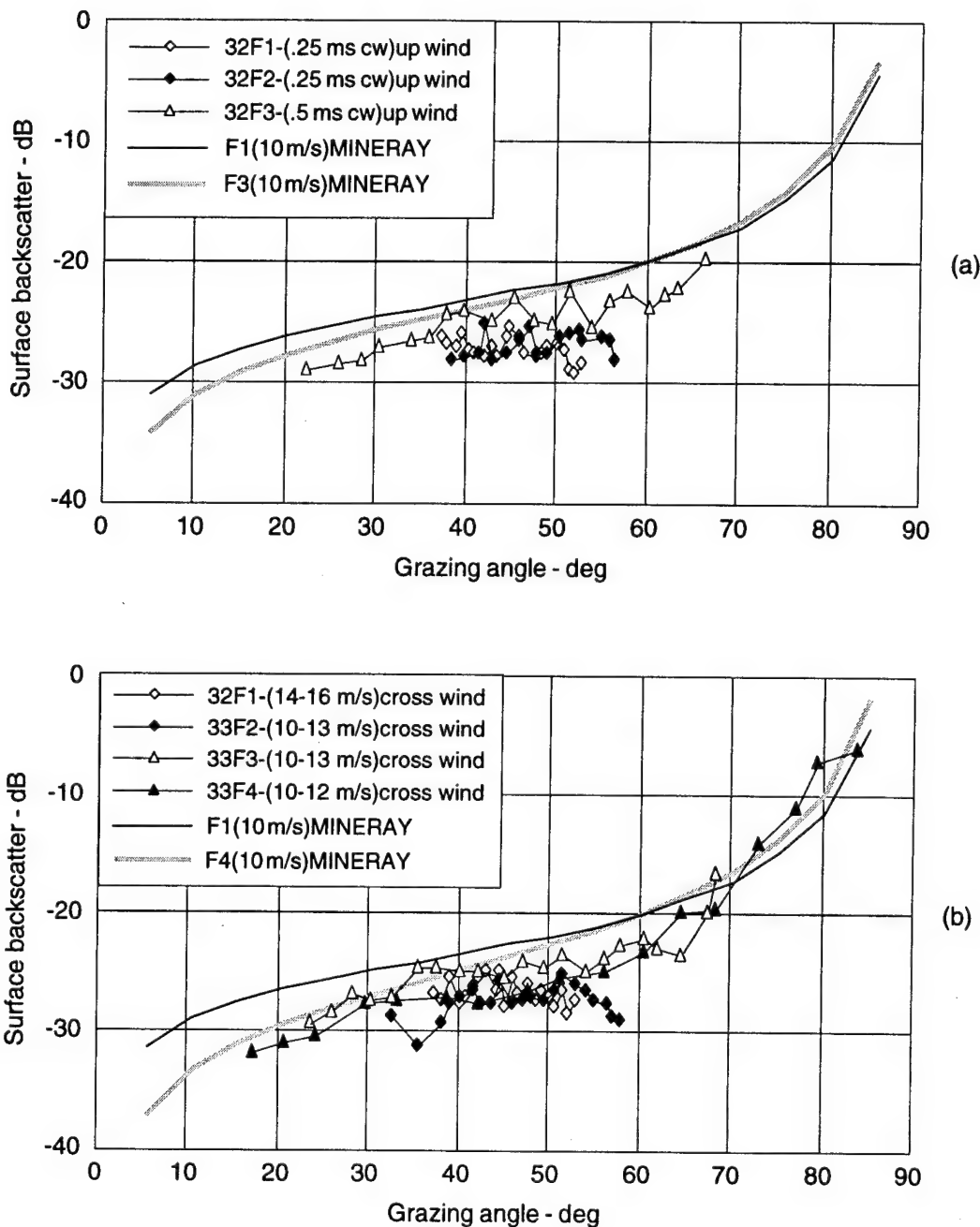
Figure 4.9
Model comparisons of surface backscattering strength versus grazing angle for high wind condition.

59

dependence that is even less than the modest dependence included in the two prediction models.

4.4   WIND DEPENDENCE AND MODEL COMPARISONS

As mentioned earlier, surface backscattering measurements were made for a variety of wind speeds and wind directions.   The acquisition of up/down/cross wind data was planned for each environmental condition; however, environmental conditions seldom remained stable for the length of time required to obtain a full set of data at all four frequencies over all grazing angles at a particular array orientation. Certain data files were selected to demonstrate the dependence upon wind speed of surface backscattering strength versus grazing angle. (As mentioned before, the wind speed was actually measured on shore.)   The resulting data plots presented separately for each of the four frequencies are shown in Figs. 4.10 - 4.13. For each frequency the data plots were further separated according to whether the vertical plane of the receiver contained the wind velocity (up/down wind orientation) or was perpendicular to the wind velocity (cross wind orientation).

The measurements at all four frequencies for both the up/down and cross wind orientations exhibit only modest wind speed dependence for grazing angles above about 60°. The backscattering strength remains fairly constant at lower grazing angles, with higher levels associated with increased wind speed, in some cases by as much as 10 dB for an increase in wind speed of about 8 m/s. For the cross wind orientation all four frequencies exhibit a rather dramatic increase in backscattering strength below about 60° grazing angle as wind speeds increase. At wind speeds of about 8-10 m/s and higher, levels for cross wind orientations are comparable with those for the up/down wind orientation at similar wind speeds.

The cross wind data exhibiting very low surface backscatter at the lower wind speeds include data file sets [38F1, 39F2, 40F3, 40F4] and [18F1, 20F2, 19F3, 19F4], as well as single data files 55F2, 55F3, and 42F4. The first data file set and the single data files have no comparative up/down wind data under similar wind conditions; thus no conclusion can be drawn with regard to wind direction dependence. There are comparative up/down wind data for the

60
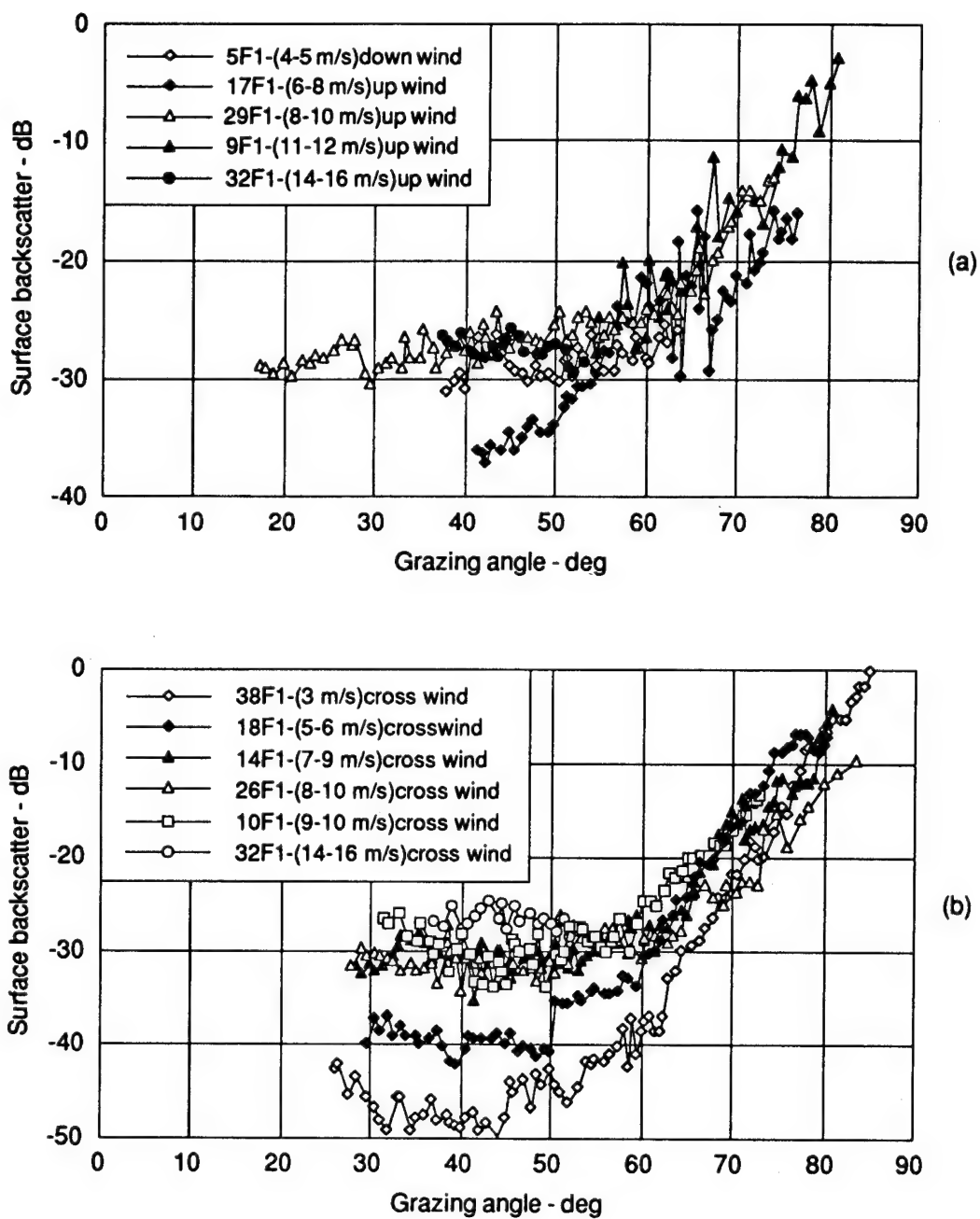
Figure 4.10
Wind dependence of surface backscattering strength
versus grazing angle (frequency = 108 kHz).
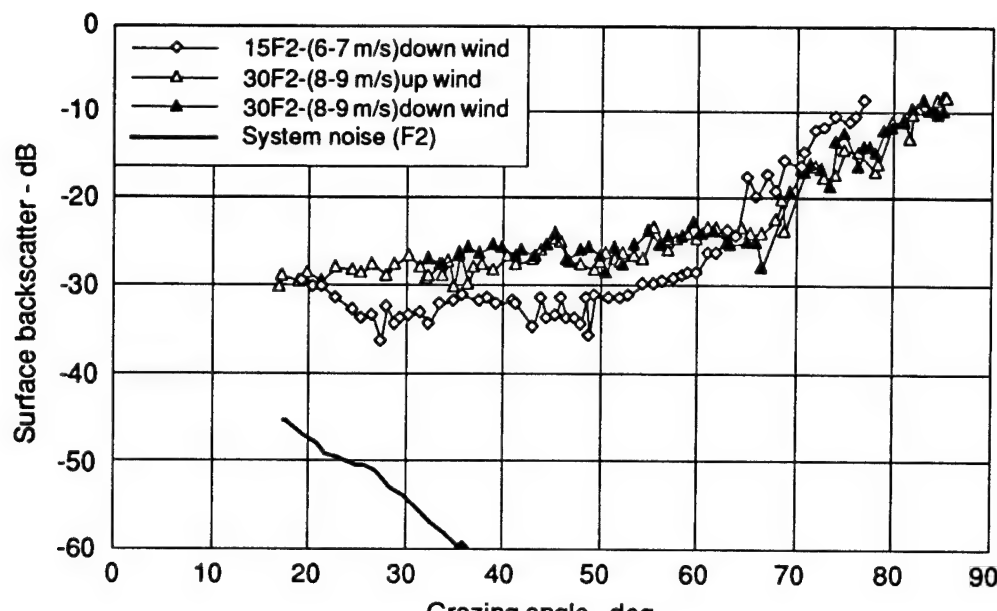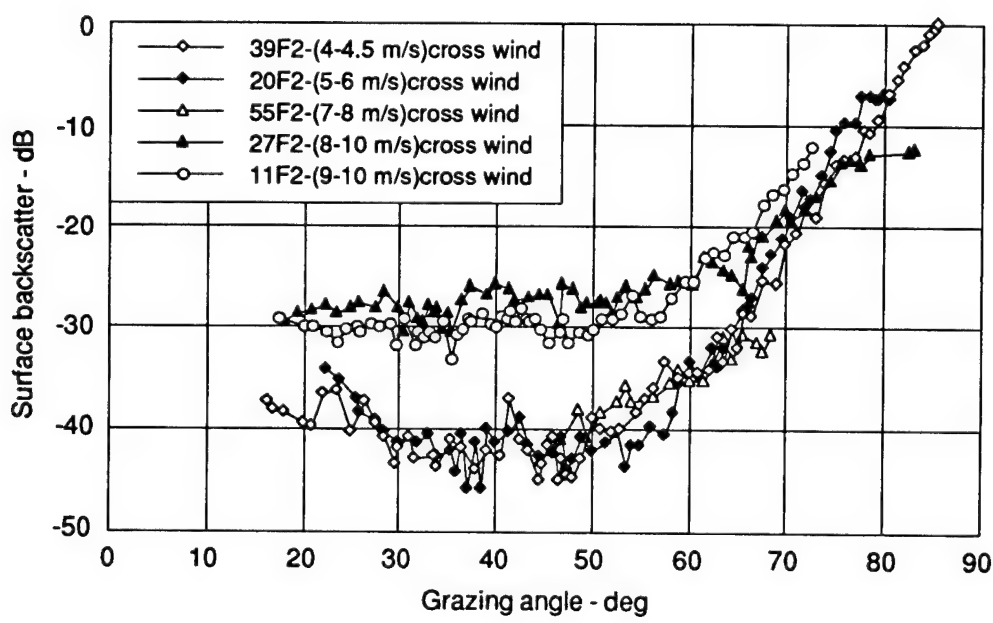
Figure 4.11
Wind dependence of surface backscattering strength
versus grazing angle (frequency = 72 kHz).
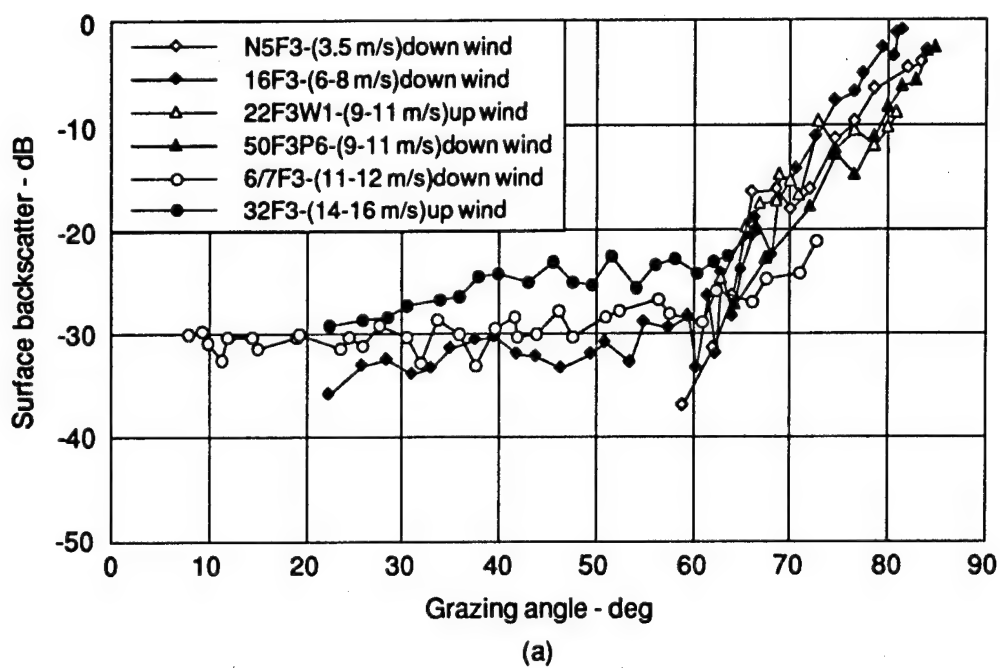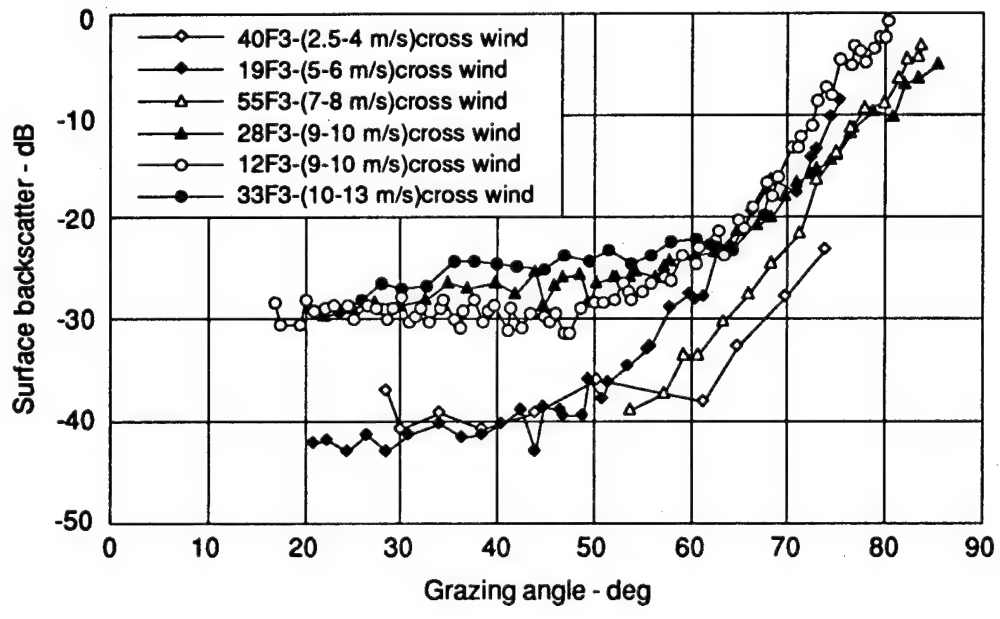
Figure 4.12
Wind dependence of surface backscattering strength
**versus grazing angle (frequency = 36 kHz).**
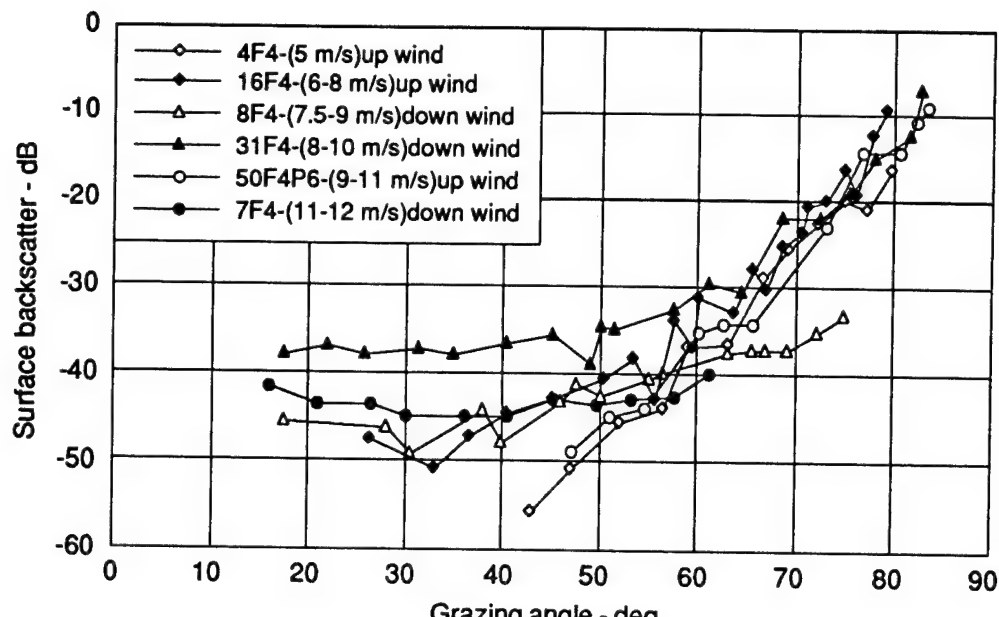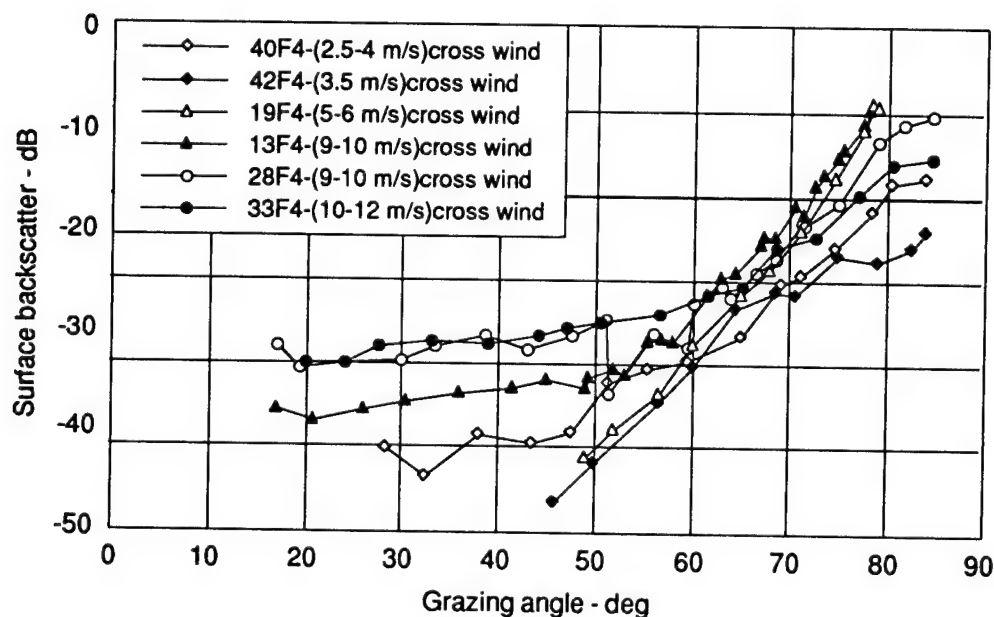
Figure 4.13
Wind dependence of surface backscattering strength
**versus grazing angle (frequency = 18 kHz).**

second data set, including the same wind direction although somewhat higher wind speeds.

Data file *18F1-(5-6m/s)cross wind* in Fig. 4.10(b) should be compared with file *17F1-(7-8m/s)up wind* in Fig. 4.10(a). In this comparison, the up wind data at a slightly higher wind speed is indeed higher than the cross wind data. However, data file *14F1-(7-9m/s) cross wind* in Fig. 4.10(b), at almost exactly the same wind speed (and also the same wind direction) as that of 17F1, is <u>higher</u> than the up wind data. Data file *20F2-(5-6m/s)cross wind* in Fig. 4.11(b) should be compared with *15F2-(6-7m/s)down wind* in Fig. 4.11(a). In this comparison cross wind values are significantly lower than the down wind values although the wind speeds are comparable.

Cross wind values are also significantly lower than corresponding down wind values in a comparison of *19F3-(5-6m/s)cross wind* in Fig. 4.12(b) and *16F3-(6-8m/s)down wind* in Fig. 4.12(a), although the wind speeds in this comparison are somewhat farther apart. The surface backscattering strengths are more comparable for *19F4-(5-6m/s)cross wind* in Fig. 4.13(b) and *16F4-(6-8m/s)up wind* in Fig. 4.13(a), while the respective wind speeds are identical to those in Fig. 4.12. From these limited comparisons there is no conclusive evidence of wind direction dependence. A comparison of vertical incidence volume backscattering data presented in Figs. 3.3 and 3.4, including the same time period as that of surface backscattering data compared above, shows that the higher wind speeds of the up/down wind data files resulted in significantly higher volume backscattering than observed for slightly lower cross wind data files. This suggests that the differences seen in up/down and cross wind surface backscattering are the result of wind speed differences rather than differences in wind direction orientations.

Surface backscattering strength versus grazing angle measurement results are compared with model prediction curves in Figs. 4.14 - 4.17. The measurement results are subdivided into relatively narrow wind speed categories spanning the wind speeds encountered during acoustic measurements. Low wind speeds ($\leq$ 6 m/s) are represented in the (a) part of the figures for all four frequencies; wind speeds of about 6-8 m/s are represented in part (b) of the figures. MINERAY and APL/UW (APL89) model predicted surface
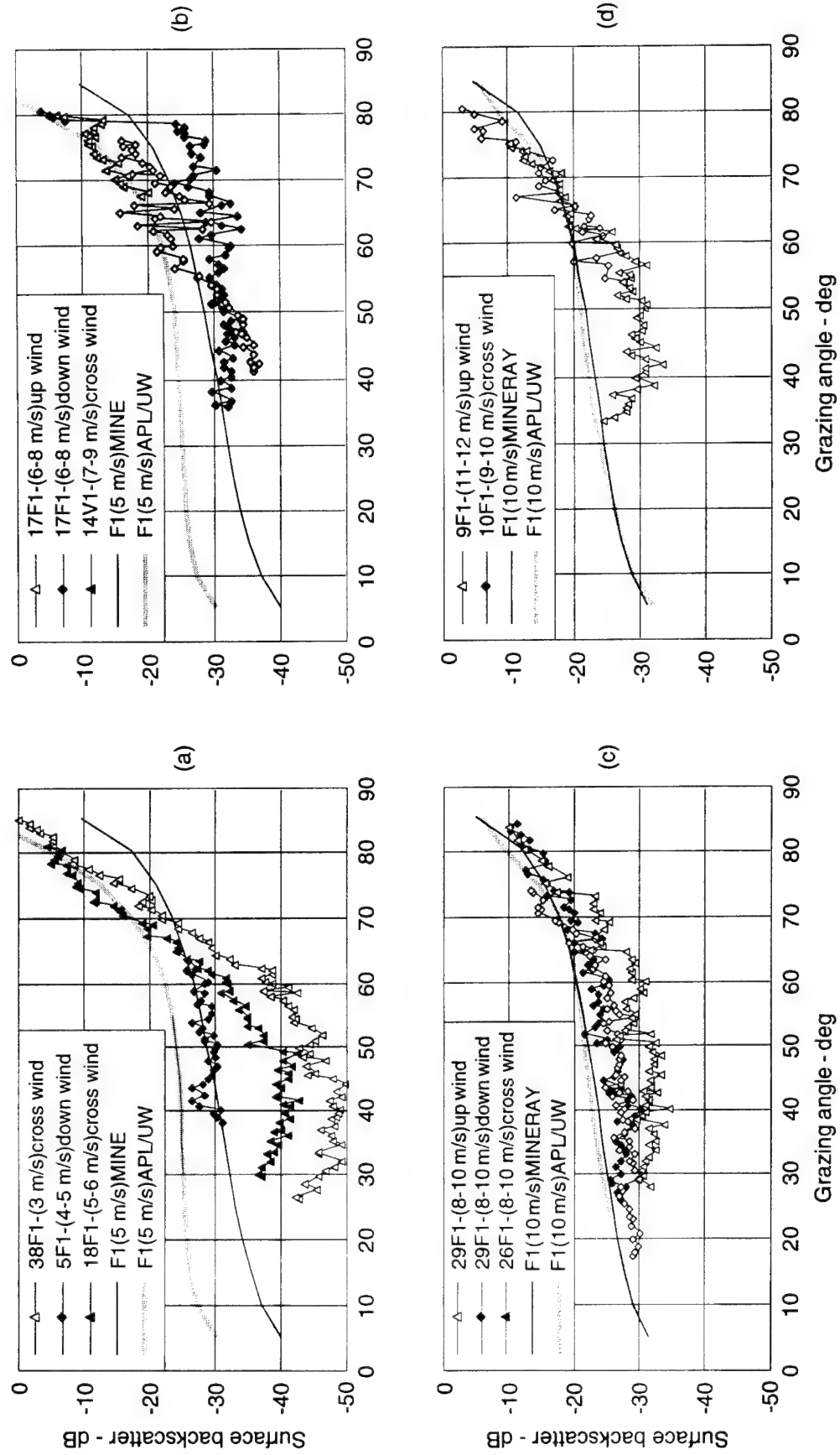
Figure 4.14

Model comparisons of surface backscattering strength versus grazing angle (frequency = 108 kHz).
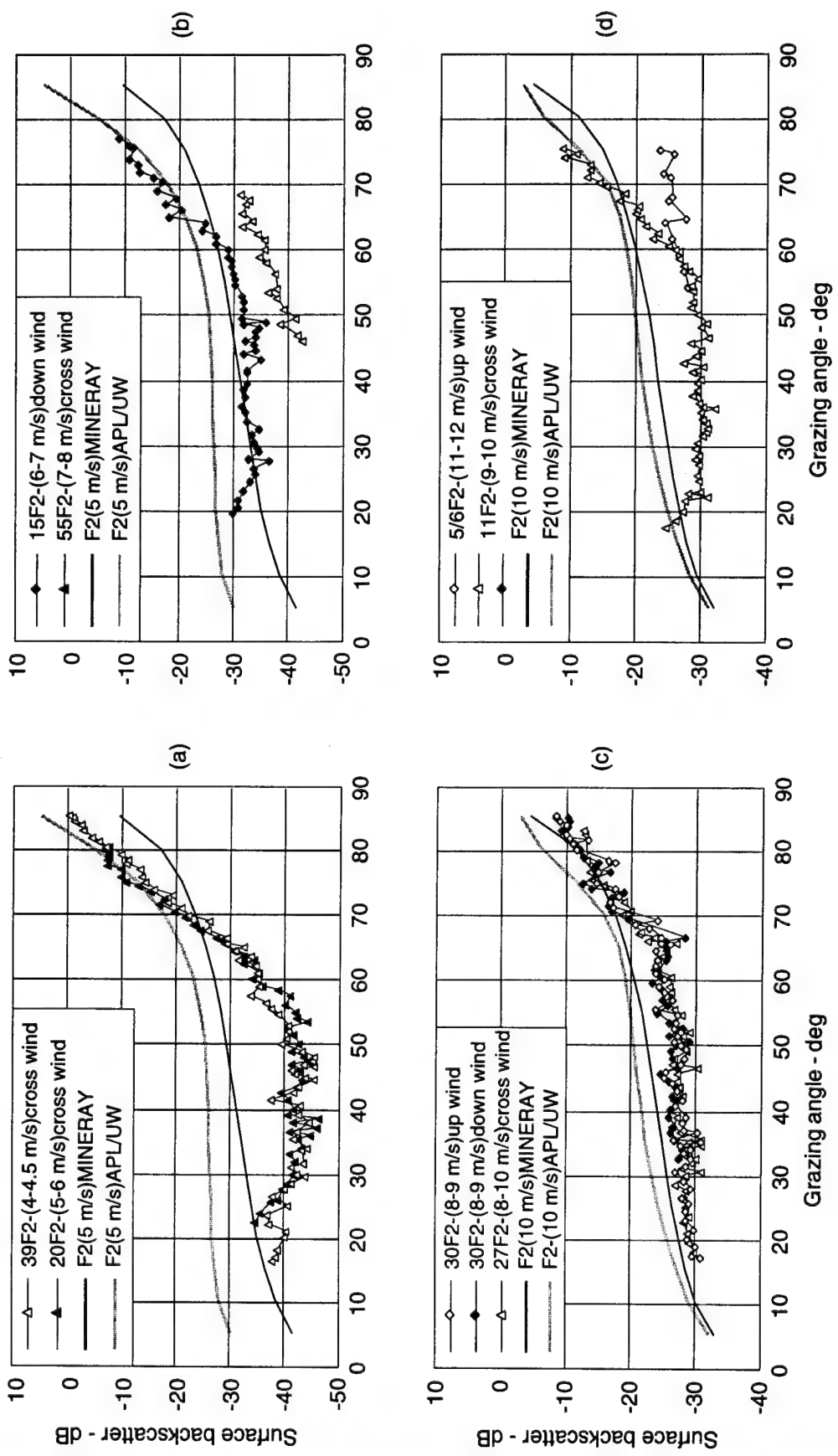
Figure 4.15

**Model comparisons of surface backscattering strength
versus grazing angle (frequency = 72 kHz).**
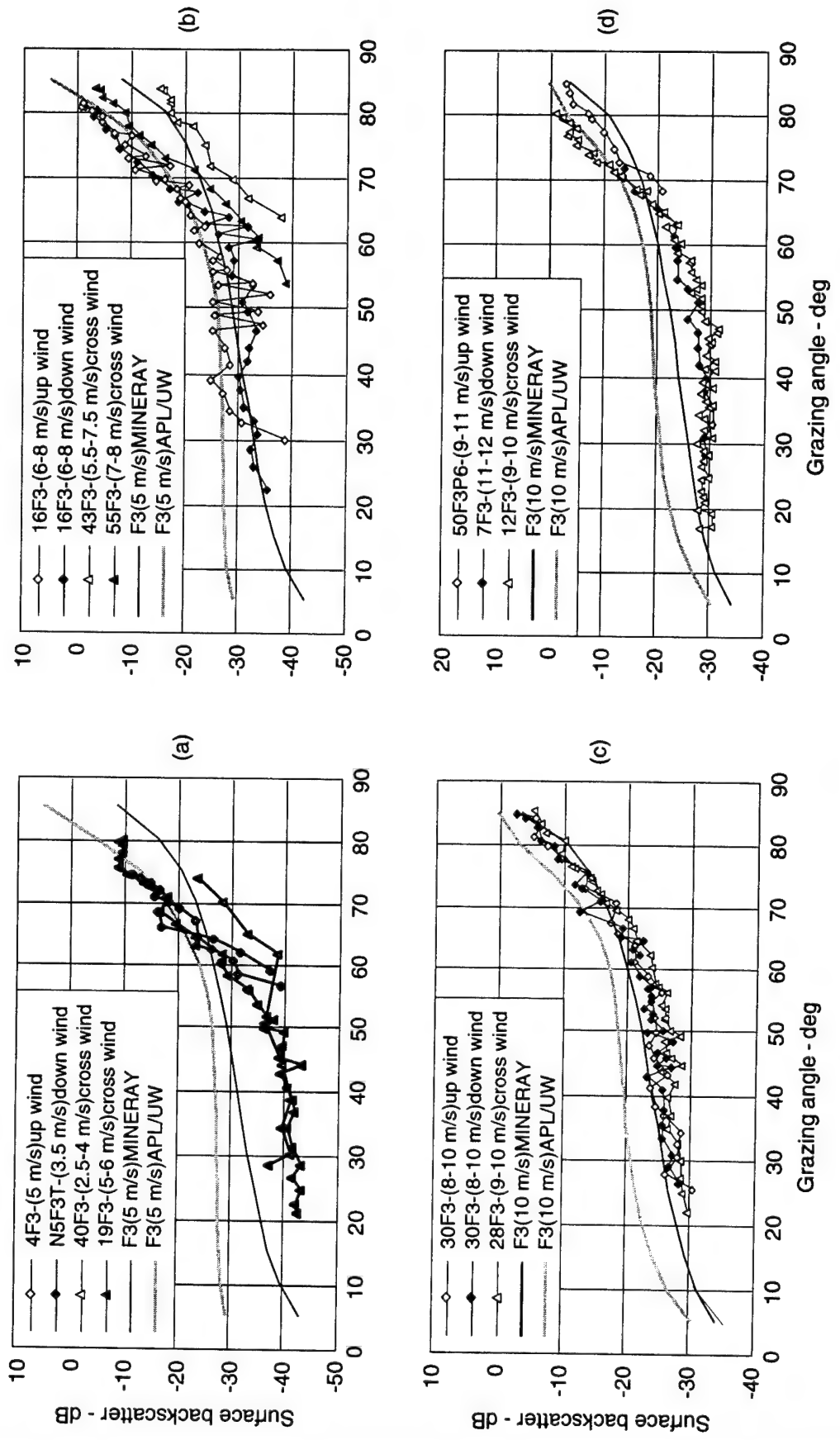
Figure 4.16

Model comparisons of surface backscattering strength versus grazing angle (frequency = 36 kHz).
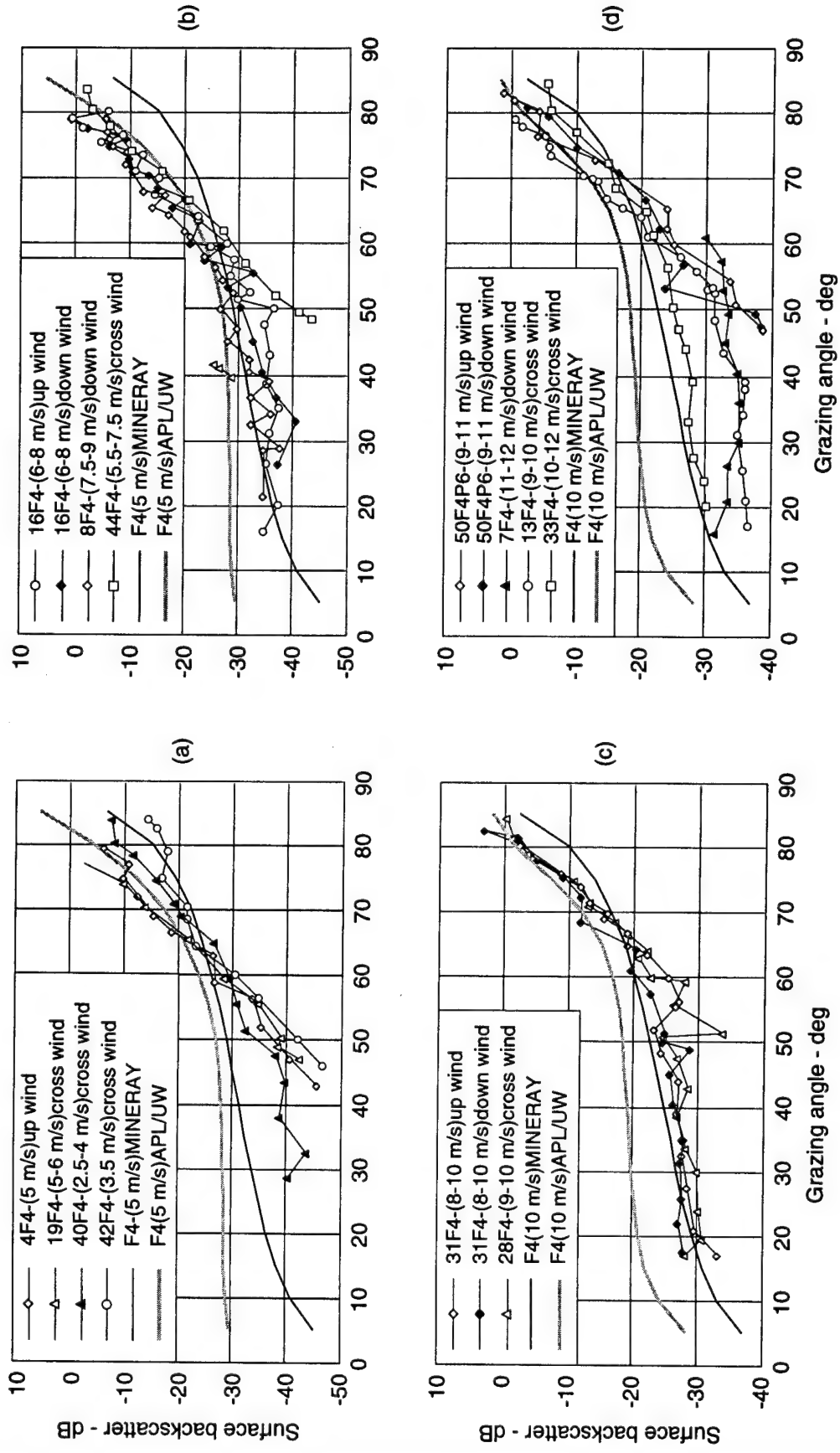
Figure 4.17

Model comparisons of surface backscattering strength versus grazing angle (frequency = 18 kHz).

69

backscatter curves for a wind speed of 5 m/s are compared with measurement results in parts (a) and (b). Wind speeds of about 8-10 m/s and ≥ 9 m/s are represented in parts (c) and (d) of the figures, respectively. Measurement results in these wind speed categories are compared with model surface backscatter curves for a wind speed of 10 m/s.

For grazing angles above about 60-65°, the measurement results in parts (a) and (b) at all four frequencies are fit fairly well by the APL/UW curves for 5 m/s wind speed. The measurement results in parts (a) and (b) generally fall below both model curves for lower grazing angles, and especially so for cross wind orientation measurements. In part (c), both MINERAY and APL/UW curves would fit the measurement results fairly well over the entire range of grazing angles if the model curves were shifted downward. The trend with frequency of the measurement results does not appear to agree with that of the APL/UW curves; i.e., an increase in backscattering strength with decreasing frequency.

In part (d), at all four frequencies, the APL/UW curves again fit the measurement results moderately well for grazing angles above about 70°. Both model curves predict levels considerably in excess of measurement results for the intermediate and lower grazing angles.

The surface backscattering strength submodels for both MINERAY and APL/UW have been reduced to dependence only upon wind speed for any selected frequency. Surface backscattering measurements support a wind speed dependence, and wind speed is relatively easily measured (or at least approximated with some degree of accuracy). Wind measurements were made in the present case at some distance from the deployed equipment, which may contribute somewhat to the substantial differences in model-predicted and measured results at lower grazing angles. Also, the model-predicted curves are intended for global sonar performance prediction applications and are inherently conservative.

Unlike MINERAY, which is empirical, the APL/UW surface backscattering submodel has physical bases and employs measurement results in parameter selection. At lower grazing angles and above a relatively low threshold wind speed, the submodel is dominated by surface bubble scattering with direct

dependence upon bubble layer characteristics as described in the appendix. Specifically, the bubble scattering model depends upon the integrated bubble total extinction coefficient which is related to the near-surface volume backscatter. Thus, the vertical incidence volume backscatter measured in the present case should be more directly applicable to an examination of the bubble scattering model than the remotely measured wind speed.

It was deemed appropriate to investigate the relative contribution of predicted bubble scattering and ripple scattering, where on the one hand both scattering contributions were based upon observed wind speeds, and where on the other hand the bubble scattering contribution was based upon observed vertical incidence volume backscatter. The integrated volume backscatter results presented in Table 3.2 were used as inputs to the APL/UW (APL89) bubble scattering model. A grazing angle of 40° was selected for these comparisons since potential noise problems at lower grazing angles could be avoided. Figure 4.18 shows the ratio of predicted bubble to ripple scattering versus wind speed for the two different bubble component inputs; WS represents (observed) wind speed inputs for both bubble and ripple scattering components while VI represents vertical incidence volume backscatter inputs for the bubble scattering component.

With wind speed as the inputs for both scattering components the curves increase smoothly and rapidly with wind speed so that bubble backscattering dominates ripple scattering ($\sigma_b/\sigma_r \geq 10$) below 5 m/s for 108 kHz and below 10 m/s for 18 kHz. However, when measured volume backscatter is used as input to the bubble scattering component, bubble scattering dominates ripple scattering only for 108 and 72 kHz and at considerably higher wind speeds. For 36 and 18 kHz, bubble scattering was less than or comparable with ripple scattering for all wind speeds observed.

The comparisons shown in Fig. 4.18 suggest that the basis for the bubble scattering model might be further validated, while simultaneously reconciling the near-surface volume backscattering and surface backscattering measurements in the present case, provided volume backscatter results were used as inputs

71
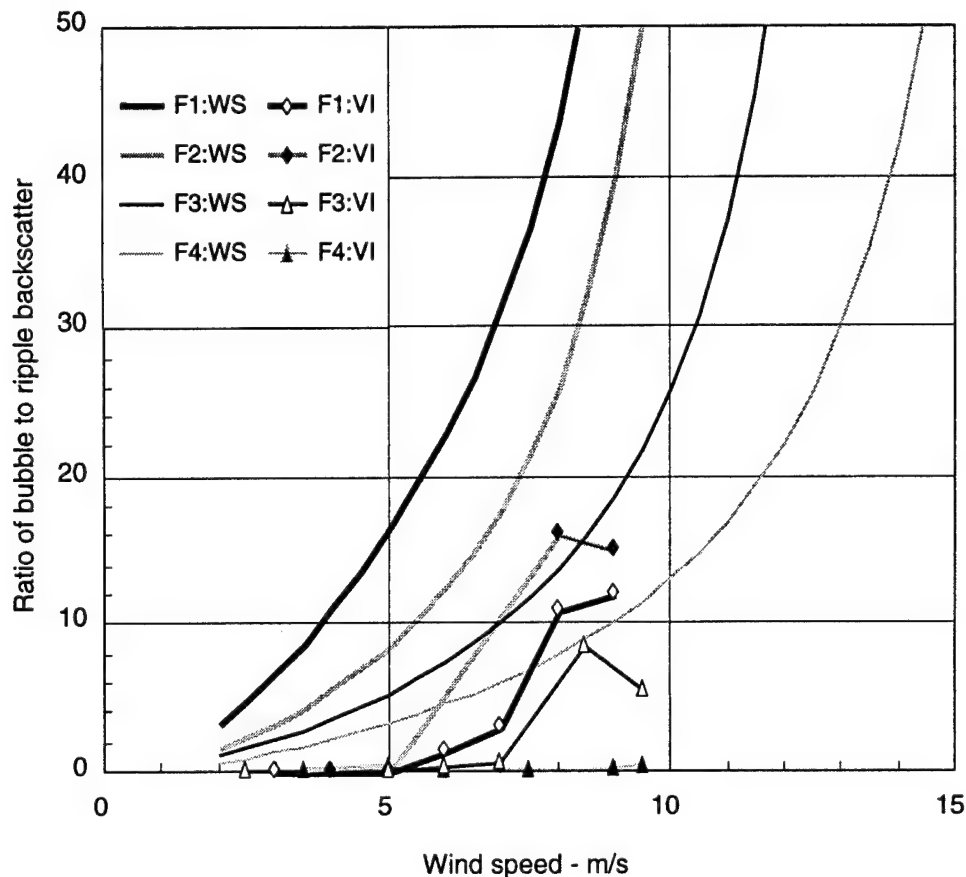
Figure 4.18
Ratio of predicted bubble and ripple backscattering contributions.

to the bubble scattering component and observed wind speeds were used as ripple scattering component inputs.

The surface backscatter measurement results presented in Figs. 4.14 - 4.17 are repeated in Figs. 4.19 - 4.22 along with model predicted curves at the lower grazing angles, using vertical incidence volume backscatter measurement results as inputs. The model predicted curves represent $10 \log (\sigma_b + \sigma_r)$ where the respective inputs to σ_b and σ_r, the bubble scattering and ripple scattering components as described in APL/UW (1989), are as discussed above. Measured volume backscattering strength and observed wind speed for corresponding data files were used as model inputs where possible. However, for data files where no volume backscatter was discernible, model inputs were selected from data files which matched wind conditions most closely.

In most cases the model predicted curves using measured volume backscatter as inputs to the bubble scattering component match measured surface backscatter strength more closely than the earlier comparisons where model curves were based on wind speed as inputs. This is particularly significant with regard to verification of the physical basis of the near-surface bubble layer component of the APL/UW surface backscattering model. The comparisons also serve to illustrate the compatibility of vertical incidence volume backscatter and surface backscatter measurements in the present case. In particular, extremely low surface backscattering strength at low grazing angles is observed to accompany those occasions where no vertical incidence volume backscatter was discernible.

The APL/UW revised surface acoustic backscatter submodel (APL/UW, 1994) predicted curves for all grazing angles were generated for 5, 8, and 10 m/s wind speeds using computer code supplied by APL/UW. The predicted curves for the revised submodel are also shown for comparison in Figs. 4.19 - 4.22.

The APL94 revised model predicted curves for 5 m/s fit the lower wind speed measurements (i.e., the (a) and (b) presentations) reasonably well for all frequencies. Model predictions using vertical incidence volume backscatter to estimate the bubble scattering component parameter generally provide a better
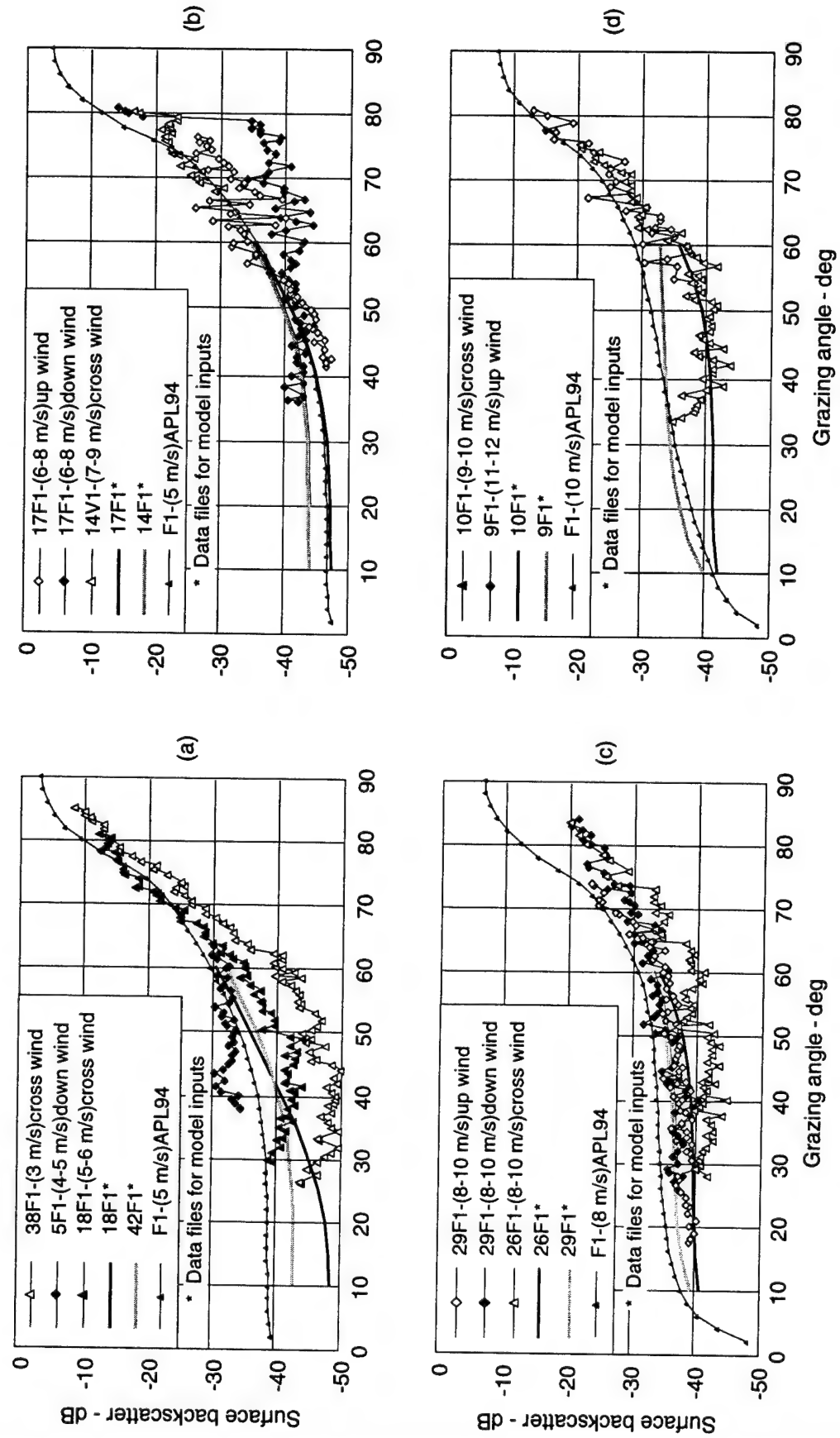
Figure 4.19
Bubble scattering model comparisons
of surface backscattering strength versus grazing angle
(frequency = 108 kHz).

74
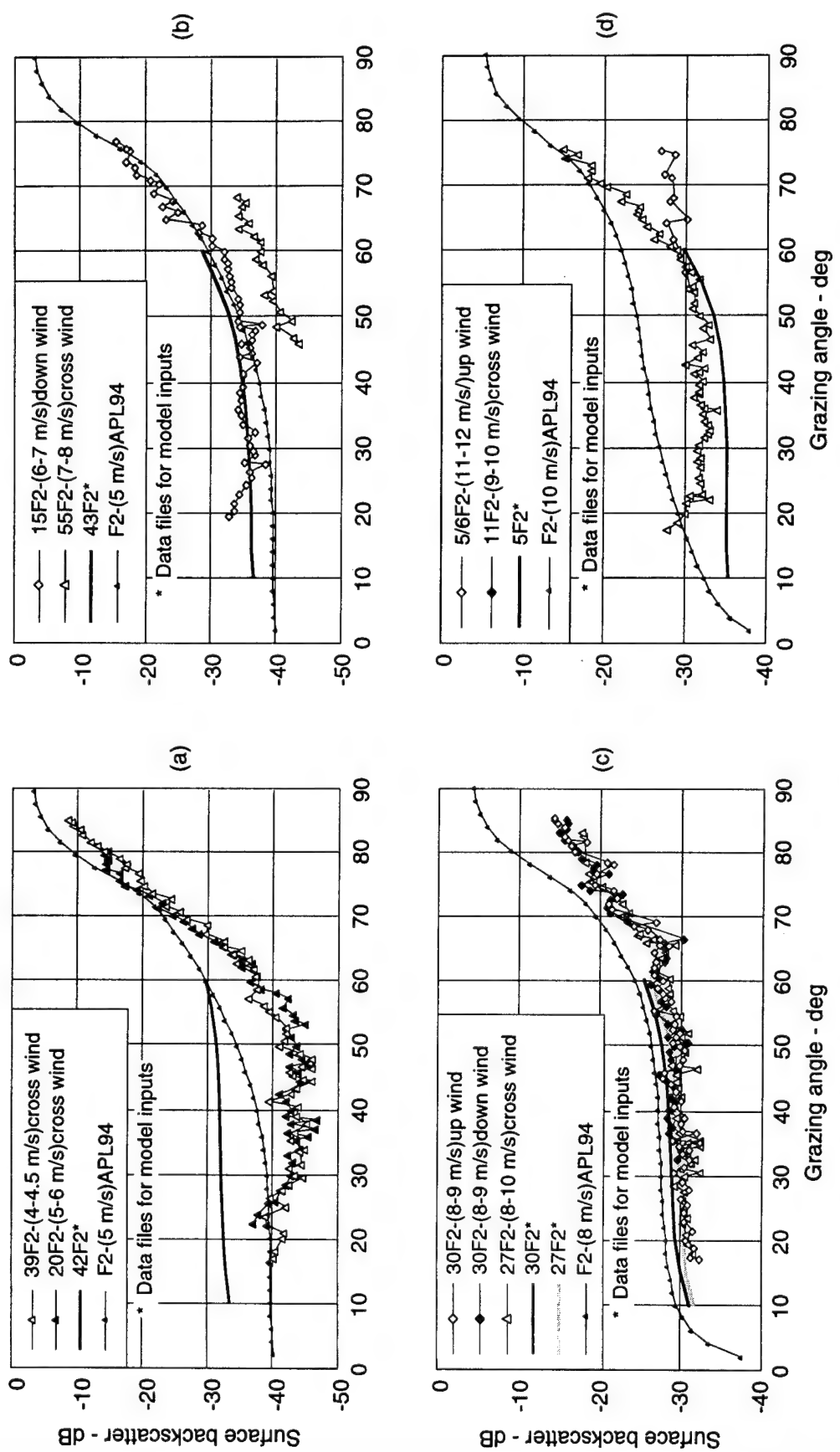
Figure 4.20
Bubble scattering model comparisons
of surface backscattering strength versus grazing angle
(frequency = 72 kHz).
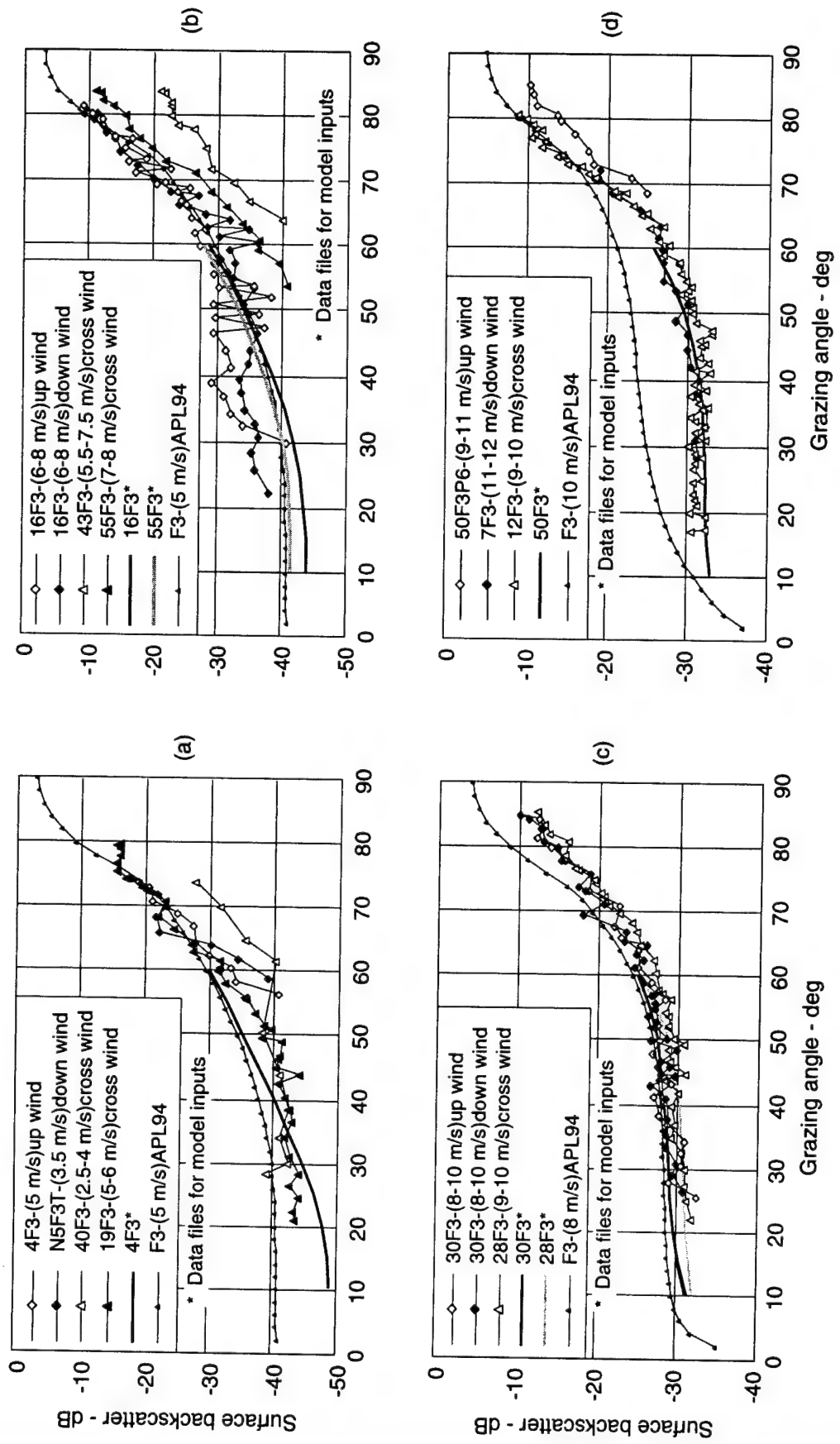
Figure 4.21
Bubble scattering model comparisons
of surface backscattering strength versus grazing angle
(frequency = 36 kHz).

76
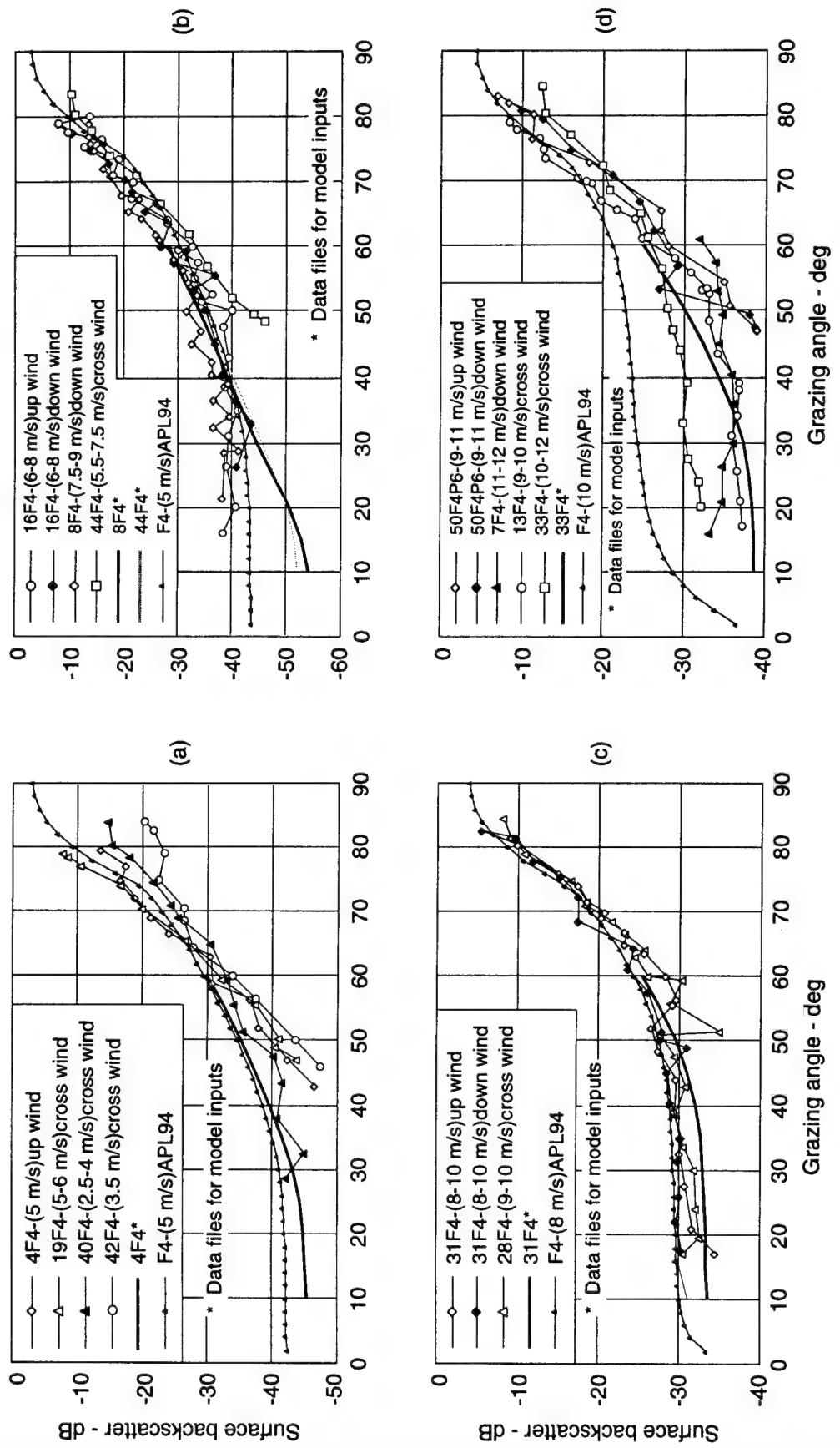
Figure 4.22
Bubble scattering model comparisons
of surface backscattering strength versus grazing angle
**(frequency = 18 kHz).**

fit to these measurements, indicating that in situ estimates of bubble density in the near time frame are more reliable than remote wind speed estimates in determining model parameters. The revised model predicted curves for 8 m/s (part (c) in the figures) overestimate surface backscatter, particularly for the two highest frequencies, but generally represent the shape of the data versus grazing angle rather well at all frequencies. For the highest wind speed data in part (d) of each figure, the revised model predicted curves fit high grazing angle data rather well, but consistently overestimate surface backscatter measurements at intermediate and low grazing angles. The overall shape of the higher wind speed predicted curves do not match very well that of the measurements at these wind speeds; the shape of the measurements at all four frequencies is more like that of the predictive curves for lower wind speeds.

The absence of near-surface volume backscatter and, presumably, dynamic surface generated bubbles at wind speeds below about 2-3 m/s have been noted by others. An apparent anomaly occurs in the present measurements for a wind speed of 5-6 m/s, in that no volume backscatter and very low surface backscatter were observed although the wind had been from the SE and diminishing for more than 24 hours preceding the measurements. A BT was taken from a work boat near the at-sea test site on the day in question and no large discrepancy between at-sea and shore site wind conditions were noted. The lack of bubble production on this occasion remains unexplained but may not be uncommon in coastal waters.

In all cases, as discussed earlier, the volume backscatter was highly variable from ping to ping, which contributes to considerable uncertainty in the model inputs. Selected surface backscattering data files were used to estimate the coefficient of variation (COV) for backscattering strength at 40° grazing angle as a function of (observed) wind speed. Figure 4.23 shows the results obtained for the selected data. For all four frequencies the COV exceeds the Rayleigh value expected for Gaussian statistics at lower wind speeds. Gaussian statistics are indicated at the highest wind speeds consistent with the trend toward domination by bubble scattering indicated in Fig. 4.18. The close connection between surface backscatter at lower grazing angles and near-surface concentrations of resonant bubble scatterers is reinforced by the current measurement results.
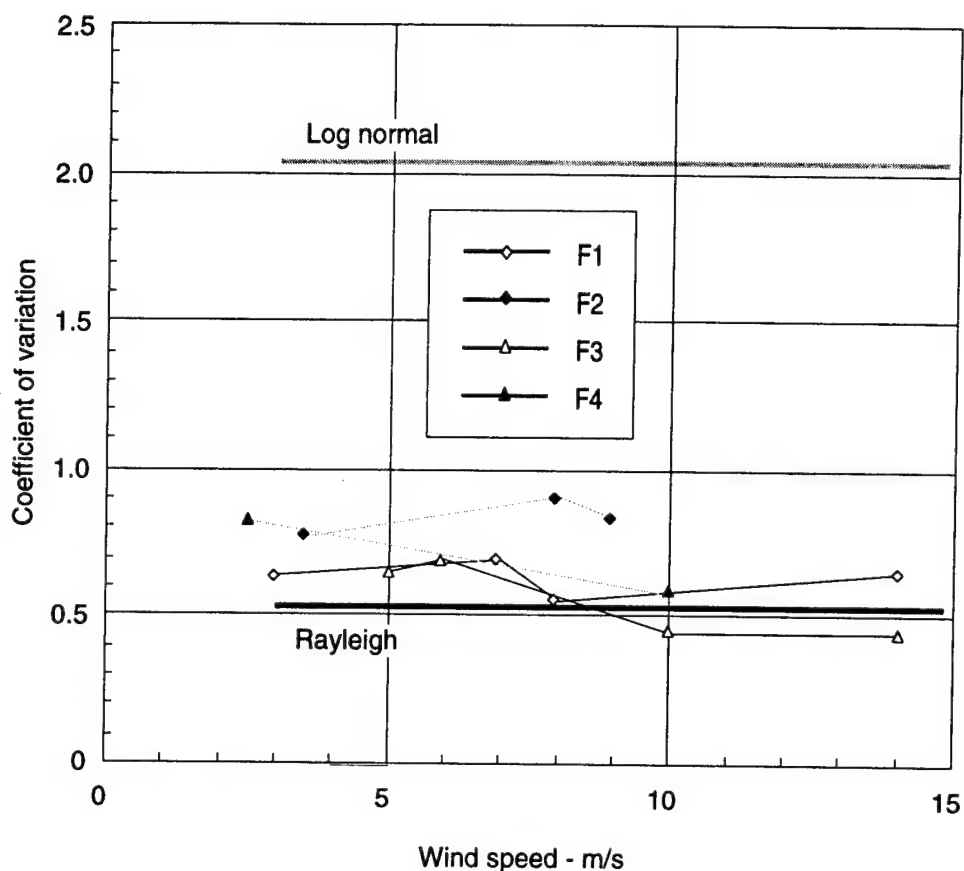
**Figure 4.23
Coefficient of variation versus observed wind speed
for selected data files.**

79

This page intentionally left blank.

5. SUMMARY AND CONCLUSION

Surface and near-surface acoustic backscatter measurements at 108, 72, 36, and 18 kHz made off the coast of Fort Lauderdale, Florida, have been analyzed and the results are presented in this report. The measurements were made with bottom mounted equipment looking upward at the ocean surface; wind speeds encountered varied from about 2.5 to about 16 m/s.

Vertical incidence acoustic measurements were used to evaluate near-surface volume backscatter. The transmit pulse types mainly used were 0.25 ms cw and 1 ms - 4 kHz FM, which provided sufficient depth resolution to obtain volume backscatter data to within 1 m of the ocean surface. In general, mean volume backscatter strength decreased exponentially with depth; integrated volume backscattering values were evaluated and compared with values reported by McConnell and Dahl (1991). Estimates of resonant bubble densities were made assuming that near-surface volume backscatter was dominated by resonant bubble scattering. Such estimates for measurements reported here indicate that bubble densities very near the surface were quite high but diminished rapidly with depth. Bubble density versus depth estimates were compared with similar estimates from acoustic measurements reported by others.

The bubble density versus depth estimates for multiple frequencies were used to evaluate bubble density versus bubble radius behavior at selected depths of 1 and 4 m. If it is assumed that resonant bubble density $n(a_R) = n_o a_R^{-m}$, where a_R is the resonant bubble radius, the estimates at the selected depths lead to values for m that are generally higher than similar values reported by others. Bubble density versus bubble radius estimates revealed no wind dependence over the range of wind speeds encountered.

Surface backscattering measurement results were examined for dependence upon transmitted pulse type; no such dependence was found for the frequencies used and the wind speeds encountered. Only modest wind speed dependence was observed for grazing angles greater than about 60°. However, a significant dependence upon wind speed was observed for all frequencies at intermediate and lower grazing angles. Surface backscattering and near-surface volume backscattering results were consistent in that very low surface

81

backscattering corresponded to occasions for which no or very low near-surface volume backscattering was observed.

Little if any frequency dependence was seen over the range of wind speeds encountered. Measured surface backscattering strengths were comparable with APL/UW model predictions at high grazing angles; however, measurement results were substantially below MINERAY and APL/UW(89) model predictions at intermediate and lower grazing angles. APL/UW(94) revised surface acoustic backscatter model predictions were in much closer agreement with measurement results at all grazing angles and wind speeds; however, substantial differences in revised model predictions and measurements were noted at intermediate and lower grazing angles for higher wind speeds.

Vertical incidence volume backscatter measurements were used to provide more direct inputs to the APL/UW bubble scattering model for prediction of surface backscattering at lower grazing angles. The model predictions using these inputs generally agreed more closely with surface backscattering measurement results than model predictions using observed wind speed as inputs. Considerable improvement in wind speed dependence has been made in the revised APL/UW(94) surface backscatter model.

These comparisons provide some substantiation of the physical basis of the bubble scattering model. The preferred physical measurement providing model inputs is vertical incidence acoustic backscatter or absorption. When such measurements are impractical, wind speed measurements can provide less direct inputs, but tend to result in overestimates of surface backscatter at lower grazing angles and higher wind speeds.

APPENDIX A
MINERAY AND APL/UW SURFACE BACKSCATTERING MODELS

This page intentionally left blank.

MINERAY INTRODUCTION

MINERAY is a sonar performance computer model developed initially by ARL:UT for evaluation of minehunting sonars. The use of this computer model extends generally to high resolution direct path sonar with operating frequencies from 10 to 400 kHz. A detailed description of the MINERAY baseline computer model is found in Jaster and Boehme (1984). MINERAY basically implements an active sonar equation and computes signal-to-interference level ratios as a function of time. Interference level estimates derive from submodels of potentially interfering noise sources including bottom, surface and volume backscattering. The surface backscattering submodel is of particular interest in this report.

MINERAY SURFACE BACKSCATTERING MODEL

The prediction of high frequency acoustic surface backscattering strength in MINERAY is based upon an empirical model (Chapman and Harris, 1962) modified (Welton and Campbell, 1975) to include results at higher acoustic frequencies (Urick and Hoover, 1956; Garrison et al., 1960).

The surface backscattering strength BS, in dB/yd^2, is given by the following equation.

$$BS = -51.3 + 20 \log(1+R) + (1/15)[R \log(f+0.1)] + 10\Gamma \log[\tan(\theta)] \quad , \quad (A.1)$$

where R is wind speed in kt (R≥0.1), f is frequency in kHz, θ is grazing angle, and Γ is a computed parameter given by the following equation.

$$\Gamma = [4(R+2)/(R+1)] + [2.5(f+0.1)^{-0.3} - 4][\cos \theta]^{0.125} \quad . \tag{A.2}$$

Figures A.1(a) and A.2(a) show surface backscattering versus grazing angle curves (MINE) computed from the above equations for wind speeds of 5 m/s and 10 m/s, respectively.
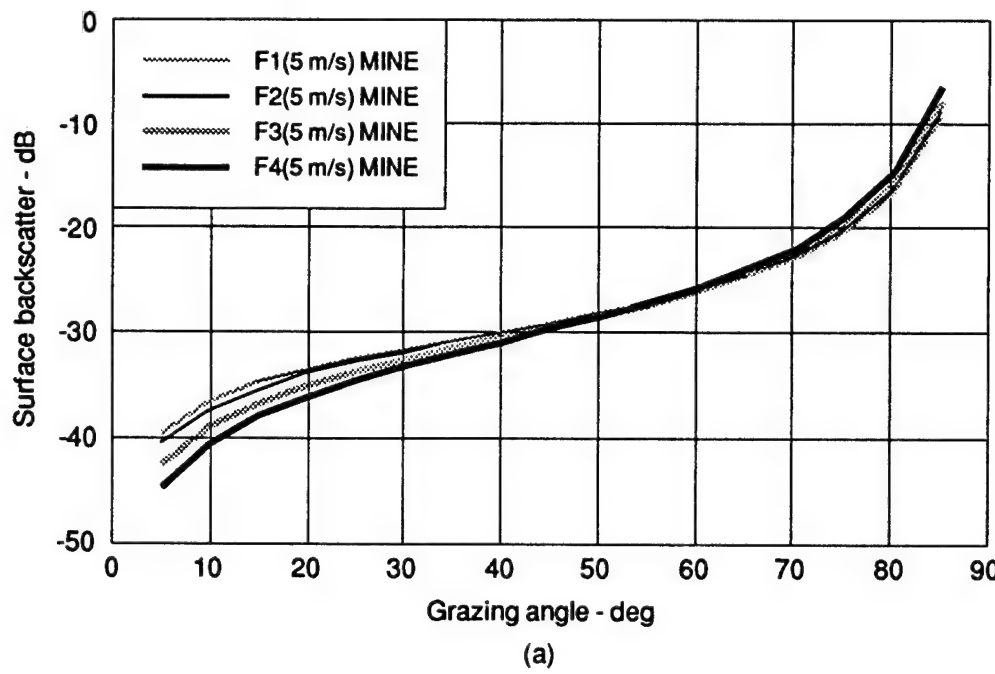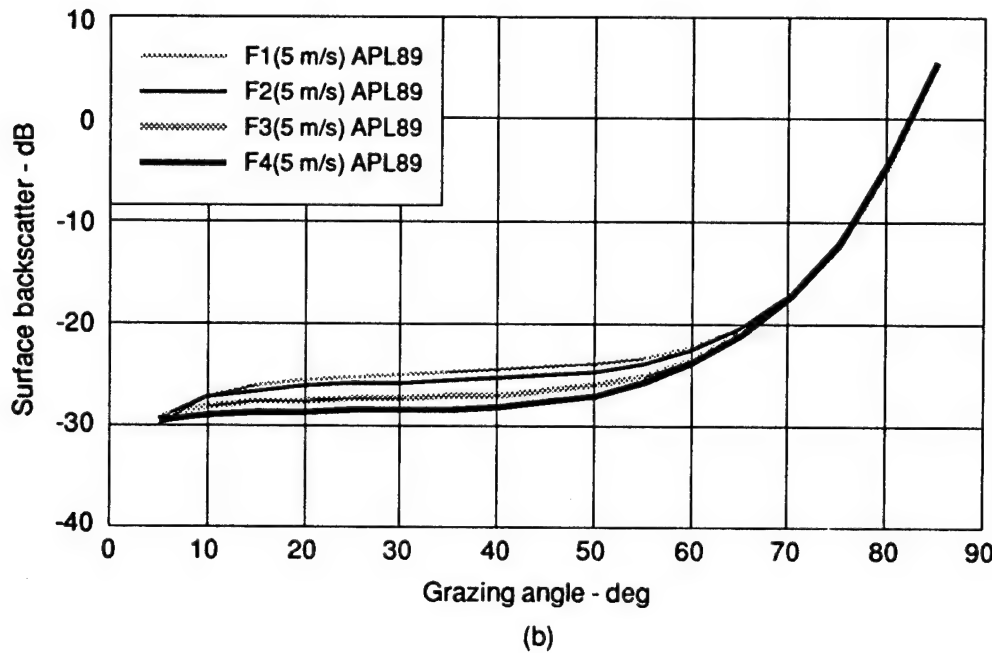
Figure A.1
MINERAY and APL/UW surface backscatter model
predicted curves for a wind speed of 5 m/s.
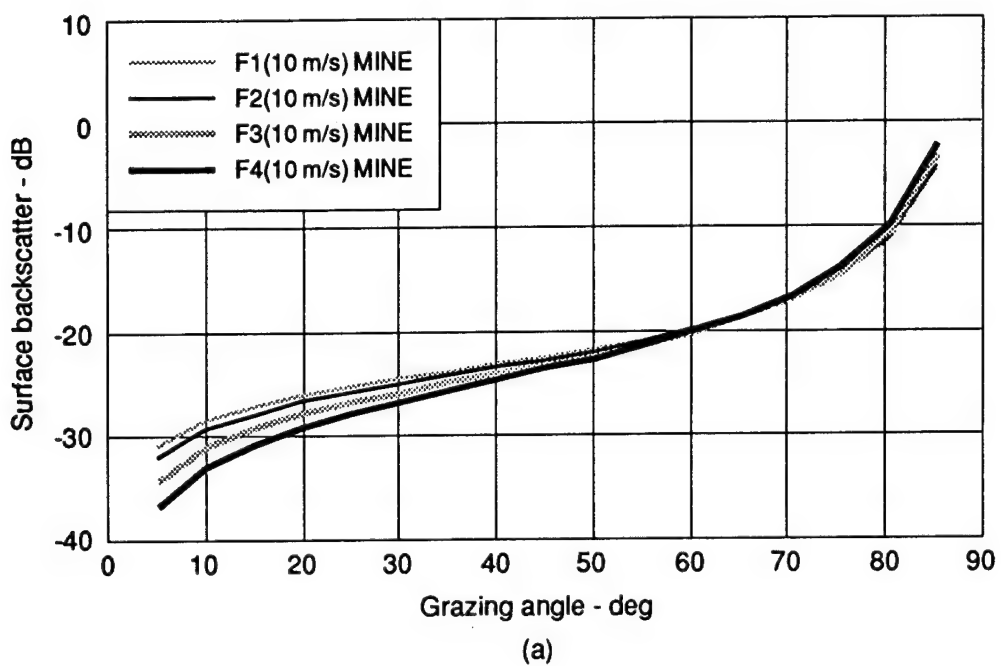
(a)
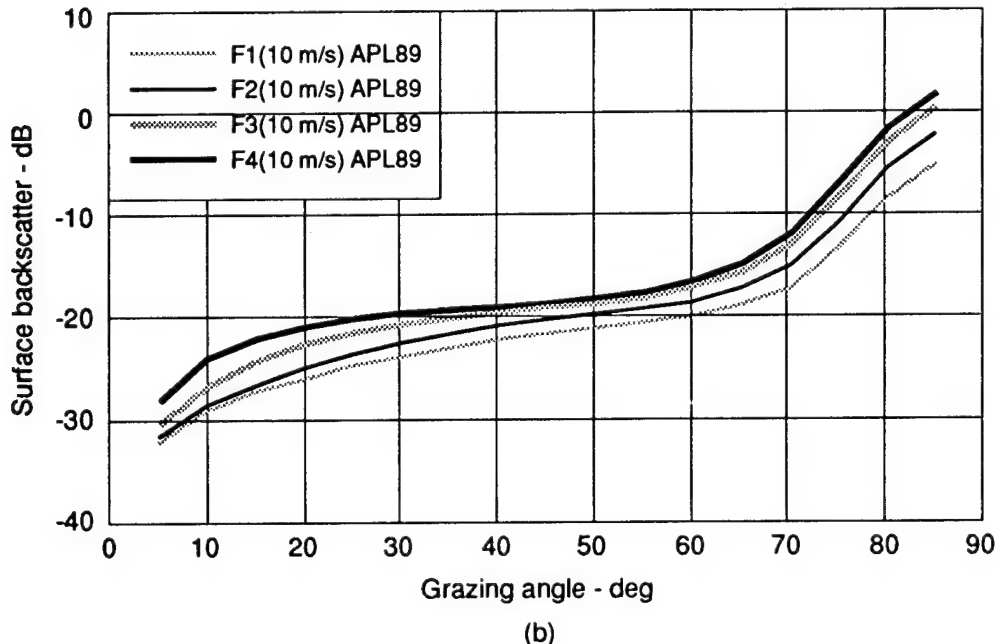
(b)

Figure A.2
MINERAY and APL/UW surface backscatter model
predicted curves for a wind speed of 10 m/s.

A.3   APL/UW HIGH FREQUENCY MODELS INTRODUCTION

The APL/UW high frequency ocean environmental acoustic models were developed primarily for use in simulations and system design within U. S. Navy torpedo and mine countermeasures programs. The models address the interaction of high frequency acoustics with the ocean volume and boundaries, including Arctic ice. The models have been periodically updated to include additional experimental results.

A.4   APL/UW SURFACE BACKSCATTERING MODEL

The APL/UW high frequency acoustic surface backscattering prediction is based upon a composite model including three scatterer mechanisms, near-surface bubbles, surface roughness, and wave 'facets'. In the following discussion the earlier APL/UW(89) model description is given with equations in plain text; the revised APL/UW(94) model parameters and equations are included in bold text.

The surface scattering strength in dB is expressed as

$$S_s = 10 \log (\sigma') \quad , \qquad \mathbf{S_s = 10 \log [\sigma_r(\theta) + \sigma_b(\theta)]}$$

$$\sigma' = \begin{cases} \sigma_b + \sigma_r & \sigma_f \le \sigma_r \\ \\ \sigma_b + \sigma_f & \sigma_f > \sigma_r \end{cases} \tag{A.3}$$

where

$$\sigma_b, \ \boldsymbol{\sigma_b(\theta)} \quad = \quad \text{bubble scattering cross section per unit surface area,}$$

$$\sigma_r, \ \boldsymbol{\sigma_{sc}} \quad = \quad \text{ripple [small-scale roughness] scattering cross section per unit surface area, and}$$

$$\sigma_f, \ \boldsymbol{\sigma_f} \quad = \quad \text{facet [large-scale wave] scattering cross section per unit surface area.}$$

The near-surface bubble contribution is based upon model structures developed by Crowther (1980) and by McDaniel and Gorman (1982). The

surface roughness contribution is based upon a composite roughness model developed by Kur'yanov (1963), Bachman (1973), and McDaniel and Gorman (1983), wherein the rough sea surface is characterized by small ripples superimposed upon larger scale waves. The third contribution, termed facet scattering, is applicable near vertical incidence and is presumed to arise from wave facets that are oriented so as to produce specular reflection. The model used is based upon developments by McDaniel (1986) and McDaniel and McCammon (1987); in addition, a Gaussian, isotropic distribution of surface slopes is used.

For the backscattering condition, the following equation applies for σ_b:

$$\sigma_b = (\sin \theta/8\pi)(\delta_r/\delta)[1 + 4\beta e^{-2\beta} - e^{-4\beta}] \quad , \tag{A.4}$$

$$\sigma_b(\theta) = (\sin \theta/8\pi)(\delta_r/\delta)[1 + 8\beta e^{-2\beta} - e^{-4\beta}] \quad ,$$

where

θ = grazing angle,

β = $\beta_v/\sin \theta$,

β_v = depth integrated total extinction cross section,

= $1.65 \times 10^{-6}\, f\, U^{3.75}$ = $10^{(-5.2577+0.4701U)}(f/25)^{0.85}$, $U < 11 m/s$,

= $\beta_v(U = 11\ m/s)(U/11)^{3.5}$, $U \geq 11 m/s$,

δ_r = 0.0136 = bubble radiation damping coefficient,

δ = $5.15 \times 10^{-2} \log f - 2.95 \times 10^{-2}$ = total damping coefficient,

= $2.55 \times 10^{-2}\, f^{1/3}$,

f = frequency, kHz, and

U = wind speed measured 10 m above the sea surface in m/s.

Bragg scattering from surface ripples superimposed on larger-scaled waves described by composite roughness theory forms the basis for the quantity σ_r [$\sigma_{sc}(\theta)$]. The following equation applies to this surface backscattering contribution.

$$\sigma_r = A(U) \tan^4 \theta\ 10^{-SBL/10} \quad , \tag{A.5}$$

$$\sigma_{sc}(\theta) = A(U) \tan^4 \theta \quad , \qquad \theta \leq 85° \quad ,$$

$$\sigma_{sc}(\theta) = 0 \quad , \qquad \theta > 85° \quad ,$$

where

A(U), **A(U)** = an adjustable coefficient fitted to data in the grazing angle range of 30-70°,

= $1.3 \times 10^{-5} U^2$

SBL(dB) = $[1.43 \times 10^{-5}/\sin\theta]\, U^{3.75}$ f = extinction loss through near-surface bubble layer.

The facet scattering term is applicable at high grazing angles and is given by the expression

$$\sigma_f = [\sec^4 \gamma/4\pi s^2]\, \exp\{-\tan^2 \gamma/s^2\}\, 10^{-SBL/10}\ ,\qquad (A.6)$$

$$\boldsymbol{\sigma_f(\theta) = [\sec^4 \gamma/4\pi s^2]\, \exp\{-\tan^2 \gamma/s^2\}}\ ,$$

where

γ, γ = $90 - \theta$ and the mean surface slope s^2 is estimated from

s^2 = $\tan^2(\Delta)$; $\Delta = 1.79 U^{0.73}$, deg,

$\boldsymbol{s^2}$ = $\boldsymbol{4.6 \times 10^{-3} \log_e(2.1U^2)}$, $\boldsymbol{U \geq 1\ m/s}$,

$\boldsymbol{s^2}$ = $\boldsymbol{0.0034}$, $\boldsymbol{U < 1\ m/s}$.

The surface roughness component $\sigma_r(\theta)$ contribution to total surface scattering strength is obtained by interpolation between $\sigma_f(\theta)$ and $\sigma_{sc}(\theta)$ using the interpolation function $f(x)=[1+e^x]^{-1}$, and first computing the quantity

$$\sigma_{r1}(\theta) = f(x)\sigma_f(\theta) + [1 - f(x)]\,\sigma_{sc}(\theta)\ ,$$

with the argument $x=0.524(\theta_f-\theta)$, where the angles θ and θ_f are in deg. The transition occurs in the vicinity of θ_f, defined as the angle at which θ_f is 15 dB below its peak value at $\theta_f=90°$. The interpolation function provides for a smooth transition between the two scattering contributions. Finally, $\sigma_r(\theta)$ is computed from $\sigma_{r1}(\theta)$ by correcting for the extinction loss due to penetration through the near-surface bubble layer, as

$$\sigma_r(\theta) = \sigma_{r1}(\theta)10^{-SBL(\theta)/10}\ ,$$

90

where

$$\mathbf{SBL(\theta)\ dB} = [1.26 \times 10^{-3}/\sin\theta]U^{1.57}f^{0.85}, \quad U \geq 6\ \text{m/s}$$

$$\mathbf{SBL(\theta)\ dB} = \mathbf{SBL(U=6m/s)}\ e^{1.2(U-6)}, \quad U < 6\ \text{m/s}$$

where U and f are as defined above.

The APL/UW(89) surface backscattering model (APL89) curves for all four frequencies and wind speeds of 5 and 10 m/s are shown in Figs. A.1(b) and A.2(b), respectively. The revised APL/UW(94) surface backscattering model (APL94) curves for all four frequencies and wind speeds of 5, 8, and 10 m/s are shown in Figs 4.19 - 4.22.

This page intentionally left blank.

REFERENCES

Applied Physics Laboratory, The University of Washington (APL/UW, 1989). "APL/UW High-Frequency Ocean Environmental Acoustic Models," APL/UW Technical Report 8907.

Applied Physics Laboratory, The University of Washington (APL/UW, 1994). "APL/UW High-Frequency Ocean Environmental Acoustic Models Handbook," APL/UW Technical Report 9407.

Bachmann, W. (1973). "A Theoretical Model for the Backscattering Strength of a Composite-Roughness Sea Surface," J. Acoust. Soc. Am. **54**(3), 712-716.

Chapman, R. P., and J. H. Harris (1962). "Surface Backscattering Strengths Measured with Explosive Sound Sources," J. Acoust. Soc. Am. **34**(10), 1592-1597.

Crawford, G. B., and D. M. Farmer (1987). "On the Spatial Distribution of Ocean Bubbles," J. Geophys. Res. **92**(C8), 8231-8243.

Crowther, P. A. (1980). "Acoustical Scattering from Near-Surface Bubble Layers," in *Cavitation and Inhomogeneities in Underwater Acoustics*, edited by W. Lauterborn (Springer-Verlag, New York), pp. 194-204.

Dalen, J., and A. Løvik (1981). "The Influence of Wind-Induced Bubbles on Echo Integration Surveys," J. Acoust. Soc. Am. **69**(6), 1653-1659.

Devin, C. (1959). "Survey of Thermal, Radiation, and Viscous Damping of Pulsating Air Bubbles in Water," J. Acoust. Soc. Am. **31**, 1654-1667.

Farmer, D. M., and S. Vagle (1989). "Waveguide Propagation of Ambient Sound in the Ocean-Surface Bubble Layer," J. Acoust. Soc. Am. **86**(5), 1897-1908.

Francois, R. E., and G. R. Garrison (1982). "Sound Absorption Based on Ocean Measurements. Part II: Boric Acid Contribution and Equation for Total Absorption," J. Acoust. Soc. Am. **72**(6), 1879-1890.

Garrison, G. R., S. R. Murphy, and D. S. Potter (1960). "Measurements of the Backscattering of Underwater Sound from the Sea Surface," J. Acoust. Soc. Am. **32**(1), 104-111.

Jaster, C. E., and H. Boehme (1984). "The MINERAY Sonar Performance Prediction Computer Model Baseline Description," Applied Research Laboratories Technical Report No. 84-9 (ARL-TR-84-9), Applied Research Laboratories, The University of Texas at Austin.

Kur'yanov, B. F. (1963). "The Scattering of Sound at a Rough Surface with Two Types of Irregularity," Sov. Phys. Acoust. **8**(3), 252-257.

Løvik, A. (1980). "Acoustic Measurements of the Gas Bubble Spectrum in Water," in *Cavitation and Inhomogeneities in Underwater Acoustics*, edited by W. Lauterborn (Springer-Verlag, New York), pp. 211-218.

McConnell, S. O. (1988). "Acoustic Measurements of Bubble Densities at 15-50 kHz," in *Sea Surface Sound*, edited by B. Kerman (Kluwer Academic Publishers, Boston), pp. 237-252.

McConnell, S. O., and P. H. Dahl (1991). "Vertical Incidence Backscatter and Surface Forward Scattering from Near-Surface Bubbles," APL/UW Technical Report 9022, Applied Physics Laboratory, The University of Washington, Seattle, Washington.

McDaniel, S. T. (1986). "Diffractive Corrections to the High-Frequency Kirchhoff Approximation," J. Acoust. Soc. Am. **79**(4), 952-957.

McDaniel, S. T. (1993). "Sea Surface Reverberation: A Review," J. Acoust. Soc. Am. **94**(4), 1905-1922.

McDaniel, S. T., and A. D. Gorman (1982). "Acoustic and Radar Sea Surface Backscatter," J. Geophys. Res. **87**, 4127-4136.

McDaniel, S. T., and A. D. Gorman (1983). "An Examination of the Composite-Roughness Scattering Model," J. Acoust. Soc. Am. **73**(5), 1476-1486.

McDaniel, S. T., and D. F. McCammon (1987). "Composite Roughness Theory Applied to Scattering from a Fetch Limited Sea," J. Acoust. Soc. Am. **82**(5), 1712-1719.

Medwin, H. (1970). "In Situ Acoustic Measurements of Bubble Populations in Coastal Waters," J. Geophys. Res. **75**(3), 599-611.

Medwin, H. (1977a). "Counting Bubbles Acoustically: A Review," Ultrasonics **15**, 7-13.

Medwin, H. (1977b). "In Situ Acoustic Measurements of Microbubbles at Sea," J. Geophys. Res. **82**(6), 971-976.

Medwin, H. (1977c). "Acoustical Determination of Bubble Size Spectra," J. Acoust. Soc. Am. **62**(4), 1041-1044.

Medwin, H., and N. D. Breitz (1989). "Ambient and Transient Bubble Spectral Densities in Quiescent Seas and Under Spilling Breakers," J. Geophys. Res. **94**(C9), 12751-12759.

Monahan, E. C., and M. Lu (1990). "Acoustically Relevant Bubble Assemblages and Their Dependence on Meteorological Parameters," IEEE J. Oceanic. Eng. **15**(4), 340-349.

Nützel, B., et al. (1986). "A Further Investigation of Acoustic Scattering from the Sea Surface," Technical Document NUSC 7685, Naval Underwater Systems Center, New London, Connecticut.

Nützel, B., H. Herwig, P. D. Koenigs, and J. M. Monti (1994). "Acoustic Backscatter Measurements in the North Sea: 3-18 kHz," J. Acoust. Soc. Am. **95**(5), 2488-2494.

Osborn, T., D. M. Farmer, S. Vagel, S. A. Thorpe, and M. Cure (1992). "Measurements of Bubble Plumes and Turbulence from a Submarine," Atmosphere-Ocean **30**(3), 419-440.

Schippers, I. P. (1980). "Density of Air-Bubbles below the Sea Surface, Theory and Experiments," in *Sea Surface Sound*, edited by B. Kerman (Kluwer Academic Publishers, Boston), pp. 205-210.

Thorpe, S. A. (1985). "Small-Scale Processes in the Upper Ocean Boundary Layer," Nature **318**, 519-522.

Thorpe, S. A. (1986). "Measurements with an Automatically Recording Inverted Echo Sounder, AIRES and the Bubble Clouds," J. Phys. Oceanogr. **16**, 1462-1478.

Thorpe, S. A. (1992). "Bubble Clouds and the Dynamics of the Upper Ocean," Q. J. Roy. Meteorol. Soc. **118**, 1-22.

Urick, R. J., and R. M. Hoover (1956). "Backscattering of Sound from the Sea Surface: Its Measurement, Causes, and Application to the Prediction of Reverberation Levels," J. Acoust. Soc. Am. **28**(6), 1038-1042.

Vagle, S., and D. M. Farmer (1992). "The Measurement of Bubble-Size Distributions by Acoustical Backscatter," J. Atmos. and Oceanic Tech. **9**, 630-644.

Weast, R. C. (1979). *CRC Handbook of Chemistry and Physics, 59th Edition*, (The Chemical Rubber Company, CRC Press, New York).

Welton, P. J., and R. J. Campbell (1975). "New Empirical Expression for Sea Surface Backscattering Strength," J. Acoust. Soc. Am. **57**(Sup. 1), S58.

DISTRIBUTION LIST
ARL-TR-95-23
**Technical Report under ARL:UT Independent
Research and Development Program**

<u>Copy No.</u>

	Director
	Office of Naval Research
	800 North Quincy Street
	Arlington, VA 22217-5660
1	Attn: F. Saalfeld (Code 01)
2	A. Bisson (Code 03)
3	S. Ramberg (Code 21)
4	J. Andrews (Code 321N)
5	E. Chaika (Code 321OA)
6	W. Ching (Code 321TS)
7	B. Wheatley (Code 321US)
8	T. Goldsberry (Code 322)
9	B. Blumenthal (Code 322TE)
10	D. Houser (Code 333)

Commander
Program Executive Office, Mine Warfare
Space and Naval Warfare Systems Command
Crystal Plaza Bldg. 6
2531 Jefferson Davis Highway
Arlington, VA 22242-5167

11	Attn: J. Grembi (PEOMIW)
12	D. Gaarde (PMO407B)
13	T. Douglass (PEO (USW)

Office of the Oceanographer of the Navy
U. S. Naval Observatory
3450 Massachusetts Avenue, NW
Washington, DC 20392-5421

14	Attn: E. Whitman (Code NO96T)

Director
Office of Naval Intelligence
4251 Suitland Road
Washington, DC 20395-5720

15	Attn: L. Edmonds

Distribution List for ARL-TR-95-23 under ARL:UT Independent Research and Development Program (cont'd)

<u>Copy No.</u>

	Commander
	Naval Meterology and Oceanography Command
	1020 Balch Boulevard
	Stennis Space Center, MS 39529
16	Attn: R. Martin (Code N5C)

	Superintendent
	U. S. Naval Postgraduate School
17	Monterey, CA 93943

	Commanding Officer
	Naval Research Laboratory
	Washington, DC 20375-5000
	Attn: Technical Library
18	E. Franchi (Code 7100)

	Commanding Officer
	Naval Surface Warfare Center
	Coastal Systems Station
	6703 West Highway 98
	Panama City, FL 32407-7001
19	Attn: Technical Library (Code E29)
20	E. Pipkin
21	D. Todoroff (Code 130)
22	K. Commander (Code 2120)

	Commanding Officer
	Naval Research Laboratory
	Stennis Space Center, MS 39529-5004
23	Attn: J. S. Stanic (Code 7174)
24	R. Love (Code 7174)
25	K. Briggs (Code 7333)
26	S. Tooma (Code 7430)
27	M. Richardson (Code 7431)

Distribution List for ARL-TR-95-23 under ARL:UT Independent Research and Development Program (cont'd)

Copy No.

	Commander
	Naval Surface Warfare Center
	Dahlgren Division, White Oak Detachment
	10901 New Hampshire Avenue
	Silver Spring, MD 20903-5000
28	Attn: Technical Library
29	C. McClure (Code A10)
30	S. Martin (Code G94)
31	M. Stripling (Code N04W)
32	B. DeSavage, Jr. (Code R02)

Officer in Charge
Naval Undersea Warfare Center
Arctic Submarine Laboratory
49250 Fleming Road
San Diego, CA 92152-7210
33   Attn: R. Anderson (Code 906)

Commanding Officer
Naval Command Control and Ocean Surveillance Center
RDT&E Division
53560 Hull Street
San Diego, CA 92152-5000
34   Attn: C. Wright, Librarian (Code 0274)
35   R. Floyd (Code 532)

Officer in Charge
Naval Undersea Warfare Center
New London Detachment
New London, CT 06320-5594
36   Attn: Technical Library
37   A. Dugas, Jr. (Code 2122)
38   H. Weinberg (Code 3122)

Distribution List for ARL-TR-95-23 under ARL:UT Independent Research and Development Program (cont'd)

<u>Copy No.</u>

	Commander
	Naval Undersea Warfare Center
	Newport Division
	1176 Howell Street
	Newport, RI 02841-1708
39	Attn: Technical Library (Code 0262)
40	A. Davis, Jr. (Code 2211)
41	J. Kelly (Code 821)
42	D. Goodrich (Code 823)
43	F. Aidala, Jr. (Code 842)

	Commander
	Advanced Research Projects Agency
	3701 North Fairfax Drive
	Arlington, VA 22203-1714
44	Attn: W. Carey
45	C. Stewart

	DTIC-OCC
	Defense Technical Information Center
	8725 John J. Kingman Road, Suite 0944
46 - 57	Fort Belvoir, VA 22060-6218

	Applied Research Laboratory
	The Pennsylvania State University
	P. O. Box 30
	State College, PA 16804-0030
58	Attn: Library
59	R. Goodman
60	E. Liszka
61	D. McCammon
62	S. McDaniel
63	H. Piper, Jr.
64	F. Symons

Distribution List for ARL-TR-95-23 under ARL:UT Independent Research and Development Program (cont'd)

<u>Copy No.</u>

	The University of Washington Applied Physics Laboratory 1013 NE 40th Street Seattle, WA 98105-6698
65	Attn: P. Dahl
66	C. Eggen
67	D. Jackson
68	C. Sienkiewicz
69	E. Thorsos
70	K. Williams
71	Matthew A. Beck, ARL:UT
72	Nancy R. Bedford, ARL:UT
73	Frank A. Boyle, ARL:UT
74	Nicholas P. Chotiros, ARL:UT
75	Karl C. Focke, ARL:UT
76	John M. Huckabay, ARL:UT
77	Mimi Z. Lawrence, ARL:UT
78	Thomas G. Muir, ARL:UT
79	S. Patrick Pitt, ARL:UT
80	Jack A. Shooter, ARL:UT
81	Library, ARL:UT